Transient Response Analysis for Fault Detection and Pipeline Wall Condition Assessment in Field Water Transmission and Distribution Pipelines and Networks

by

Mark Leslie Stephens

February 2008

A Thesis Submitted for the Degree of Doctor of Philosophy

School of Civil and Environmental Engineering
The University of Adelaide, SA 5005
South Australia

Chapter 9

Leak and Blockage Detection for Transmission Mains Using Transients

---

The inverse calibration of quasi-steady friction (QSF), unsteady friction (UF), discrete gas cavity with unsteady friction (DGCUF) and unsteady friction and "viscous" Hanson pipeline and offtake branch (UFVHOB) models described in Chapter 8 revealed that identifying the correct pipeline roughness, the quantity of in-situ entrained air and effects of mechanical dispersion and damping is not straight forward. The inverse calibrations to no-fault measured responses from the Hanson Transmission Pipeline (HTP) improved the match between the measured and predicted responses. However, as emphasised in Chapter 8, this did not necessarily mean that the correct physical mechanisms were identified, that realistic parameters were derived for the physical mechanisms that were included in the models or that transient response analysis and/or Inverse Transient Analysis (ITA) can be successfully undertaken, using the calibrated forward transient models, to identify faults.

Field tests, as described in Chapter 7, have been conducted with an artificial 9L/s leak. The measured responses from these tests will be analysed to determine whether the direct reflection information from the leak is sufficient to allow it to be identified. Inverse Transient Analysis (ITA) will then be conducted, using long and short term measured responses, and the calibrated QSF, UF and UFVHOB forward transient models developed in Chapter 8. Varying the length of the measured response used in the inverse analysis enables the influence of damping versus reflection information to be assessed. The accuracy with which the artificial leak can be identified is assessed without and with the use of prior information regarding the leak flowrate.

The results of field tests conducted on the Morgan Transmission Pipeline (MTP) with an artificial discrete blockage, as described in Chapter 7, are presented to illustrate its effect upon the transient response of a pipeline. While ITA is not performed, the results of forward transient modelling are presented to demonstrate how a measured response can be interpreted to diagnose such a fault.

9.1 Comparison of numerical and measured leak reflections

It was hoped that a low level of hydraulic noise coupled with the minimisation of instrumentation noise, would enable the detection of relatively small leak reflections. This hydraulic noise is primarily due to fluctuations in the flow along the Hanson Transmission Pipeline (HTP) but is also contributed to by a random component of mechanical motion and vibration. Unfortunately, as the diameter of a transmission pipeline increases, it appears that hydraulic noise levels remain relatively constant while the relative size of the leak reflections decrease (i.e., as the signal (leak reflection) to noise (hydraulic noise) ratio decreases). An assessment of the size of the numerically estimated and measured leak reflections for the HTP is presented below.

9.1.1 Estimated leak reflection using direct formulation

Providing the pressure under steady conditions, the transmitted and reflected pressures and the transient pressure rise at the location of a leak are known, and the friction in the pipe system is not significant (nor any mechanical dispersion or damping), the size of the lumped leak coefficient C_dA_L can be determined using the relation:

$$C_d A_L = \frac{A}{a}\sqrt{\frac{g}{2}}\frac{(H_1 - H_2)}{\left(\sqrt{\frac{1}{2}(H_1 + H_2)} - \sqrt{H_0}\right)} \tag{9-1}$$

where the terms, H_0, H_1, H_2 and C_dA_L, the steady state pressure, the magnitude of the incident wavefront, the magnitude of the wavefront transmitted after interaction with the leak and the lumped leak coefficient, respectively, are illustrated in Appendix R

Equation 9-1 can be rearranged to form Equation 9-2 (below) which can be solved iteratively to determine a value for H_2 and the maximum anticipated leak reflection when friction and other mechanical effects are ignored:

$$\frac{A}{a}\sqrt{\frac{g}{2}}\left(\frac{(H_1 - H_2)}{\left(\sqrt{\frac{1}{2}(H_1 + H_2)} - \sqrt{H_0}\right)}\right) - C_d A_L = 0 \qquad (9\text{-}2)$$

The leak on the Hanson Transmission Pipeline (HTP) was simulated using the galvanised pipe section connected to an existing fire plug/air valve as described in Chapter 6. The geometry of the galvanised steel pipe section and height of vertical leak discharge were used to estimate the initial vertical velocity of the leak jet and hence a discharge of approximately 9L/s. This was confirmed, as described in Appendix T, using the orifice equation and geometric details of the fire plug/air valve (including the geometry of the seat of the valve). Finally, chart records from the insertion flowmeter in the HTP, included in Appendix J, confirmed that an additional 9L/s discharge occurred in the HTP when the fire plug/air valve was partially opened.

Knowing that the seat of the fire plug/air valve was opened 6.5 of 10 turns, giving and equivalent orifice diameter of approximately 25mm across the seat of the valve, the C_dA_L for the simulated leak on the Hanson Transmission Pipeline (HTP) is approximately 0.000295m^2 (for a C_d of approximately 0.6). The orifice equation can be used to calculate the initial pressure at the leak location:

$$H_0 = \frac{1}{2g}\left(\frac{Q_L}{C_d A_L}\right)^2 = 47.46\text{m}$$

Furthermore, the Joukowsky pressure rise can be estimated, for the customised 50mm ball valve mounted in the transient generator, as described in Chapter 6, after it is closed over approximately 10ms to induce a transient through an existing 200mm diameter scour valve mounted on the side of the HTP. Based on a flow rate through the transient generator of 43L/s, the theoretical Joukowsky pressure rise can be calculated:

$$\Delta H = -\frac{a \times \Delta V}{g} = 15.06\text{m}$$

where $a = 1055\,\text{m/s}$ and $\Delta V = -0.14\,\text{m/s}$

The pressure rise is split equally as the transient propagates from the scour valve into the HTP such that an increase in pressure of approximately 7.53m (H_J) occurs upstream and downstream of the point of generation. As confirmed below, this theoretical pressure rise is approximately equal to that observed in the measured responses.

Given the area of the HTP is approximately 0.3072m^2, its wave speed is 1055m/s, H_0 is equal to 47.46m, H_1 (= H_0 + H_J) is equal to 54.99m and, finally, C_dA_L is equal to 0.000295m^2, the pressure after the leak reflection can be calculated as H_2 equal to 54.75m giving a leak reflection size of 0.24m. This is a maximum estimate of the size of the leak reflection ignoring the effects of fluid friction and mechanical dispersion and damping.

9.1.2 Estimated leak reflection using a forward transient model

Equation 9-1 can only provide a maximum estimate of the size of a leak reflection in pipelines without significant friction or other dispersion and damping phenomena. The Hanson Transmission Pipeline (HTP) is a relatively long field pipeline with, amongst other things, significant friction loss and so it is more accurate to estimate the size of anticipated leak reflections using a forward transient model that includes the effect of friction. Numerous forms of forward transient model have been identified and calibrated in Chapters 7 and 8. A forward transient model with unsteady friction, but without any mechanical “viscous” mechanism, will be used for the purpose of estimating the reflections for various leak sizes on the HTP. A roughness value of 2mm will be used for both the HTP and offtake branch.

Figures 9-1 and 9-2 show the size of the reflections for 9, 15, 21 and 27L/s leaks, with C_dA_L values of 0.000295, 0.000484, 0.000678 and 0.000873m^2, respectively. The sizes of the leak reflections are listed in Table 9-1. Importantly, the sizes of the

reflections for the 9L/s leak are only 0.108m and 0.110m at stations 1 and 2, respectively. These values are less than half the estimate of 0.24m obtained when using Equation 9-1 and neglecting friction.

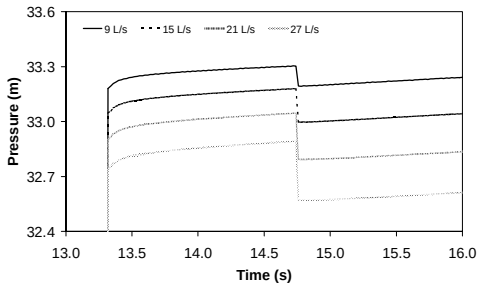

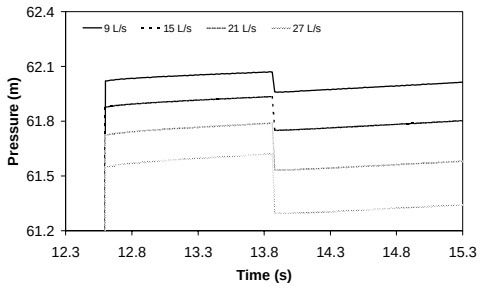

Figures 9-1 and 9-2 – Comparison of leak reflection sizes obtained for 9, 15, 21 and 27L/s leaks on the HTP, at stations 1 and 2, respectively

Table 9-1 – Comparison of leak reflection sizes determined, using an unsteady friction model, at stations 1 and 2, for 9, 15, 21 and 27L/s leaks on the HTP

Leak Size (L/s)	Measurement Station 1				Measurement Station 2			
	Pressure rise(m)	H_R (m)	H_T (m)	Reflection (m)	Pressure rise(m)	H_R (m)	H_T (m)	Reflection (m)
9	7.397	33.303	33.195	0.108	7.493	62.070	61.960	0.110
15	7.382	33.179	32.999	0.180	7.483	61.934	61.751	0.183
21	7.365	33.045	32.795	0.250	7.472	61.787	61.534	0.254
27	7.349	32.891	32.573	0.318	7.460	61.619	61.296	0.323

where H_R = magnitude of the reflected wavefront from the leak and H_T = magnitude of the transmitted wavefront from the leak

The pressure rises acting at stations 1 and 2 reduce marginally as the size of the leak increases and are lower at station 1 because of the effect of friction (station 2 is closer to the transient source than station 1). Nevertheless, the pressure rises are in the range of 7.35m to 7.49m for both stations and are comparable with the pressure rise predicted using the Joukowsky equation (i.e., 7.53m). Unfortunately, for these pressure rises the maximum leak reflection sizes for a discharge of 27 L/s are only 0.318m and 0.323m at stations 1 and 2, respectively. While the pressure rises are slightly lower than the operator imposed limit of 10m, the results indicate that the leak

reflection information that can be induced in pipelines such as the HTP will be relatively weak.

It is important to confirm that the predicted pressure rises are comparable with those observed in the measured responses. Table 9-2 shows the average pressure for 1s prior to and following the induction of the controlled transients for tests 1 (without leakage) and 3 (with the artificial leak). The pressure for test 1 rises by an average of 7.40m (for stations 1 and 2). The pressure for test 3 rises by an average of 7.28m. The pressure rises predicted without and with the leak are of the same order as those predicted using the transient model (they are marginally lower). Discrepancies may be attributed to local variations in friction and mechanical damping effects.

Table 9-2 – Transient overpressures from measured responses for tests 1 and 3

Test No.	Measurement Station 1			Measurement Station 2			Average Pressure Rise (m)
	Steady (m)	Plateau (m)	Pressure Rise (m)	Steady (m)	Plateau (m)	Pressure Rise (m)	
1	25.94	33.32	7.38	54.80	62.21	7.41	7.40
3	25.80	33.06	7.26	54.50	61.80	7.30	7.28

9.1.3 Measured leak reflection from Hanson Transmission Pipeline

Figures 9-3 and 9-4 show the measured leak reflections for test 3 at stations 1 and 2, respectively. The predicted leak reflections, respectively 0.108m and 0.110m, are superimposed for the purpose of comparison. It is apparent that the leak reflections are barely discernable amongst background hydraulic noise. Given the conclusions of Stoianov et al. (2003a), regarding small leak reflections and large diameter pipelines, the result is not unexpected. The results for Covas et al. (2004a) stand in contrast but can be explained by the fact that the pipeline tested was only 300mm in diameter, had a very high static pressure (132m) and was subjected to a pressure rise (13.2m) above the limits determined by both Stoianov et al. (2003a) and in this research.

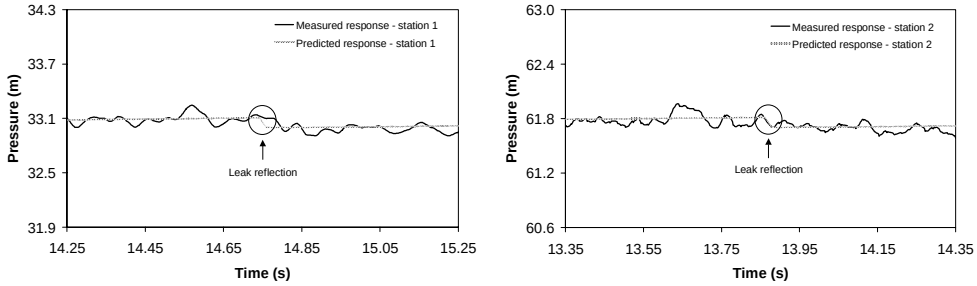

Figures 9-3 and 9-4 – Measured versus predicted leak reflections for test 3, conducted on the HTP, at stations 1 and 2, respectively

Figures 9-5 and 9-6 show the measured and predicted leak reflections in more detail. A marginal fall in the measured response is discernable at the location of the leak. The average pressures for 0.5s prior to and following the time of the leak reflection, for test 3 at station 1, are 33.092m and 32.989m, respectively. This gives an average drop of 0.103m. For station 2, the average pressures are 61.789 and 61.693m giving an average drop of 0.096m. These measurements are inconsistent with the expectation that the measured reflection at station 2, located closer to the transient generator and artificial leak, should be greater than that at station 1.

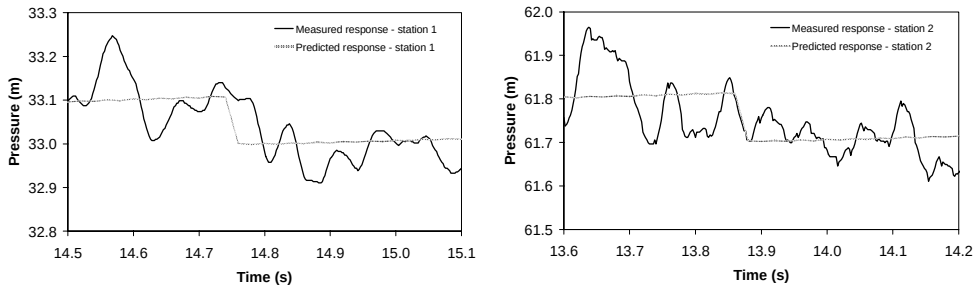

Figures 9-5 and 9-6 – Focus on measured versus predicted leak reflections for test 3, conducted on the HTP, at stations 1 and 2, respectively

The results may indicate that mechanical dispersion and damping near the source of the transient have a disproportionately greater effect. However, it may also be because the reflection recorded at station 2 is obscured, to a greater degree than at station 1, by localised hydraulic noise. The results confirm that, for the size of leak and maximum

permissible pressure rise specified by South Australian system operators, weak leak reflections occur in larger transmission pipelines.

The sources of the hydraulic noise are discussed in Chapter 10 and include flow variability or "flutter" through the nozzle mounted in the transient generator, particularly for the tests conducted in May 2004, interaction of the relatively sharp wavefronts with wall lining (and wall) thickness and other material variations and reflections from the saddle supports and collar restraints (and changes in pipeline profile in elevation and plan). Once the side discharge valve mounted in the transient generator has been closed, the effect of flow variability is greatly reduced leaving reflections from wall lining (and wall) thickness changes and the saddle supports and collar restraints as the main sources of the hydraulic noise. Unfortunately, for leak sizes around the threshold of interest, the measured reflections are within the hydraulic noise band giving a very low signal to noise ratio.

9.2 Problems with wavefront dispersion

9.2.1 Wavefront dispersion and transient models

Traditional transient models, which neglect the effects of unsteady friction and mechanical dispersion and damping (and flexural and shear wave formation) do not account for wavefront dispersion. This problem has not been previously contemplated by researchers investigating hydraulic transient methods for fault detection because of a lack of measured responses from field pipelines. As described in Chapter 7, the measured responses from both the Hanson Transmission Pipeline (HTP) and the Morgan Transmission Pipeline (MTP) exhibit significant dispersion that increases as the induced wavefronts continue propagating within the pipeline. This dispersion will progressively obscure reflection information from any leak along the pipelines.

This problem is distinct from the problem of hydraulic noise obscuring weak leak reflections. In the case of tests 3 and 4, conducted on the HTP, the close proximity of the transient generator, the artificial 9L/s leak and measurement station 2 are such that the hydraulic noise described above has not dispersed at the times the initial leak reflection is recorded at station 2. Furthermore, while the dispersion has increased in

the measured responses observed at station 1 (located approximately 878m to the east of the transient generator), both the hydraulic noise and weak leak reflection remain discernable.

The wavefront dispersion considered in this section increases as the length of pipeline over which the wavefronts travel increases. As shown in Chapter 7, this results in considerable dispersion of the reflected wavefronts from the Hanson summit tanks and closed butterfly valve at "Sheep Dip" that cannot be explained in terms of the inertial effects described by Skalak (1956). Hence, both the hydraulic noise and the weak leak reflections themselves are dispersed and the leaks remain relatively obscured.

Transient models have been developed in Chapter 8 that include unsteady friction and mechanical dispersion and damping. These models have been calibrated to the no-leak responses from the HTP. However, as previously discussed, "viscous" mechanisms only provide for equivalent dispersion and damping. They do not describe the physical behaviour of a pipeline and are unable to replicate the precise structure of the measured responses. Furthermore, while the damping in the measured response is, on average, correctly predicted, the observed dispersion is not accurately approximated over the initial stages of the transient, unless separate long and short term calibrations are performed.

9.2.2 Use of prior information regarding leak size

The use of prior information, in the form of knowledge of the leak discharge, can partially compensate for structural deficiencies in the forward transient models presented in Chapter 8, including an inability to model significant dispersion over the initial stages of a measured transient response as well as over the longer term, and/or low sensitivity leak information.

Prior information regarding leak discharge can be used, during Inverse Transient Analysis (ITA) to fix the size of a leak at each potential leak location. Hence, both the location and the size of the leak are fixed, as each potential leak location is assessed, leaving the determination of the goodness of the fit (i.e., the objective function) as the

only variable. The results presented below, for both short and long term analysis, without and with prior information regarding the leak discharge, have been determined using the quasi-steady friction (QSF), the unsteady friction (UF) and the unsteady friction and "viscous" Hanson pipeline and offtake branch (UFVHOB) models as previously developed and calibrated in Chapter 8.

9.2.3 Use of leak damping information

While the reflections from the artificial 9L/s leak introduced to the Hanson Transmission Pipeline (HTP) are difficult to discern amongst significant hydraulic noise, the long term measured responses nevertheless exhibit significant leak related damping. Figures 9-7 and 9-8 show the numerically estimated effect, over the long term, of 9, 15, 21 and 27L/s leaks at the location of the simulated leak on the HTP, at measurement stations 1 and 2, respectively (the measured responses from the HTP for tests 3 and 4 exhibit similar damping, as shown below, for a 9L/s leak).

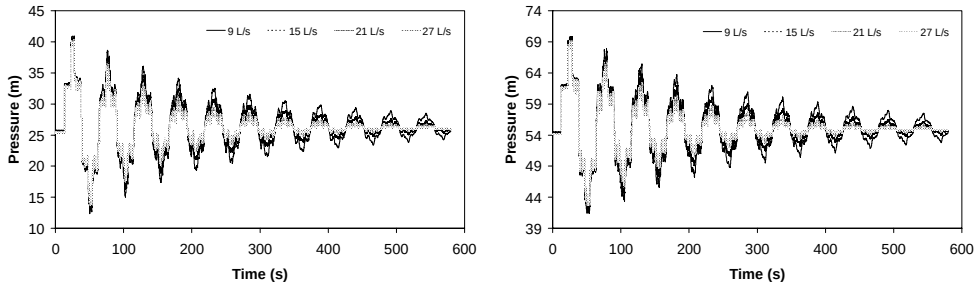

Figures 9-7 and 9-8 – Comparison of leak damping for 9, 15, 21 and 27L/s leaks on HTP, at stations 1 and 2, respectively

The leak damping significantly increases with the size of the leak. Furthermore, the leak damping effect is more significant than the damping associated with unsteady friction and mechanical dispersion and damping. This confirms that important leak damping information is available in the measured responses from the HTP. The challenge, is applying transient response analysis or Inverse Transient Analysis (ITA), to interpret this leak related damping information.

9.3 Leak detection using quasi-steady friction (QSF) model

9.3.1 Results of Inverse Transient Analysis performed over 580s

Given that the quasi-steady friction (QSF) model was only calibrated over the long term (580s), Inverse Transient Analysis (ITA) will only be performed, to locate and size the artificially introduced 9L/s leak, using long term measured responses. Figures 9-9 and 9-10 show the logarithm of the ratios between the objective functions determined for each potential leak location and the minimum objective function obtained when ITA is performed by fixing the leak location at individual nodes along the Hanson Transmission Pipeline (HTP) and then fitting for the optimum leak size, without and with prior information regarding the leak discharge, respectively.

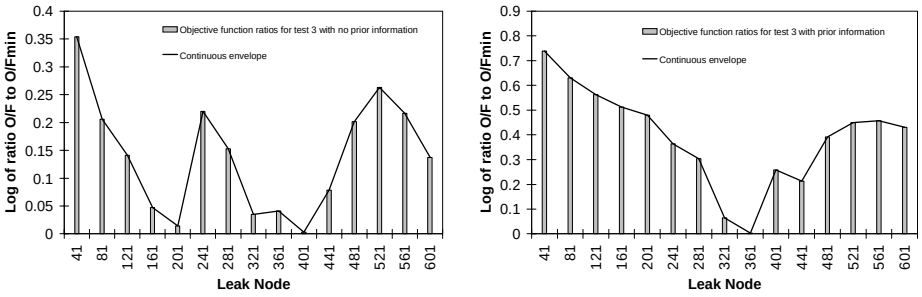

Figures 9-9 and 9-10 – Using the QSF model, calibrated over the long term, to perform long term ITA for test 3, without and with prior information, respectively

Figure 9-9 shows that, without prior information regarding the leak discharge, the minimum objective function is obtained when the leak location is fixed at node 401. The objective function when the leak is fixed at its "true" location (node 441) is ranked 6th from the minimum value for the leak at node 401. There is a significant difference between the fitted leak sizes, at nodes 401 and 441, of 0.000527m^2 and 0.000474m^2, respectively. The fitted leak size at node 441 is closer to the "true" leak size of 0.000295m^2. Figure 9-10 shows that, with prior information regarding the leak discharge, the minimum objective function is obtained when the leak location is fixed at node 361. The objective function when the leak is fixed at its "true" location (node 441) is ranked 3rd from the minimum value. This represents an improvement relative to the results obtained without prior information regarding the leak discharge.

Figures 9-11 and 9-12 show the measured and predicted responses at station 1, over a time scale of 580s, when the leak is located at its "true" position (node 441), and ITA is performed without and with prior information regarding the leak discharge, respectively. Figure 9-11 confirms that the QSF model does not replicate non-leak related dispersion. However, the measured damping is approximated because a leak size of $0.000474m^2$ is erroneously fitted (compared to the "true" leak size of $0.000295m^2$). Figure 9-12 shows that, by fixing the leak size to its "true" value, the measured damping cannot be replicated by inaccurately calibrating for the size of the leak and the structural inadequacy in the QSF model is exposed. This example shows how fitting a parameter (in this case, the size of a leak rather than pipe roughness) can incorrectly compensate for other phenomena affecting a transient response.

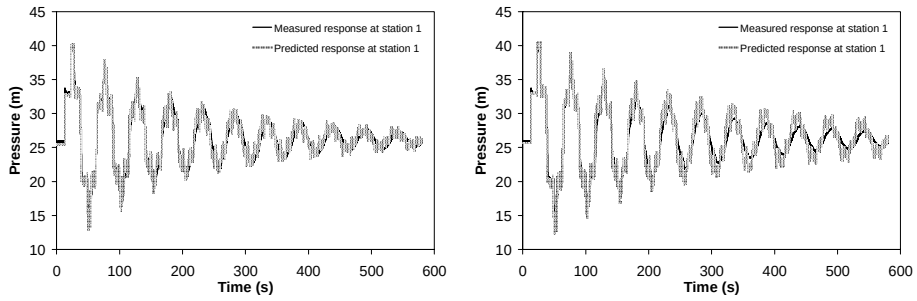

Figures 9-11 and 9-12 – Comparison between measured and predicted responses, over 580s, when ITA is performed without and with prior information, respectively

Figures 9-13 and 9-14 show the measured and predicted responses at station 1, over a time scale of 40s, when the leak is located at its "true" position (node 441), and ITA is performed without and with prior information regarding the leak discharge, respectively. Figure 9-13 shows a discrepancy between the measured and predicted steady state pressures due to the erroneously fitted leak size. Figure 9-14 shows that, by constraining the leak size to its "true" value, the error between the measured and predicted steady state pressures is reduced. Figures 9-13 and 9-14 confirm that the measured and predicted leak reflection information is relatively indistinct in the context of the observed hydraulic noise and dispersion.

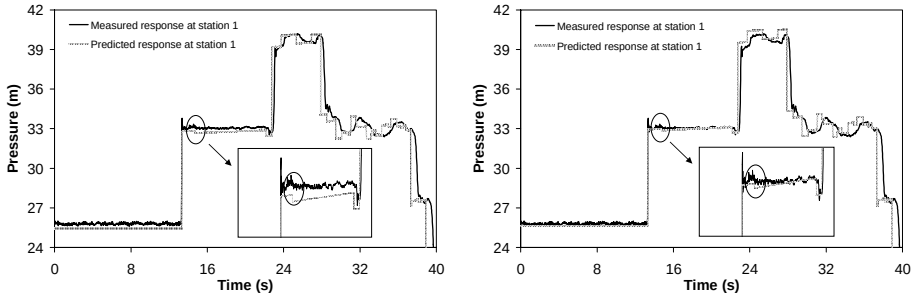

Figures 9-13 and 9-14 – Comparison between measured and predicted responses, over 40s, when ITA is performed without and with prior information, respectively

9.3.2 Regression diagnostics for the QSF model following ITA

Figures 9-15 and 9-16 show the standardised residual plotted against time for Inverse Transient Analysis (ITA) performed without and with prior information regarding the leak discharge. The leak is located at its "true" location (i.e., node 441). Prime facie, the deterioration in the residual error when the prior information is used suggests that the fixed ("true") leak size is incorrect. However, the correct interpretation is that the leak damping should not be used to compensate for the effects of other phenomena and that the quasi-steady friction (QSF) model is structurally inadequate.

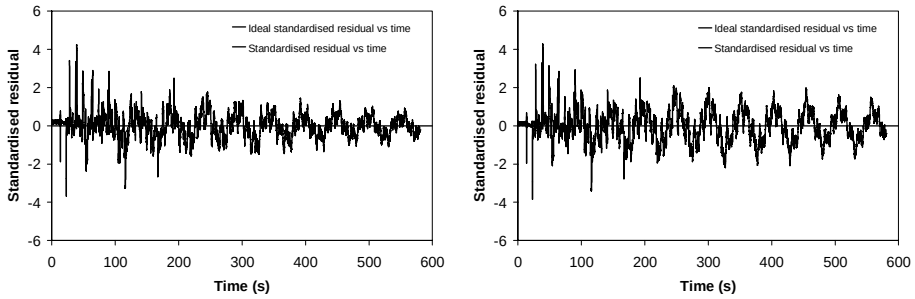

Figures 9-15 and 9-16 – Standardised residual versus time plots for test 3, when using the QSF model, without and with prior information, respectively

9.4 Leak detection using unsteady friction (UF) model

9.4.1 Results of Inverse Transient Analysis performed over 580s

As for the analysis performed using the quasi-steady friction (QSF) model, Inverse Transient Analysis (ITA) will only be performed, using the unsteady friction (UF) model, to locate and size the artificially introduced 9L/s leak using the long term measured responses. Figures 9-17 and 9-18 show the logarithm of the ratios between the objective functions determined for each potential leak location and the minimum objective function obtained when ITA is performed by fixing the leak location at individual nodes along the Hanson Transmission Pipeline (HTP) and then fitting for the optimum leak size, without and with prior information regarding the leak discharge, respectively.

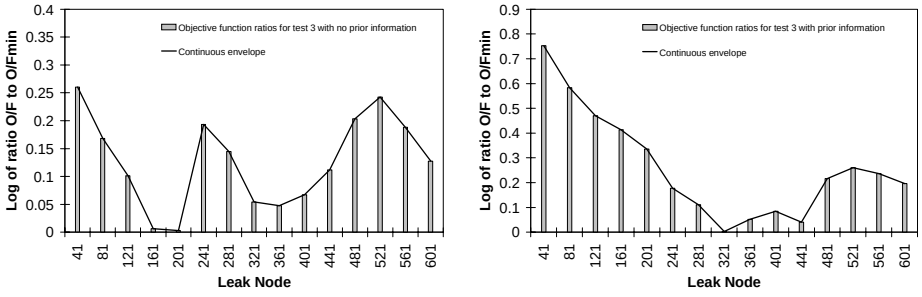

Figures 9-17 and 9-18 – Using the UF model, calibrated over the long term, to perform long term ITA for test 3, without and with prior information, respectively

Figure 9-17 shows that, without prior information regarding the leak discharge, the minimum objective function is obtained when the leak location is fixed at node 201. The objective function when the leak is fixed at its "true" location (node 441) is ranked 7th from the minimum value for the leak at node 201. This represents a deterioration relative to the results obtained using the QSF model. There is a significant difference between the fitted leak sizes, at nodes 201 and 441, of 0.000777m^2 and 0.000333m^2, respectively. The fitted leak size at node 441 is relatively close to the "true" leak size of 0.000295m^2. Figure 9-18 shows that, with prior information regarding the leak discharge, the minimum objective function is obtained when the leak location is fixed at node 321. The objective function when the

leak is fixed at its "true" location (node 441) is ranked 2rd from the minimum value. This represents an improvement relative to the results obtained without prior information regarding the leak discharge and to those obtained using the QSF model.

9.4.2 Regression diagnostics for the UF model following ITA

Figures 9-19 and 9-20 show the standardised residual plotted against time for Inverse Transient Analysis (ITA) performed without and with prior information regarding the leak discharge. The leak is located at its "true" location (i.e., node 441). In contrast to the results obtained using the quasi-steady friction (QSF) model (presented for comparison), the cyclical error apparent in the residual reduces with increasing time regardless of whether prior information regarding the leak size is used. Furthermore, there is only a marginal difference between the residual obtained without and with prior information. This is a consequence of the similarity between the fitted and "true" leak sizes specified above.

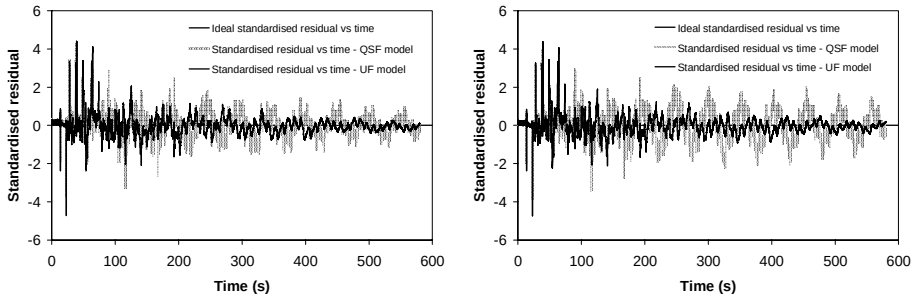

Figures 9-19 and 9-20 – Standardised residual versus time plots for test 3, when using the UF model, without and with prior information, respectively

9.5 Leak detection using "viscous" UFVHOB model

9.5.1 Results of Inverse Transient Analysis performed over 580s

As for the Inverse Transient Analysis (ITA) performed using the quasi-steady friction (QSF) and unsteady friction (UF) models, ITA will be performed, using the unsteady friction and "viscous" Hanson pipeline and offtake branch (UFVHOB) model, to locate and size the artificially introduced 9L/s leak using the long term measured

responses. Figures 9-21 and 9-22 show the logarithm of the ratios between the objective functions determined for each potential leak location and the minimum objective function obtained when ITA is performed by fixing the leak location at individual nodes along the Hanson Transmission Pipeline (HTP) and then fitting for the optimum leak size, without and with prior information regarding the leak discharge, respectively.

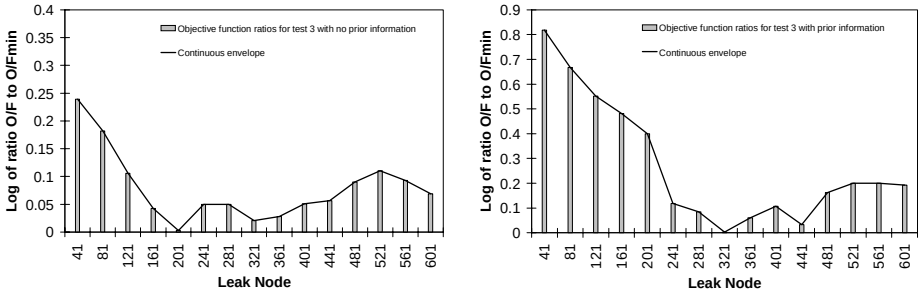

Figures 9-21 and 9-22 – Using the UFVHOB model, calibrated over the long term, to perform long term ITA for test 3, without and with prior information, respectively

Figure 9-21 shows that, without prior information regarding the leak discharge, the minimum objective function is obtained when the leak location is fixed at node 201. The objective function when the leak is fixed at its "true" location (node 441) is ranked 8th from the minimum value for the leak at node 201. This represents a deterioration relative to the results obtained using the QSF and UF models. There is a significant difference between the fitted leak sizes, at nodes 201 and 441, of 0.000768m^2 and 0.000328m^2, respectively. The fitted leak size at node 441 is relatively close to the "true" leak size of 0.000295m^2. Figure 9-22 shows that, with prior information regarding the leak discharge, the minimum objective function is obtained when the leak location is fixed at node 321. The objective function when the leak is fixed at its "true" location (node 441) is ranked 2rd from the minimum value.

Figure 9-23 shows the measured and predicted responses at station 1, over a time scale of 580s, when the leak is located at its "true" position (node 441), and ITA is performed without prior information regarding the leak discharge. The measured response is best replicated when an erroneous leak size of 0.000328m^2 is fitted

(compared to the "true" leak size of 0.000295m^2). As for the results obtained using the QSF model, this indicates that the fitted leak size is acting to compensate for non-leak related damping.

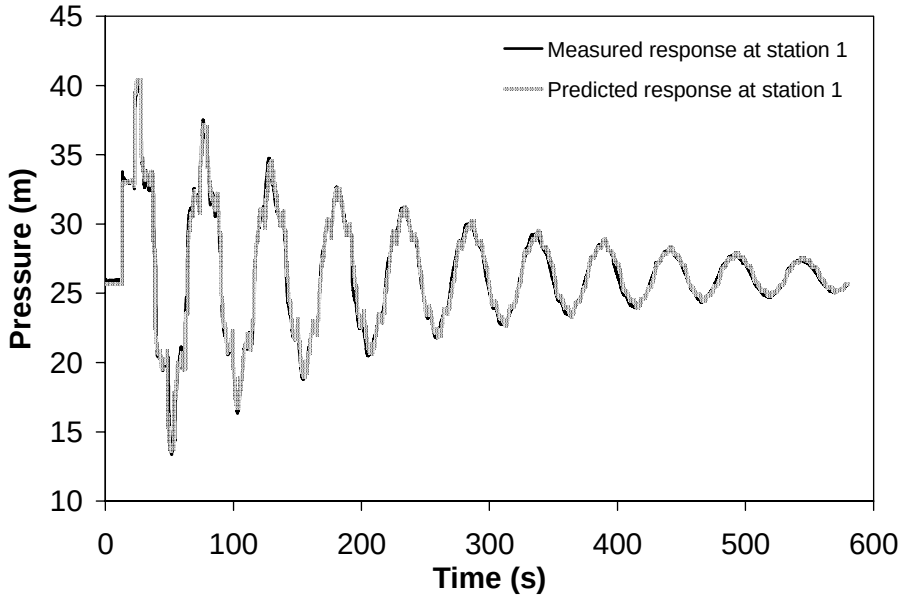

Figure 9-23 – Comparison between measured and predicted responses, over 580s, when the leak is located at node 441, and ITA is performed without prior information

9.5.2 Regression diagnostics for the UFVHOB model following ITA

Figures 9-24 and 9-25 show the standardised residual plotted against time for Inverse Transient Analysis (ITA) performed without and with prior information regarding the leak discharge. The leak is located at its "true" location (i.e., node 441). A marginal reduction in the residuals is apparent relative to the results obtained using the unsteady friction (UF) model (presented for comparison). However, a cyclical error persists in the residuals regardless of whether prior information regarding the leak size is used. Furthermore, there is only a marginal difference between the residual obtained without and with prior information. Unfortunately, the cyclical residual is significant and is related to the inability of the unsteady friction and "viscous" Hanson pipeline and offtake branch (UFVHOB) model to replicate the dispersion and damping over the later stages of the transient responses with sufficient accuracy. This

inaccuracy is critical in the context of accessing the leak damping information in the context of Inverse Transient Analysis (ITA).

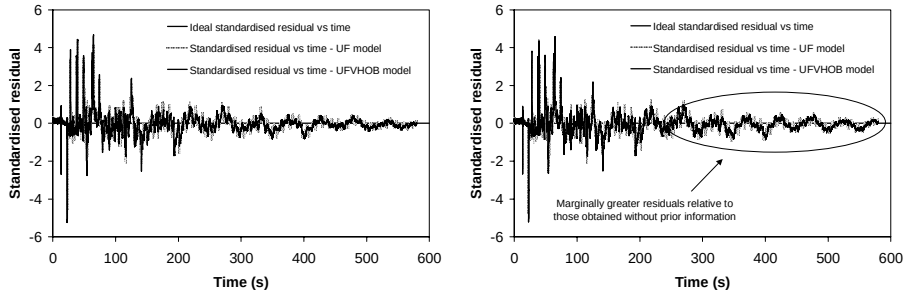

Figures 9-24 and 9-25 – Standardised residual versus time plots for test 3, when using the UFVHOB model, without and with prior information, respectively

9.6 Using UFVHOB model over a period of 2L/a seconds

9.6.1 Results of ITA performed over 2L/a seconds

Based on the model calibration performed in Chapter 8, it is known that the unsteady friction and "viscous" Hanson pipeline and offtake branch (UFVHOB) model, calibrated over the long term, does not approximate the dispersion of the measured responses, particularly over their initial stages, as accurately as when calibration is performed over the short term. Inverse Transient Analysis (ITA) will therefore be performed, using the UFVHOB model calibrated over the short term, to locate and size the artificially introduced leak using 2L/a seconds (38.1s) of the measured responses. Figures 9-26 and 9-27 show the logarithm of the ratios between the objective functions determined for each potential leak location and the minimum objective function obtained when ITA is performed by fixing the leak location at individual nodes along the Hanson Transmission Pipeline (HTP) and then fitting for the optimum leak size, without and with prior information regarding the leak discharge, respectively.

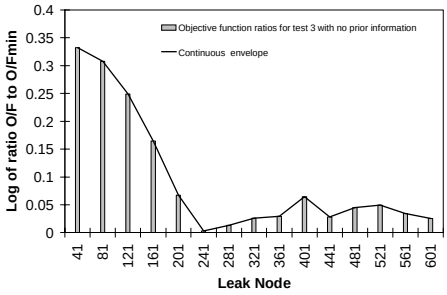

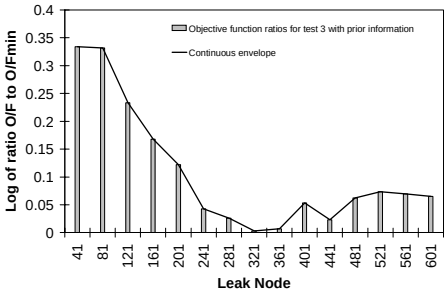

Figures 9-26 and 9-27 – Using the UFVHOB model, calibrated over the short term, to perform short term ITA for test 3, without and with prior information, respectively

Figure 9-26 shows that, without prior information regarding the leak discharge, the minimum objective function is obtained when the leak location is fixed at node 241. The objective function when the leak is fixed at its "true" location (node 441) is ranked 5th from the minimum value for the leak at node 241. This represents a significant improvement relative to the results obtained when long term ITA was performed using the UFVHOB model. However, a significant difference persists between the fitted leak sizes, at nodes 241 and 441, of 0.000649m^2 and 0.000365m^2, respectively. The fitted leak size at node 441 is closer to the "true" leak size of 0.000295m^2. Figure 9-27 shows that, with prior information regarding the leak discharge, the minimum objective function is obtained when the leak location is fixed at node 321. The objective function when the leak is fixed at its "true" location (node 441) is ranked 3rd from the minimum value. This is a deterioration relative to the result obtained using the UFVHOB model calibrated over the long term.

Figure 9-28 shows the measured and predicted responses at station 1, over a time scale of 2L/a seconds (38.1s), when the leak is located at its "true" position (node 441), and ITA is performed, over the short term, without prior information regarding the leak discharge. The measured response is best replicated when an erroneous leak size of 0.000365m^2 is fitted (based on objective function minimisation). The inset shows that this erroneously fitted leak size results in an inaccurate offset of the predicted steady state pressure and initial transient plateau below the measured pressures. As for the long term ITA, the fitted leak size is compensating for non-leak related uncertainties rather than giving a more accurate estimate of the leak size.

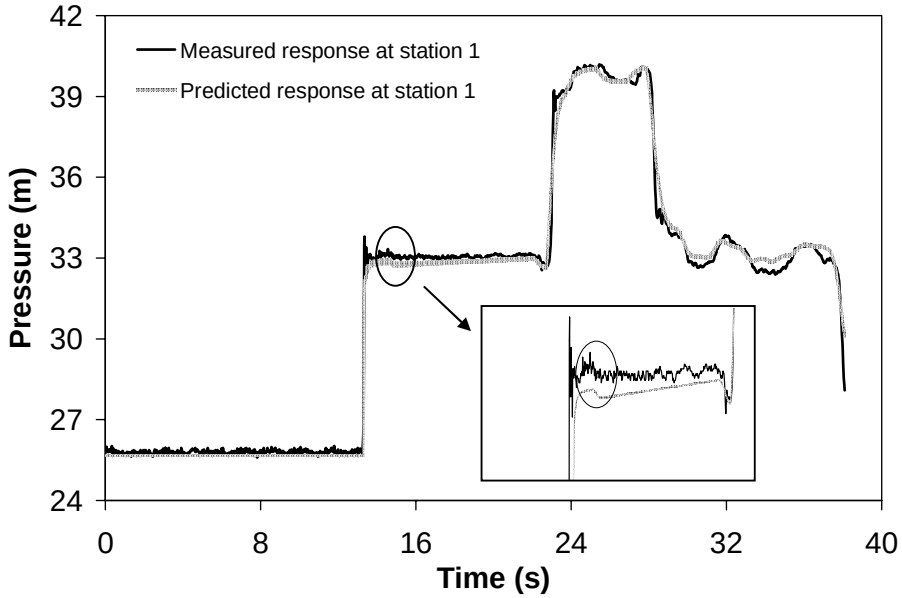

Figure 9-28 – Measured and predicted responses, over 40s, when the leak is located at node 441, and ITA is performed over the short term, without prior information

While the magnitude of the measured and predicted incident transient wavefront and reflections from the closed in-line valve and tanks compare reasonably, the discrepancy between the observed and predicted responses, caused by the inability of the UFVHOB model to replicate the measured dispersion, even when calibrated over the short term, is evident. More importantly, the weakness of the leak reflection along the transient plateau, and difficulty in discerning it amongst hydraulic noise, is also evident. Given the weakness of the reflection information, and the combined effects of hydraulic noise and neglected dispersion, it is not surprising that ITA, performed over the short term without prior information regarding the leak discharge, failed to either correctly locate or size the leak.

9.6.2 Regression diagnostics following short term ITA

Figure 9-29 shows the standardised residual plotted against time for Inverse Transient Analysis (ITA) performed, using the unsteady friction and “viscous” Hanson pipeline and offtake branch (UFVHOB) model calibrated over the short term, without prior

information regarding the leak discharge. The leak is located at its "true" location (i.e., node 441). The discrepancies between the measured and predicted responses, evident for the quasi-steady friction (QSF) and unsteady friction (UF) models, have been reduced.

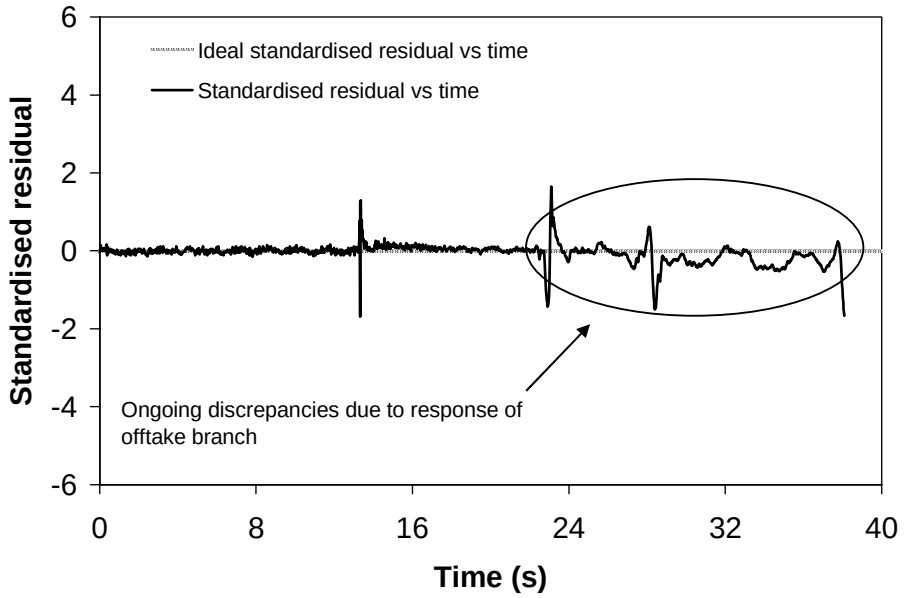

Figure 9-29 – Standardised residual versus time plot, for ITA over 2L/a seconds using the UFVHOB model, calibrated over the short term, without prior information

9.7 Summary of problems affecting ITA for leak detection

Table 9-3 summarises the results of the Inverse Transient Analysis (ITA) performed over the long term (i.e., 580s) using the quasi-steady friction (QSF), the unsteady friction (UF) and the unsteady friction and "viscous" Hanson pipeline and offtake branch (UFVHOB) models. Erroneous leak locations and sizes are determined, without any prior information regarding the leak discharge, using the QSF, UF and UFVHOB models. Erroneous leak locations are determined, when the leak size is fixed using prior information regarding the leak discharge, using all three models. Furthermore, the objective function does not minimise when the leak is fixed at its "true" location and its size is determined without and with prior information regarding the correct leak discharge.

Table 9-3 – Comparison of results when ITA is performed over the long term

Model	Calibration	Without prior information			With prior information		
		Leak node/location	Rank	Size (m^2)	Leak node/location	Rank	Size (m^2)
QSF	Long term	401/8440m	1	0.000527	361/7596m	1	0.000295
QSF	Long term	441/9284m	6	0.000474	441/9284m	3	0.000295
UF	Long term	201/4220m	1	0.000777	321/6752m	1	0.000295
UF	Long term	441/9284m	7	0.000333	441/9284m	2	0.000295
UFVHOB	Long term	201/4220m	1	0.000768	321/6752m	1	0.000295
UFVHOB	Long term	441/9284m	8	0.000328	441/9284m	2	0.000295

* true leak location taken as node 441 (CH 9284m) approximately equal to actual location at CH 9290m

Table 9-4 summarises the results of the ITA performed over the short term (i.e., 2L/a seconds) using the UFVHOB model (calibrated to short term no-leak measured responses). As for the ITA performed over the long term using a long term calibration, an erroneous leak location and size is determined without any prior information regarding the leak discharge. An erroneous leak location is determined when the leak size is fixed using prior information regarding the leak discharge. The objective function does not minimise when the leak is fixed at its "true" location and its size is determined without and with prior information regarding the correct leak discharge.

Table 9-4 – Comparison of results when ITA is performed over the short term

Model	Calibration	Without prior information			With prior information		
		Leak node/location	Rank	Size (m^2)	Leak node/location	Rank	Size (m^2)
UFVHOB	Short term	241/4220m	1	0.000649	321/6752m	1	0.000295
UFVHOB	Short term	441/9284m	5	0.000365	441/9284m	3	0.000295

* true leak location taken as node 441 (CH 9284m) approximately equal to actual location at CH 9290m

9.7.1 Weak leak reflection information and hydraulic noise

As noted previously, the magnitude of the theoretically anticipated leak reflection, neglecting friction, was approximately 0.24m. The inclusion of friction in a numerical

transient model led to a reduction in the anticipated leak reflection to approximately 0.110m at station 2 (closest to the transient generator). The measured leak reflection was approximately 0.096m at station 2. The reduction in the size of the numerically predicted leak when unsteady friction is included in the numerical transient model suggests that the effect of friction is significant and should not be ignored. The residual difference between the size of the leak reflection predicted with unsteady friction and the measured leak reflection suggests that additional phenomena, thought to be related to mechanical dispersion and damping, may be further reducing the size of the leak reflections.

The measured leak reflections are small and difficult to discern amongst significant hydraulic noise. This hydraulic noise is thought to derive from a combination of the effects of flow variability and mechanical motion and vibrations and/or reflections from changes to the pipeline walls. As a consequence, the signal to noise ratio for the leak to hydraulic noise is low and the latter acts to confound the optimisation of the leak location and size when performing Inverse Transient Analysis (ITA). The ITA becomes reliant upon low sensitivity steady state pressure information.

9.7.2 Effect of wavefront dispersion on damping information

Considerable dispersion of the measured wavefronts propagating along the Hanson Transmission Pipeline (HTP) was observed for no-leak as well as leak tests. Furthermore, the magnitude of the dispersion observed for all four tests was similar suggesting that the dispersion was not leak related. It was hoped that the leak damping information in the measured responses could be used to locate and size the artificial 9L/s leak introduced to the HTP if non-leak related sources of dispersion and damping could be accounted for with sufficient accuracy using calibrated quasi-steady friction (QSF), unsteady friction (UF) and unsteady friction and “viscous” Hanson pipeline and offtake branch (UFVHOB) models.

While discrepancies in the replication of the no-leak measured response were reduced significantly by the implementation of unsteady friction, and to a lesser degree, calibration for mechanical dispersion and damping, the calibrated forward transient models were not sufficiently accurate to enable the isolation of differences in leak

damping related to different potential leak locations. This confirms that while the effect of leak damping on a transient is significant, and will vary with the size of the leak, there are many non-unique combinations of leak location and size that will give rise to the same or similar damping effect. Uncertainties in pipeline roughness (or friction effects) and the extent of mechanical dispersion and damping may prevent the successful isolation of the damping effect of a particular leak (e.g., the 9L/s artificial leak introduced to the HTP).

9.7.3 Use of prior information regarding leak discharge

Flowmeter records are often available for transmission pipelines (as they were for the Hanson Transmission Pipeline (HTP)). The use of these records as prior information regarding the magnitude of the leak discharge significantly constrained the solution space during Inverse Transient Analysis (ITA) such that the identification of the "true" leak was significantly improved despite the weakness of the leak reflection information and the dispersion of leak damping information. That said, the use of prior information regarding the leak size is a very significant concession in terms of the potential for ITA for leak detection. In practical terms, South Australian Water Corporation operators would have been able to identify the presence of the leak by examining the flowmeter records and then visually inspecting the HTP.

9.8 Blockage detection in the Morgan Transmission Pipeline

In the case of transient response analysis and/or Inverse Transient Analysis (ITA) for leak detection, South Australian Water Corporation operators were consulted to determine the threshold size of interest for leak detection using hydraulic transients. Field tests on the Hanson Transmission Pipeline (HTP) were then conducted to determine whether leaks near the threshold of interest could, in fact, be successfully located and sized. It is tempting to trivialise the inverse problem, particularly during the early stages of the transfer of techniques using hydraulic transients for fault detection to the field, by introducing a severe fault to a pipeline. The effect is that problems afflicting transient model accuracy become less significant as the signal to hydraulic noise ratio is increased.

The introduction of a discrete blockage to the Morgan Transmission Pipeline (MTP), as described in Chapter 6, demonstrates how a severe fault is easier to detect using transient response analysis and/or ITA. As reported in Chapter 7, transient field tests were conducted with in-line gate valve "No.3" along the MTP closed 54 of 58 turns. This left an open aperture with an equivalent orifice diameter of approximately 50mm. In a pumped transmission pipeline, such as the MTP, a blockage of this severity would become immediately apparent and could not form gradually. It is difficult to envisage the circumstances under which such a blockage might form and fortunately one never has along the MTP. As a consequence, the simulation of a discrete blockage of the severity described above was considered unrealistic.

Figures 9-30 and 9-31 show the comparison between the measured and predicted response of the MTP, over relatively short time periods, with a 50mm equivalent diameter in-line orifice located at in-line valve "No.3", at stations 1 and 2, respectively. A relatively strong reflection (approximately 2.5m as recorded at station 1) is apparent because of the severity of the discrete blockage, and this reflection is far greater than the magnitude of the hydraulic noise band. As a consequence, the location and size of the discrete blockage are obvious and can be replicated with little effort by simply conducting trial and error modelling with different blockage locations and sizes. Figure 9-31 shows that the corresponding transmitted wavefront can also be relatively easily modelled.

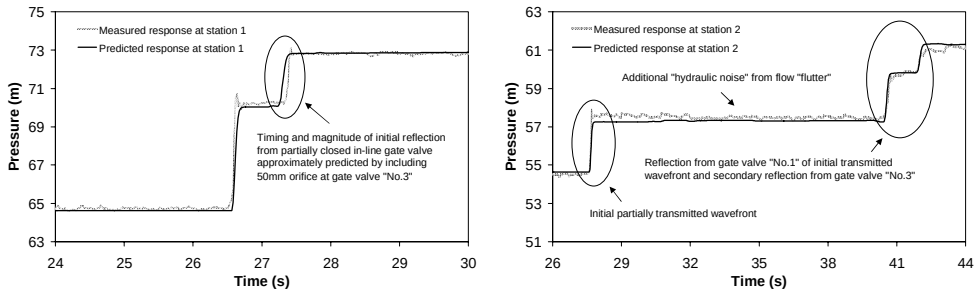

Figures 9-30 and 9-31 – Measured and predicted reflected and transmitted wavefronts, from a discrete blockage, at stations 1 (over 6s) and 2 (over 18s), respectively

Figures 9-32 and 9-33 show the comparison between the measured and predicted response of the MTP, over a longer time period of 540s, with a 50mm equivalent diameter in-line orifice located at in-line valve "No.3", at stations 1 and 2, respectively. It is apparent that the severity of the discrete blockage gives rise to a significant damping effect upon the measured and predicted responses of the MTP and a distinct secondary oscillation.

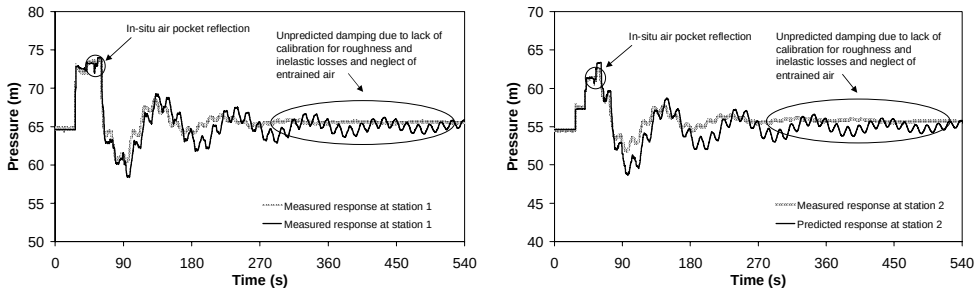

Figures 9-32 and 9-33 – Measured and predicted reflected and transmitted waveforms, from a discrete blockage, at stations 1 and 2, respectively (over 540s)

While the blockage induced damping and secondary oscillation is dominant, a discrepancy, exists between the measured and predicted damping and waveforms. This is probably due to the effect of friction losses (pipeline roughness) and mechanical dispersion and damping that have not been calibrated to no-blockage responses (and possibly the presence of a small percentage of entrained air). Nevertheless, the damping and secondary oscillation due to the presence of the blockage are obvious and have been reasonably replicated, with no calibration effort, by conducting trial and error modelling with different blockage locations and sizes. The same blockage location and size gives the best fit over the short and long term response of the MTP.

9.9 Summary

The size of the reflections from a range of leaks have been numerically assessed in this chapter, for large transmission pipelines, and compared with the size of the measured reflection from an artificial 9L/s leak introduced to the Hanson Transmission Pipeline (HTP). It was found, by comparing results obtained using a

frictionless reflection formulation and a forward transient model including unsteady friction, that the effect of friction, and, to a lesser extent, mechanical dispersion and damping, significantly reduce the size of leak reflections. The measured reflection from the 9L/s leak was of the order of 0.1m and difficult to discern amongst background hydraulic noise. Furthermore, significant dispersion of the leak reflected wavefront reduced the effective interpretation of reflection and damping information from the 9L/s leak.

The quasi-steady friction (QSF), unsteady friction (UF) and unsteady friction and "viscous" Hanson pipeline and offtake branch (UFVHOB) models, developed and calibrated in Chapter 8, have been used to perform Inverse Transient Analysis (ITA) for leak detection. Furthermore, regression diagnostics, including, in particular, standardised residual versus time plots, were used to assess the performance of each forward transient model. ITA was performed over both the long and short term, using the UFVHOB model, to assess the sensitivity of the results to the length of measured response and to the proportion of reflection versus damping information. The QSF model performed least well, in terms of correctly identifying the 9L/s leak, while the UFVHOB model gave the best results. However, none of the proposed models correctly identified the leak location or size. The use of prior information regarding the leak discharge was proposed to compensate for the weakness of the direct leak reflection and dispersion of reflection and damping information. This improved the results of the ITA but the leak location and size were still not correctly identified.

The QSF and UF models were expected to perform less well given neglected mechanical dispersion and damping. The UFVHOB model, although incorporating a calibrated "viscous" mechanism, only provided for equivalent dispersion and damping and did not accurately replicate the hydraulic noise and wavefront dispersion obscuring the leak reflection information. The weakness of the leak reflection, relative to background hydraulic noise, and the dispersion of leak reflection and damping information were identified as the main reasons for the failure of the ITA.

If leak reflections in or near the band of hydraulic noise identified in this study are to be used to successfully perform ITA then a more comprehensive understanding of the phenomena contributing to the hydraulic noise is required. The mechanisms calibrated

to replicate mechanical dispersion and damping make an “on-average” correction and do not replicate the actual physical mechanisms at work (e.g., at individual restraints). As a consequence, the calibrated quasi-steady friction (QSF), unsteady friction (UF) and unsteady friction and “viscous” Hanson pipeline and offtake branch (UFVHOB) models do not replicate the microstructure response over, in particular, the initial stages of the measured transient responses. The microstructure response of the Morgan Transmission Pipeline (MTP) will be examined in Chapter 10 to determine whether variations in the condition of the pipeline wall help to explain the hydraulic noise observed in the measured responses.

Another interesting reality is that the closer the leak is to the source of the induced transient, the more significant will be the effect of obscuring hydraulic noise from, in particular, mechanical motion and vibration. However, the further the leak is from the source of the induced transient, the more significant will be the effect of progressive dispersion which, unfortunately, also has the effect of obscuring the leak reflection by broadening its associated wavefront. While the way in which the leak reflection is obscured by hydraulic noise and dispersion differ, the common effect is to decrease the accessibility of the leak reflection information in the measured response. This insight is critical to the design of future field investigations seeking to develop methods for leak detection using hydraulic transients.

Chapter10

Wall Condition Assessment for Transmission Mains Using Transients

---

The results presented in Chapter 9 identify hydraulic noise that cannot be explained using either a complex forward transient model, incorporating unsteady friction, entrained air and fluid structure interaction effects, or a conceptual model based on the calibration of a "viscous" mechanism to approximate equivalent mechanical dispersion and damping. This hydraulic noise is a significant problem if transient response analysis and Inverse Transient Analysis (ITA) are to be used to identify specific faults along transmission pipelines. Furthermore, it is not known whether the hydraulic noise is associated with mechanical motion and vibration, or if there is some other physical explanation, or a combination of both.

Misiunas et al. (2005) hypothesised that there was a correlation between an increase in the standard deviation of the measured pressure response of the Morgan Transmission Pipeline (MTP) and sections of pipe along which there was internal damage. Specifically, the standard deviation of the measured pressure response following the induction of a transient was determined, along 1km sections of the MTP, and relative levels of hydraulic noise were reported. Misiunas (2005) suggested that the oscillations were caused by reflections from deposits of internal lining material built-up along the bottom of the MTP.

The hypothesis that a significant proportion of the hydraulic noise observed in the measured transient responses is related to reflections from changes in lining and pipe wall thickness, along the Hanson Transmission Pipeline (HTP) and, in particular, the Morgan Transmission Pipeline (MTP), is presented in this chapter and, while different from the explanation offered by Misiunas et al. (2005), derives from the same physical observations. The hypothesis is developed in this chapter by applying

forward transient models to investigate the effect of entrained air, discrete air pockets, reflections from minor loss elements and, finally, changes in the thickness of cement mortar lining and metal wall thickness along the MTP. The intention is to systematically eliminate alternate physical explanations and confirm the hypothesis that there is a correlation between the hydraulic noise and the internal condition of the wall of the MTP. In this regard, it has already been demonstrated, in Chapter 8, that the inertial effects of a pipeline, as formulated in the equations presented by Skalak (1956), do not explain the hydraulic noise in the transient responses of the pipelines. This analysis is not repeated in this chapter.

10.1 Characteristics of observed hydraulic noise

10.1.1 Hydraulic noise in measured responses from pipelines

The measurements reported by Stoianov et al. (2003a) appear to have contained hydraulic noise (not instrumentation noise) making it difficult to identify leak reflections of a size less than approximately 0.25m. A similar level of hydraulic noise, recorded both before and over the initial period after the induction of controlled transients, was observed for the field tests conducted on the Hanson Transmission Pipeline (HTP) and Morgan Transmission Pipeline (MTP) in May 2004. For the tests conducted on the MTP in August 2004, the noise was largely restricted to the period after the induction of the controlled transients.

Figure 10-1 shows the measured response of the MTP for test 9 conducted on the 11th August 2004. Distinct line packing is evident (i.e., a positive slope along the initial transient plateau). This suggests that the MTP has a significant average roughness and this is consistent with the information obtained from the CCTV camera logs (see below). The insets in Figure 10-1 are magnified approximately 5 times and each plotted at the same scale. Inset 1 shows that the degree of noise prior to the induction of the transient event is not significant because of the use of a new nozzle with a discharge coefficient of approximately 0.9 (and the minimisation of flow variability or "flutter" through the nozzle). Inset 2 shows a level of hydraulic noise after the induction of the transient that may, if other physical explanations are eliminated, be

related to the interaction of transient wavefronts with wall lining (and wall) thickness and other material variations, saddle supports and collar restraints, in-line valves and cross-connections. Inset 3 shows that by the time reflections from the closed in-line valve "No.1" and the tanks have arrived, the hydraulic noise has dissipated leaving a relatively smooth response.

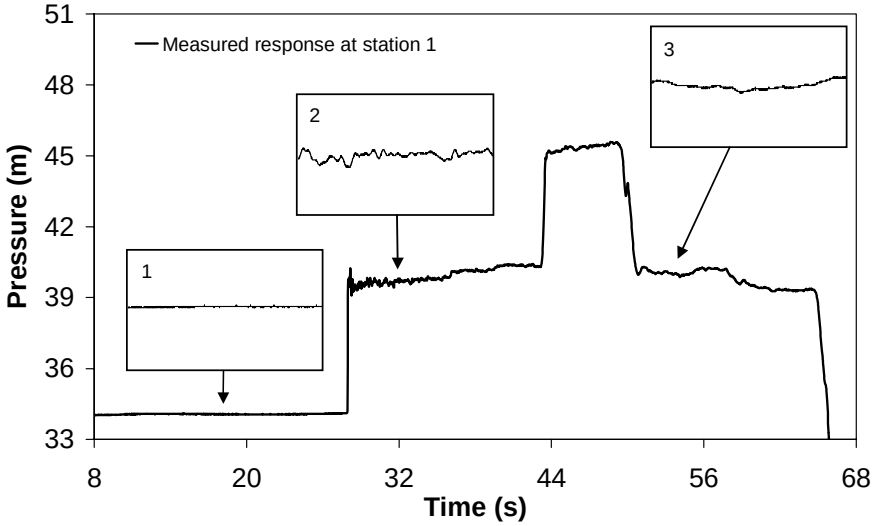

Figure 10-1 – Detailed views of hydraulic noise variation for test 9, conducted on the 11th August 2004, before and during the transient event induced in the MTP

10.1.2 Structured reflections in observed hydraulic noise

Figure 10-2 focuses in detail on the measured responses after the initiation of the transient event for tests 7, 8 and 9, conducted in August 2004, and reveals that the hydraulic noise is not random. In fact, almost identical structure is observed in the measured responses for each test despite in-line gate valves "No.1", "No.2" and "No.3" being closed to form downstream boundary conditions, respectively. Flow variation or "flutter" is relatively insignificant prior to the initiation of the transient and negligible following the initiation of the transient with no other discharges from the Morgan Transmission Pipeline (MTP). Furthermore, dispersion from flexural and shear wave formation is not significant over the early stages of the measured response. This leaves mechanical motion and vibration, and reflections from changes

to the lining and wall thickness along the MTP, as the likely causes of the structured hydraulic noise observed in the measured responses.

That said, Fluid Structure Interaction (FSI), related to pipeline inertia and precursor wave formation, does not account for the observed pattern of reflections (as explained in Chapter 7). This does not preclude other effects from mechanical motion and vibration and, in particular, flexural wave formation. Indeed, measurements taken subsequent to the research reported in this thesis, presented by way of example in Chapter 7, have confirmed inertial effects and structural accelerations and displacements in lateral (horizontal), vertical and axial directions. However, the structural oscillations are relatively small and do not contribute to significant dispersion over the first few seconds of the measured responses. Furthermore, the structural accelerations and displacements are dispersive and do not generate reflections in the measured pressure responses.

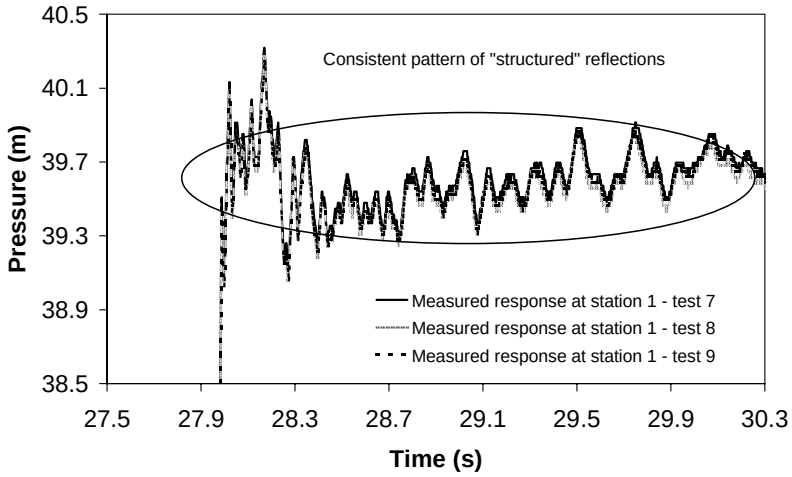

Figure 10-2 – Consistent pattern of structured reflections for tests 7, 8 and 9 conducted on the Morgan Transmission Pipeline in August 2004

10.2 Internal condition of the Morgan Transmission Pipeline

CCTV camera footage of sections of the Morgan Transmission Pipeline (MTP) was made available by the South Australian Water Corporation and used to determine the average pipeline roughness over the sections to which the footage relates. The log of

lining and wall damage, between chainages 15000m and 15400m, is presented below, and is of particular interest because this section is in close proximity to the location of the transient generator (chainage 15709m) and measurement station 1 (chainage 15627m) for the tests conducted in August 2004. As a consequence, the measured response at station 1, including reflections from features within and along the MTP, is relatively unaffected by dispersion. Figure 10-3 shows the relative positions of the transient generator, measurement stations 1 and 2, and the surveyed section of the MTP.

CCTV camera footage was also available for the section of the MTP between chainage 17200m and chainage 17700m and a log for this section is presented in Appendix N. Furthermore, CCTV camera investigation was conducted between chainage 16000m and chainage 16400m. Unfortunately, the South Australian Water Corporation could not make this footage available at the time of enquiry by the author. That said, the South Australian Water Corporation officers confirmed that there was insignificant damage along this section of the MTP.

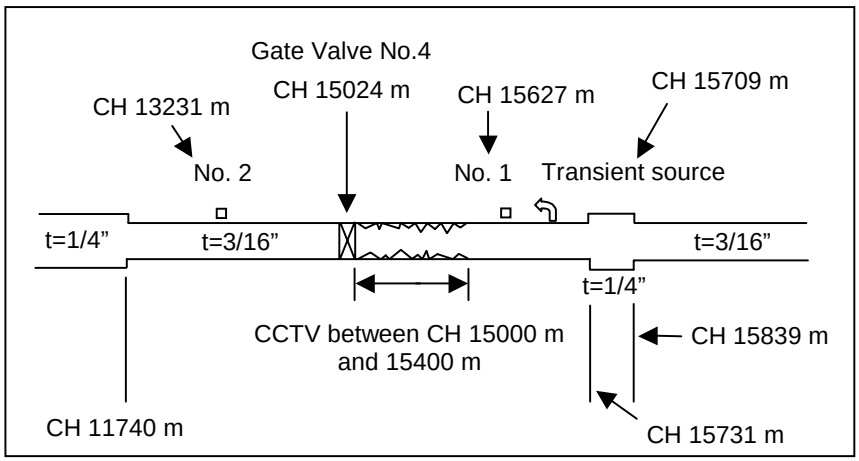

Figure 10-3 – Close proximity of damaged section of pipeline to transient generator and measurement station 1

A summary of the damage to the pipeline, as derived from the logs of the CCTV camera footage between chainages 15000m and 15400m, with the accumulation of

pieces of cement lining, delamination and the presence of corrosion surmised every 10m, is presented in Table 10-1. At particular locations, a direct estimate of the area of exposed wall steel was made and a total of 28.3m^2 of lining had been lost along the 400m of the MTP surveyed. Figures 10-4 and 10-5 show typical damage to the cement lining and wall steel along the MTP between chainages 15000m and 15400m. Figure 10-4 shows delamination and corrosion of exposed steel along a 4m section of pipeline. Figure 10-5 shows the same section and a collection of pieces of cement lining in the bottom of the pipeline.

Table 10-1 – Summary of log of CCTV camera investigation for the Morgan Transmission Pipeline between chainage 15000m and 15400m

Chainage (m)	Damage classification	Exposed steel (m^2)	Roughness (mm)	Chainage	Damage classification	Exposed steel (m^2)	Roughness (mm)
15000	Nil	0	1	15210	Nil	0	1
15010	Nil	0	1	15220	**P+D**	0.1	8
15020	**P+D**	0.2	8	15230	Nil	0	1
15030	Nil	0	1	15240	Nil	0	1
15040	Nil	0	1	15250	Nil	0	1
15050	Nil	0	1	15260	**P+D**	0.6	8
15060	Nil	0	1	15270	**P+D+R**	4.7	8
15070	**P+D+R**	6.0	8	15280	**P+D+R**	12.2	8
15080	Nil	0	1	15290	**P+R**	0.7	8
15090	Nil	0	1	15300	Nil	0	1
15100	**P+R**	0.1	6	15310	Nil	0	1
15110	**P**	0	2	15320	Nil	0	1
15120	Nil	0	1	15330	**P+D**	0.5	8
15130	**P**	0	2	15340	**P+R**	0.2	8
15140	Nil	0	1	15350	Nil	0	1
15150	**P+R**	0.2	8	15360	**P+D**	0.1	6
15160	**P+D+R**	0.6	8	15370	Nil	0	1
15170	Nil	0	1	15380	Nil	0	1
15180	**P**	0	2	15390	**P+D**	0.6	8
15190	Nil	0	1	15400	**P+D+R**	1.5	8
15200	Nil	0	1	**Average**			**3.5mm**

where P, D and R represent pieces of cement mortar lining (protrusions), delamination of the cement mortar lining and corrosion/rust, respectively

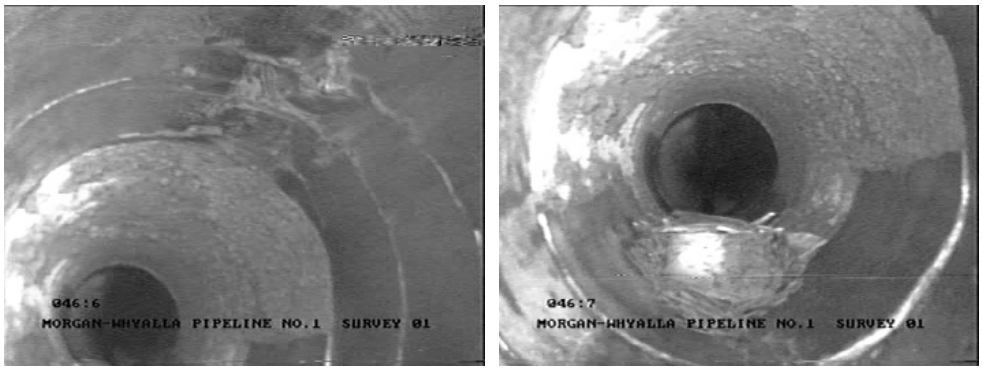

Figures 10-4 and 10-5 – Delamination and corrosion damage, with accumulated pieces of cement lining, for the MTP between chainages 15000m and 15400m

10.3 Potential explanations for observed hydraulic noise

10.3.1 Modelling and assessment of discrete air pockets/entrained air

Given the damage to the internal surface of the Morgan Transmission Pipeline (MTP) identified in the logs of the CCTV camera investigation and rationalised in Table 10-2 (below) to exclude sections where only pieces of cement mortar lining have accumulated, it was conceivable that discrete air pockets might accumulate at a number of locations between chainages 15000m and 15400m (and/or between chainages 17200m and 17700m) along the MTP. The accumulation of such air pockets was thought to be most likely at locations where the damage included delaminated lining and/or exposed and corroded steel (as listed in Table 10-2). The sizes of the discrete air pockets were assumed to be roughly proportional to the level of observed damage at particular locations.

The discrete air pockets listed in Table 10-2 were included in a forward transient model of the MTP. Figure 10-6 shows the measured and predicted responses obtained using a forward transient model without any air pockets and with the distribution of air pockets described above. The result is predictable and confirms that while the air pockets give reflections of the correct order of magnitude, the dispersive characteristics of the air pockets lead to the formation of an amalgam response that is unrepresentative of the measured response.

Table 10-2 – Rationalised log of damage between chainage 15000m and 15400m on the Morgan Transmission Pipeline and proportional air pockets

Chainage (m)	Damage type	Exposed steel (m^2)	Potential air pocket (m^3)	Chainage (m)	Damage type	Exposed steel (m^2)	Potential air pocket (m^3)
15020	P+D	0.2	0.00002 (0.2L)	15280	P+D+R	12.2	0.0002 (2.0L)
15070	P+D+R	6.0	0.0001 (1.0L)	15290	P+R	0.7	0.00003 (0.3L)
15100	P+R	0.1	0.00001 (0.1L)	15330	P+D	0.5	0.00003 (0.3L)
15150	P+R	0.2	0.00002 (0.2L)	15340	P+R	0.2	0.00002 (0.2L)
15160	P+D+R	0.6	0.00003 (0.3L)	15360	P+D	0.1	0.00001 (0.1L)
15220	P+D	0.1	0.00001 (0.1L)	15390	P+D	0.6	0.00003 (0.3L)
15260	P+D	0.6	0.00003 (0.3L)	15400	P+D+R	1.5	0.00005 (0.5L)
15270	P+D+R	4.7	0.0001 (1.0L)	Total		28.3	0.00069 (6.9L)

where P, D and R represent pieces of cement mortar lining (protrusions), delamination of the cement mortar lining and corrosion/rust, respectively

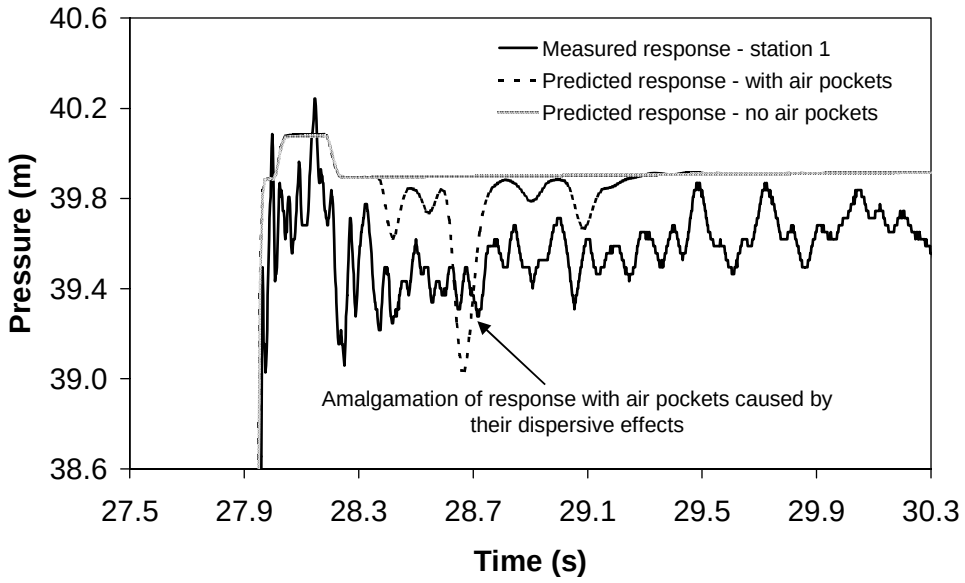

Figure 10-6 – Comparison of measured response of the MTP for test 7, conducted in August 2004, and predicted responses without and with air pockets

It was shown in Chapter 7 that a small percentage of entrained air (0.0001%) could account for dispersion in the measured response of the MTP for test 9 conducted in August 2004. Figure 10-7 confirms that the inclusion of 0.0001% of entrained air

improves the comparison between the measured and predicted responses in terms of the initial pressure rise following the induction of the controlled transient. Figure 10-8 confirms that, over the period encompassing the detailed reflections noted above, 0.0001% of entrained air gives a satisfactory match with the timing and slope of the incident wavefront. Higher percentages of air excessively reduce the initial pressure rise and overly delay and disperse the predicted wavefront. That said, the inclusion of 0.0001% of entrained air does not account for the observed pattern of reflections.

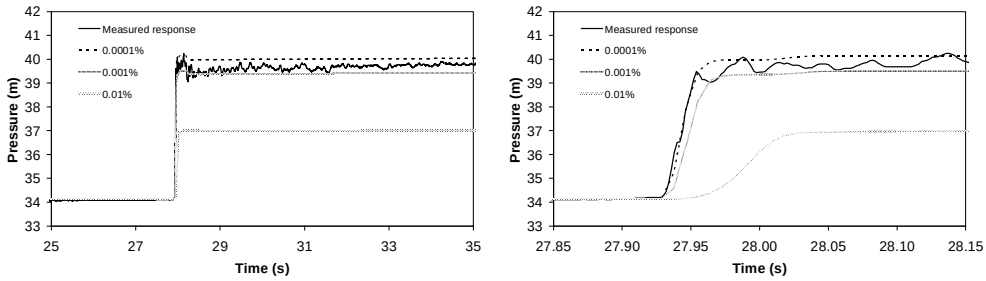

Figures 10-7 and 10-8 – Effect of different percentages of entrained air, relative to the measured response for test 7, over time scales of 10s and 0.3s, respectively

10.3.2 Modelling and assessment of minor losses

Misiunas et al. (2005) hypothesised that sections of the Morgan Transmission Pipeline (MTP) that exhibited higher densities of reflections, with greater magnitudes, when subject to controlled transient inputs, might have damaged internal linings and walls. A method was proposed whereby the standard deviation of the measured response for different 1km long sections of the MTP could be compared to quantitatively gauge relative levels of damage. The method was not verified against the available CCTV camera logs because it applied to long lengths of pipeline (greater than or equal to 1km) and could not be used to identify damage with greater specificity. Transient models incorporating the effects of unsteady friction, discrete and entrained air and Fluid Structure Interaction (FSI) effects were not developed to assess the potential impact of these phenomena.

Misiunas (2005) suggested that the mechanism responsible for the observed reflections was the interaction of the transient wavefront with protrusions, largely

comprised of delaminated cement lining, from the internal surface of the wall of the MTP. Based on the CCTV camera logs of the section of the MTP between chainages 15000m and 15400m, the distribution and degree of protrusions from the delaminated cement lining (and corrosion/tuberculation) has been directly estimated and summarised in Table 10-3.

Table 10-3 – Log of wall damage and cement lining delamination between chainage 15000m and 15400m on the MTP with corresponding extent of protrusion

Chainage (m) / point	Damage type	Approx. intrusion (m)	Approx. diameter (m)	Chainage (m) / point	Damage type	Approx. intrusion (m)	Approx. diameter (m)
15020 – 1	P+D	0.2	0.53	15260 – 8	P+D	0.1	0.63
15070 – 2	P+D+R	0.3	0.43	15270	P+D+R	0.3	0.43
15100 – 3	P+R	0.2	0.53	15280	P+D+R	0.3	0.43
15110	P	0.3	0.43	15290	P+R	0.1	0.63
15130 – 4	P	0.1	0.63	15330 – 9	P+D	0.1	0.63
15150 – 5	P+R	0.1	0.63	15340	P+R	0.3	0.43
15160	P+D+R	0.2	0.53	15360 – 10	P+D	0.3	0.43
15180 – 6	P	0.2	0.53	15390 – 11	P+D	0.1	0.63
15220 – 7	P+D	0.3	0.43	15400	P+D+R	0.3	0.43

where P, D and R represent pieces of cement mortar lining (protrusions), delamination of the cement mortar lining and corrosion/rust, respectively

Figure 10-9 illustrates the distribution and degree of protrusion, formed by pieces of cement lining, listed in Table 10-3 (with chainages corresponding to point labels). The horizontal scale is distorted to extend from chainage 15000m to 15400m. In contrast to smaller distribution pipelines with tuberculation, the corrosion and tubercules on the exposed steel wall surfaces do not form protrusions more than 25mm high. As a consequence, the bulk of each protrusion comprises loose pieces of cement lining heaped in piles at the locations shown along the pipeline. These piles of cement lining should not be represented as an integral change in the internal pipeline diameter over an extended length. Instead, they are better characterised as a sequence of in-line orifices or discrete blockages.

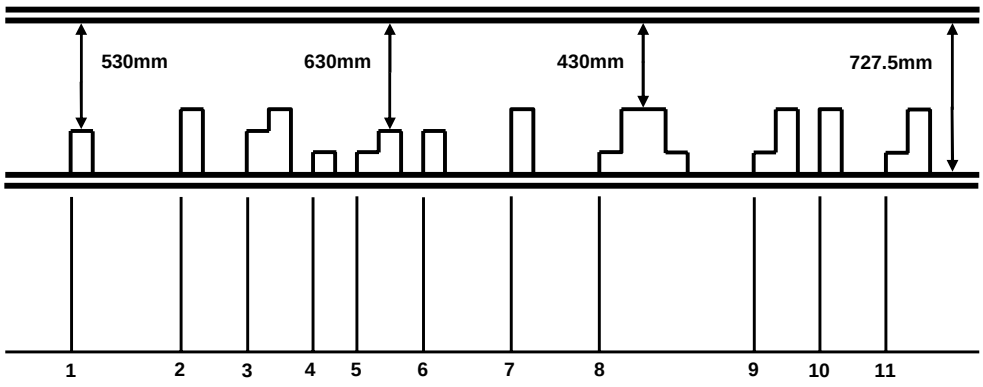

Figure 10-9 – Distribution and degree of protrusions between chainage 15000m and 15400m along the Morgan Transmission Pipeline

The distribution and extent of the protrusions listed in Table 10-3 were included in a forward transient model of the MTP as in-line orifices. Figure 10-10 shows the measured and predicted responses obtained using a forward transient model without any protrusions and with the distribution of protrusions described above.

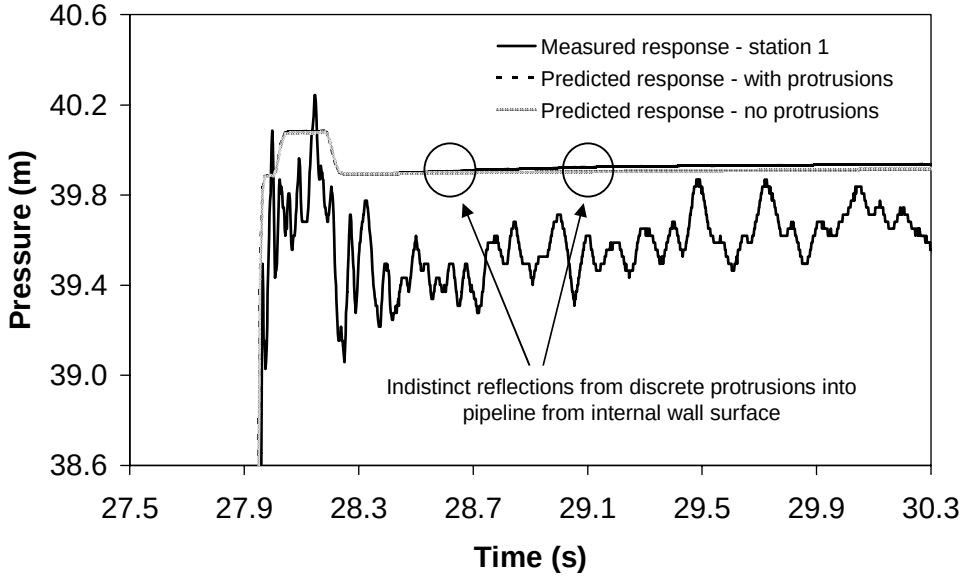

Figure 10-10 – Comparison of measured response of MTP for test 7, conducted in August 2004, and predicted responses without and with discrete protrusions

The result confirms that direct reflections from protrusions of the magnitude listed in Table 10-3, and illustrated in Figure 10-9, are not significant. The result can be confirmed by simple application of the direct equations for reflection and transmission from a discrete blockage or in-line orifice as presented by Wylie and Streeter (1993) and summarised in Chapter 3. The behaviour of reflections from discrete blockages, equivalent to the protrusions illustrated in Figure 10-9, is further investigated in Chapter 13 in the context of field tests on a water distribution pipeline. The analysis presented in Chapter 13 and, in particular, Appendix S identifies the percent constrictions required to create discernable reflections from discrete constrictions or protrusions. None of the protrusions identified in the CCTV camera investigation of the MTP are of a sufficient extent so as to give rise to the reflections observed in the measured response.

10.4 Correlating internal pipe condition with reflections

The observation by Misiunas et al. (2005), that there is a correlation between damage to the inside of the wall of the Morgan Transmission Pipeline (MTP) and the density and magnitude of reflections observed from 1km long sections of the pipeline subject to transient tests (i.e., the standard deviation of the pressure response), is thought to be correct. However, it has been necessary to develop complex forward transient models of the MTP in order to assess the potential impact of lateral pipes, cross-connections, discrete air pockets, entrained air and fluid structure interaction effects (as far as they relate to inertial effects). Furthermore, the mechanism identified by Misiunas (2005), which suggests that there are reflections from the deposits of internal lining that have built-up along the bottom of the MTP, is contradicted by the results of transient modelling and the application of the direct equations for reflection and transmission presented by Wylie and Streeter (1993).

Given the systematic elimination of other plausible explanations, and the fact that the reflections occur with the same magnitude and distribution for repeated tests (suggesting that they are related to the invariant (or very slowly varying) physical characteristics of the MTP), it is postulated that the reflections are correlated with changes in the wave speed of the MTP at locations at which there has been

delamination of the cement lining around the internal circumference of the pipeline and where wall corrosion has occurred.

10.4.1 Theoretical effect of changes to lining and wall thickness

The wave speed for the sections of the Morgan Transmission Pipeline (MTP) with 3/16 of an inch (4.76mm) thick wall is theoretically 1015m/s when the pipeline is taken to be fully restrained. This wave speed was determined assuming composite action between the steel wall and cement lining with the physical and geometric properties shown in Figure 10-11. If in good condition, nearly all of the pipeline in close proximity to the location of the transient generator and measurement station 1, for tests 7, 8 and 9, conducted in August 2004, has a 4.76mm thick wall. However, there is a relatively short section of pipeline with a 1/4 of an inch (6.35mm) thick wall between chainage 15731m and chainage 15839m as shown in Figure 10-3 (above). The wave speed for the section of pipeline with this wall thickness is theoretically 1074m/s.

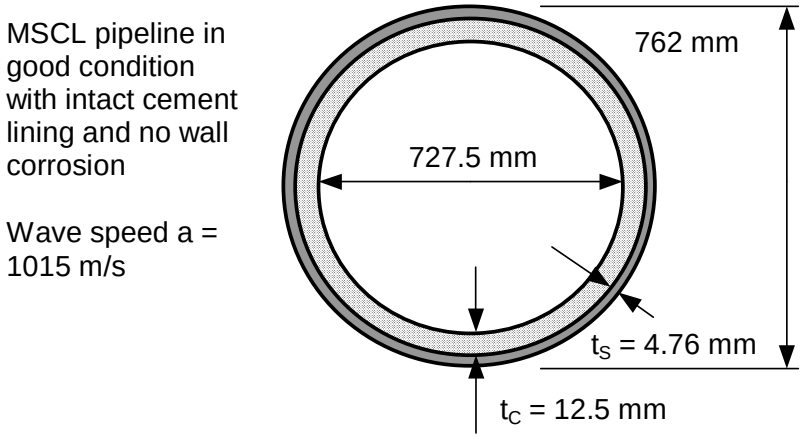

Figure 10-11 – Morgan Transmission Pipeline in good condition with intact cement lining

The transient response of the MTP is extremely sensitive to the wave speed, which is, in turn, sensitive to the condition of the pipeline wall. If we recall the traditional

Method of Characteristics (MOC) solution for the C^+ and C^- compatibility equations along the characteristic lines of the MOC grid, with a quasi-steady representation of friction, then the solution for the transient pressure can be obtained using:

$$H(x,t)^+ = \left[H(x-\Delta x, t-\Delta t) + \frac{a}{gA} Q(x-\Delta x, t-\Delta t) \right] - \left[\frac{a}{gA} + \frac{f}{2gDA^2} a\Delta t \left| Q(x-\Delta x, t-\Delta t) \right| \right] Q(x,t)^+ \quad (10\text{-}1)$$

and

$$H(x,t)^- = \left[H(x+\Delta x, t-\Delta t) - \frac{a}{gA} Q(x+\Delta x, t-\Delta t) \right] + \left[\frac{a}{gA} + \frac{f}{2gDA^2} a\Delta t \left| Q(x+\Delta x, t-\Delta t) \right| \right] Q(x,t)^- \quad (10\text{-}2)$$

where f is a steady state friction factor, a is the wave speed, A is the internal area of the pipeline and the impedance of the pipeline $B = \frac{a}{gA}$

It is apparent, through the impedance term, that the transient response of the pipeline is sensitive to the wave speed and the internal area of the pipeline. The loss of the cement lining reduces the stiffness of the pipeline wall by an amount proportional to the thickness and modulus of elasticity of the cement. Once exposed, the pipe wall begins to corrode leading to a reduction in the thickness of the metal retaining its original elastic modulus. If the pipeline wall is damaged, and has lost cement lining and/or developed wall corrosion, the wave speed will decrease, and the internal area of the pipeline will increase, such that there will be a reduction of pipeline impedance. As the variability in the condition of the pipeline wall increases so too does the magnitude and density of reflections following the passage of a sharp transient wavefront. As a consequence, it may be possible to replicate the effect of a damaged section of pipeline by varying its physical and geometric properties along its length.

Based on examination of the CCTV camera footage for the sections of the MTP between chainage 15000m and chainage 15400m, and also chainage 17200m and 17700m, it was decided to characterise the damage to the internal surface of the walls of the MTP in terms of four discrete categories of damage. While individual pits (i.e., points of specific corrosion) could not be represented, the loss of cement lining could be specified, as could average reductions in pipeline wall thickness for different degrees of corrosion. Table 10-4 summarises the four categories of damage, the change to internal pipe diameter, the status of the cement lining, thickness of steel that has corroded and, finally, the wave speed corresponding to each level of damage. The wave speed is a function of the change to internal pipe diameter and remaining thickness of cement lining and steel in the pipeline wall and has been calculated using the relationship presented by Wylie and Streeter (1993) and described in Appendix S.

Table 10-4 – Physical and geometric properties of the Morgan Transmission Pipeline for four discrete levels of damage

Level of Damage	Description of Damage	Internal Diameter (mm)	Cement Lining	Corroded Metal Thickness (mm)	Un-corroded Metal Thickness (mm)	Wave Speed (m/s)
0	Nil	727.5	Intact	0	4.76	1015
1	Loss of cement lining	752.5	None	0	4.76	932
2	1mm of corrosion	754.5	None	1	3.76	865
3	2mm of corrosion	756.5	None	2	2.76	778
4	3mm of corrosion	758.5	None	3	1.76	655

Figure 10-12 shows the idealised physical characteristics of the MTP for the four discrete levels of damage that include the pipeline without cement lining and with 0mm, 1mm, 2mm and 3mm of wall corrosion, respectively.

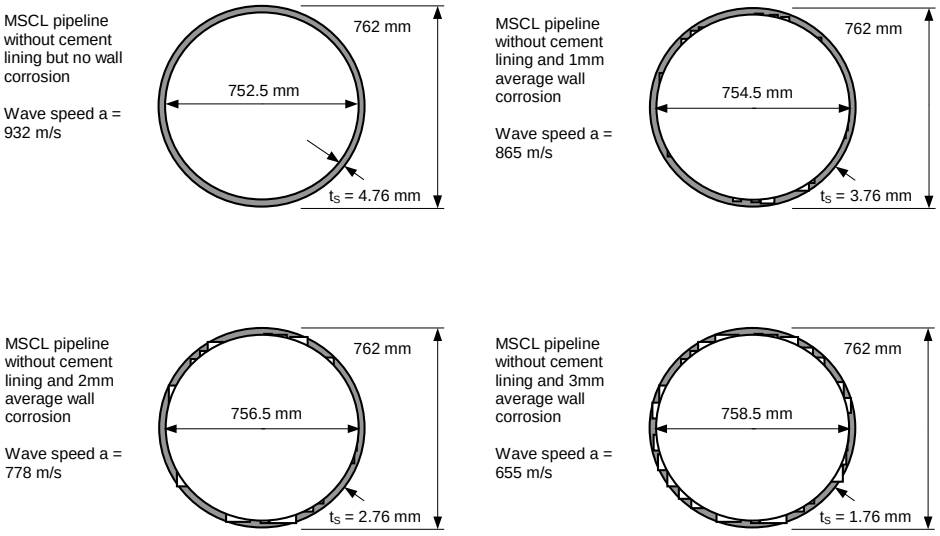

Figure 10-12 – Four discrete levels of pipe wall damage for the Morgan Transmission Pipeline

10.4.2 Representing the effects of known damage and wall changes

Table 10-5 summarises the condition of the Morgan Transmission Pipeline (MTP), in terms of the categories of damage identified above over 10m lengths of pipeline, between chainage 15000m and chainage 15400m. Loss of cement lining without significant corrosion was observed, on average, over the 10m lengths of pipeline centred on chainages 15020m, 15110m and 15180m. For all other damaged sections, the loss of cement lining was accompanied by various degrees of corrosion of the internal pipeline wall.

Figure 10-13 shows the effect of the known change in wall thickness between chainage 15731m and 15839m from 4.76mm to 6.35mm, and back to 4.76mm, and the distribution and extent of categorised damage, estimated using the CCTV camera footage, between chainage 15000m and 15400m, upon the wave speed of the MTP.

Table 10-5 – Approximate known condition of the MTP, in terms of diameter and wave speed, per 10m length, between chainage 15000m and 15400m

Chainage (m)	Damage Level	Internal Diameter (m)	Wave Speed (m/s)	Chainage (m)	Damage Level	Internal Diameter (m)	Wave Speed (m/s)
15000	Nil	0.7275	1015	15210	Nil	0.7275	1015
15010	Nil	0.7275	1015	15220	2	0.7545	865
15020	1	0.7525	932	15230	Nil	0.7275	1015
15030	Nil	0.7275	1015	15240	Nil	0.7275	1015
15040	Nil	0.7275	1015	15250	Nil	0.7275	1015
15050	Nil	0.7275	1015	15260	2	0.7545	865
15060	Nil	0.7275	1015	15270	3	0.7565	778
15070	3	0.7565	778	15280	3	0.7565	778
15080	Nil	0.7275	1015	15290	2	0.7545	865
15090	Nil	0.7275	1015	15300	Nil	0.7275	1015
15100	2	0.7545	865	15310	Nil	0.7275	1015
15110	1	0.7525	932	15320	Nil	0.7275	1015
15120	Nil	0.7275	1015	15330	3	0.7565	778
15130	Nil	0.7275	1015	15340	2	0.7545	865
15140	Nil	0.7275	1015	15350	Nil	0.7275	1015
15150	2	0.7545	865	15360	2	0.7545	865
15160	3	0.7565	778	15370	Nil	0.7275	1015
15170	Nil	0.7275	1015	15380	Nil	0.7275	1015
15180	1	0.7525	932	15390	3	0.7565	778
15190	Nil	0.7275	1015	15400	3	0.7565	778
15200	Nil	0.7275	1015				

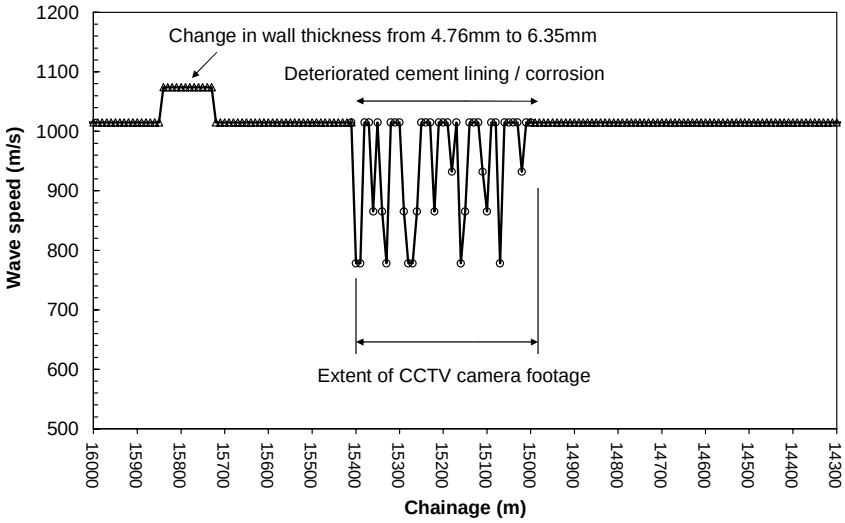

Figure 10-13 – Distribution and extent of changes to the MTP wave speed, estimated over 10m lengths, between chainage 15000m and 15400m

10.4.3 Transient modelling of known wall changes

Although Equations 10-1 and 10-2 presented above represent a traditional transient solution scheme with quasi-steady friction, the forward transient model developed for the following analysis includes turbulent rough pipe unsteady friction, using the roughness values determined on the basis of the CCTV camera footage, and 0.0001% of entrained air (as previously determined in Chapter 7 as the most realistic quantity). "Viscous" damping mechanisms have not been included in the forward transient model. A 10m discretisation, and hence 10m resolution for the classification of damaged sections of the Morgan Transmission Pipeline (MTP), has been adopted. This length matches that over which the average condition of the MTP was catergorised using the CCTV camera footage. A 5m discretisation has also been used, to assess the sensitivity of the modelled response to discretisation and interpolation errors, below.

Apart from the estimated changes to the wall of the MTP between chainage 15000m and 15400m, it was known that the pipeline wall thickness changed between chainage 15731m and 15839m from 4.76mm to 6.35mm, and back to 4.76mm, and that it changed from 4.76mm to 6.35mm at chainage 11740m. Figure 10-14 shows the comparison between the measured (test 7) and predicted responses, at station 1, when these known changes in the wall thickness are included, as well as the known damage inferred from the CCTV camera footage between chainage 15000m and 15400m. Unfortunately, the effects of the change in thickness between chainage 15731m and chainage 15839m are partially obscured by the incident wavefront because of its close proximity to the transient generator and station 1. That said, the additional reflections (positive and negative) associated with the changes in wall thickness are apparent and have a magnitude of approximately 0.16m.

The reflection from the change in pipeline wall thickness at chainage 11740m is clearly discernable and is also approximately 0.16m in magnitude. The measured and predicted magnitude of the reflection, and the timing, compare favourably. The results confirm that reflections from changes in pipe wall thickness from 4.76mm to 6.35mm (i.e., 25%) are observed in the measured response and can be predicted using the forward transient model. Furthermore, this magnitude of change in pipe wall thickness

is comparable with that for the damage categories identified above. The discrepancy between the measured and predicted transient plateau, once the limits of the known information regarding the damage to the pipe wall are reached, appears to be related to the neglect of further damage along the pipeline that has not been included in the forward transient model. Similarly, the lag between the predicted and measured reflection is likely to be related to an unaccounted for reduction in the wave speed along damaged sections of pipeline.

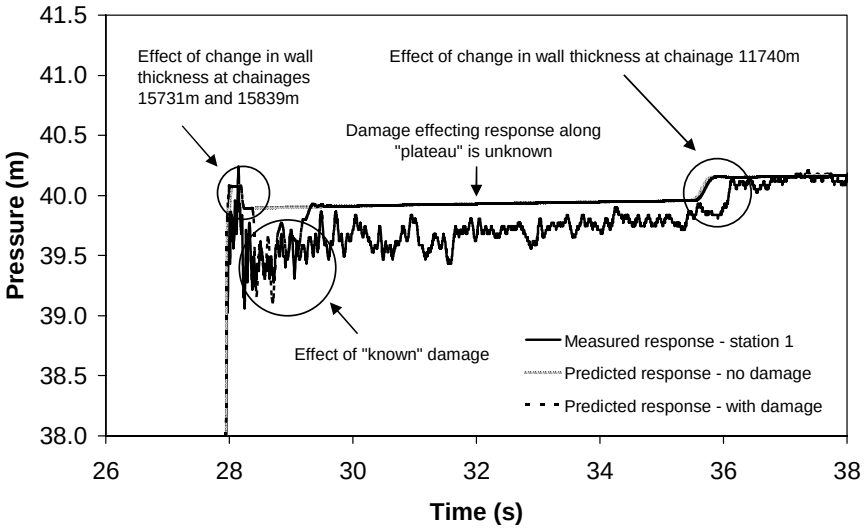

Figure 10-14 – Measured and predicted responses when known changes in wall thickness and known damage are included in a forward transient model of the MTP

10.4.4 Inferring the condition of a section of the MTP

Figure 10-15 shows the measured (test 7) and predicted responses when known damage, between chainage 15000m and chainage 15400m, is included in the forward transient model. The validity of the comparison is restricted, to between times 28.35s and 29.20s, because the range over which the lining and wall condition are known is limited to the extent of the CCTV camera footage. Within this range, trends in the predicted response approximately match those in the measured response.

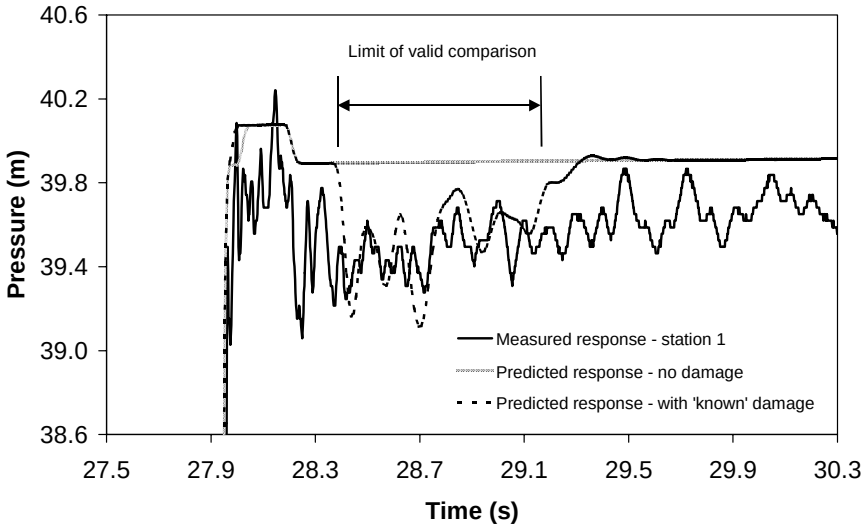

Figure 10-15 – Measured and predicted responses when known damage between chainage 15000m and 15400m is included in the forward transient model

Discrepancies are likely to be due to the categorisation process by which the damage is included in the forward transient model and differences between the damage inferred from the CCTV footage and the actual physical condition of the pipe wall. However, the important point is that the inclusion of the idealised damage, at locations that were physically confirmed using the CCTV camera footage, has led to a significant improvement in the comparison between the measured and predicted responses. Neither the inclusion of entrained air pockets nor discrete protrusions in the forward transient model gave this improvement.

An inferred distribution of damage has been determined for the remainder of the MTP between chainage 14300m and 16000m. Figure 10-16 shows the inferred pattern of damage, in terms of changes in wave speed, combined with the known damage, between chainage 14300m and 16000m. South Australian Water Corporation officers provided advice that there was insignificant damage to the MTP between chainage 16000m and 16400m. This has been relied upon when determining the inferred distribution of damage.

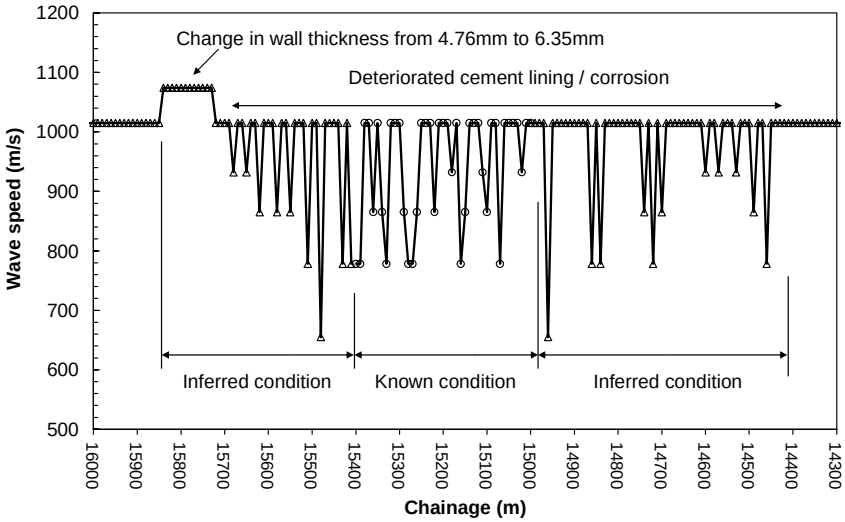

Figure 10-16 – Inferred and known distribution and extent of changes to the MTP wave speed, estimated over 10m lengths, between chainage 14300m and 16000m

Figure 10-17 shows that this combined distribution of inferred and known damage improves the comparison between the measured and predicted responses (over the full range between times 27.9s and 30.3s). It appears the changes in the wall condition, and corresponding changes in wave speed and impedance, provide an explanation for the observed reflections and, potentially, a way of inferring the damage to the pipeline wall by interpreting reflections using a forward transient model when known information is not available.

That said, the inferred distribution of damage has been determined by limited trial and error analysis and is not an optimal representation of the likely damage to the pipeline wall. This explains, in part, the discrepancies between the measured and predicted responses and represents a further complication additional to those introduced by the categorisation of the damage and the use of a 10m discretisation in the forward transient model.

Apart from suggesting that dispersion due to entrained air and/or mechanical dispersion and damping is not significant over the initial stages of the response, the density of reflection detail in the measured responses suggests that variations in damage to the pipe wall are significant on a metre for metre basis. The use of a finer

discretisation in the forward transient model is feasible and would increase the specificity with which known or inferred damage, could be represented. Figure 10-18 shows the predicted response obtained for a forward transient model with a 5m discretisation.

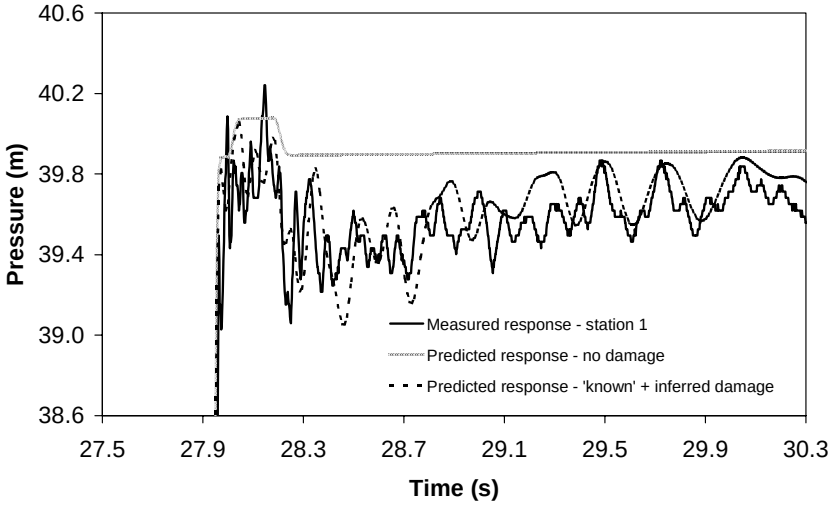

Figure 10-17 – Measured and predicted responses with known and inferred damage in a forward transient model with a 10m discretisation

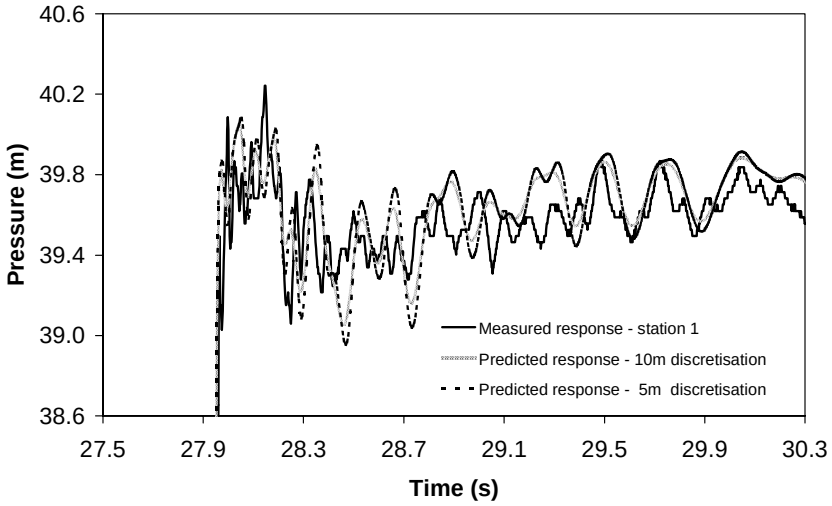

Figure 10-18 – Measured and predicted responses with known and inferred damage in a forward transient model with 10m and 5m discretisations, respectively

10.4.5 Use of evolutionary algorithm for inferring pattern of damage

The intention in this chapter has been to identify a physical mechanism that can explain the observed reflections and explore the possibility that a forward transient model could be applied to both confirm the effect of a known distribution of damage and predicatively infer a distribution of damage from a measured response. The inferred distribution of damage presented above has been determined on the basis of limited trial and error variation of the magnitude and distribution of damage and does not represent the optimal inferred distribution that gives the best match between the measured and predicted responses.

The use of trial and error analysis cannot be relied upon in future investigation of the methodology because of the number of potential combinations of damage magnitudes and distributions over even relatively short sections of pipeline. In the case of the Morgan Transmission Pipeline (MTP), between chainage 14300m and 16000m, there are 170 by 10m long sections that can each have one of 5 conditions (i.e., either undamaged or category 1, 2, 3 or 4). This gives an extremely large number of possible combinations of magnitude and distribution of damage.

The application of global optimisation algorithms is required to determine the distribution of damage that gives the optimal fit between the measured and predicted responses. In this regard, either a Genetic Algorithm, or the Shuffled Complex Evolution Algorithm used in the inverse analysis presented in this research, may be used to fit for discrete levels of damage at 10m (or other) intervals along a section of pipeline. At the time of writing, the author has completed the programming work required to combine a Genetic Algorithm with the forward transient model BSOLVER (previously described).

10.4.6 Numerical exploration of operation of evolutionary algorithm

Unfortunately, for the tests conducted on the Morgan Transmission Pipeline (MTP) in August 2004, measurement station 2 is not close enough to the damaged section of pipeline between chainage 15000m and 15400m, or the transient generator and station

1, to enable the measured response at station 2 to be used as input for the program combining the Genetic Algorithm and forward transient model. This is because the reflections measured at this station are significantly dispersed and the transient model required to include measurement stations 1 and 2, and the transient generator, with a discretisation of 10m, requires too many sub-pipe sections (nearly 500).

That said, issues can be numerically explored and the operation of the combined Genetic Algorithm and BSOLVER developed in this research can be demonstrated. This will be done using a 1000m long numerical pipe example and then a 1500m long representation of the MTP encompassing the location near SC22, AV39 and AV41. The pattern of damage along the 1500m pipeline will be a composite of the known damage identified using the CCTV camera footage, the damage inferred from the trial and error analysis described above and an artificial pattern for the remainder of the pipeline.

Description of numerical pipeline and results of inverse analysis

Figure 10-19 shows the 1000m long numerical pipeline example. The pipeline diameter is 727.5mm (i.e., the same as for the Morgan Transmission Pipeline (MTP)). However, the pipeline is treated as frictionless with a roughness of 0mm. Furthermore, the pipeline is at the same relative elevation along its entire length. An assumed reservoir depth of 40m is applied to give similar static pressures to those observed in the MTP at the location of scour valve 22. As for test 7, conducted on the MTP in August 2004, the pressure response is determined at three locations (namely, measurement stations 1 and 2 and at the transient generator). These locations are 250m, 500m and 750m from the closed valve, respectively.

Four categories of damage are used to simulate the deterioration of the wall of the MTP over 10m lengths as described above. The loss of cement mortar lining (CML) without corrosion of the steel pipeline wall is category 1, and categories 2, 3 and 4 have lost CML and 1mm, 2mm and 3mm of corroded wall thickness, respectively. The different categories of damage are shown in Figure 10-19 at seven arbitrary locations selected for the purpose of this example. Each damaged section of pipeline is 10m long.

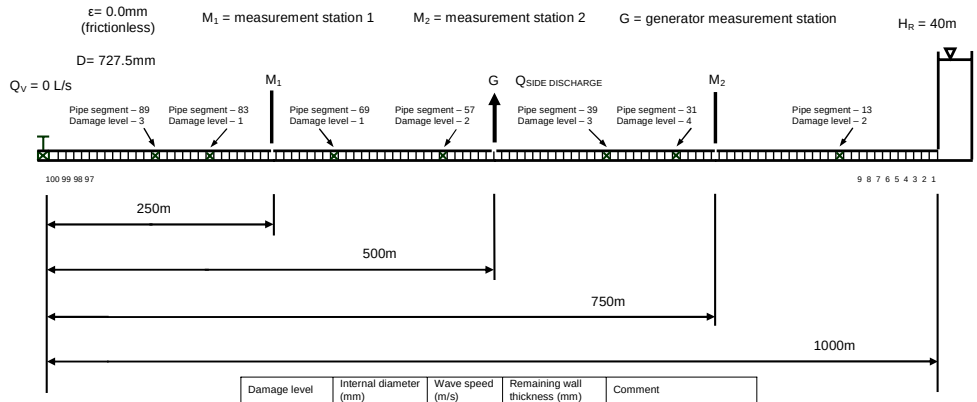

Damage level	Internal diameter (mm)	Wave speed (m/s)	Remaining wall thickness (mm)	Comment
0	727.5	1015	100%	Undamaged
1	752.5	932	100%	No CML + no corrosion
2	754.5	865	79%	No CML + 1mm corrosion
3	756.5	778	58%	No CML + 2mm corrosion
4	758.5	655	37%	No CML + 3mm corrosion

Figure 10-19 – Example pipeline used to numerically test the inverse transient model for wall condition assessment using a Genetic Algorithm and BSOLVER

Figure 10-20 shows the pattern of damage along the numerical pipeline, represented in terms of reduction in wave speed and loss of CML and/or corrosion of wall thickness, artificially established for this example, and the pattern of damage predicted after performing inverse analysis. Forward transient responses were determined for the numerical example using BSOLVER and these were used as artificial measurements when performing the inverse analysis using NLFIT, BSOLVER and a Genetic Algorithm.

The inverse analysis was performed with 64 (i.e., 2^6) divisions of the potential values for wave speed, between bounds of 655m/s and 1015m/s, for each 10m sub-pipe segment (i.e., one of 64 uniformly distributed wave speeds, increasing in 5.625m/s increments from 655m/s to 1015m/s, could be fitted for each sub-pipe length). This number of divisions was selected after performing sensitivity checks to determine the balance between the number of potential wave speed values between the bounds, and the resultant improvement in accuracy of fit, and the size of the inverse search space which increased with the number of wave speed values. Further investigation of the optimum number of divisions is continuing outside the scope of this research.

The lower and upper bounds were determined using the minimum and maximum wave speeds that could feasibly give rise to the observed pattern of reflections (i.e., the magnitude of the lowest reflection was such that a wave speed of less than 655m/s in any one sub-pipe segment was not feasible). This result follows from the fact that the lowest artificial wave speed for the numerical example was 655m/s. The importance of bounding the search space is investigated further below. In the case of a field pipeline, the lower bound can be determined, before conducting inverse analysis, by examining the measured responses and identifying the lowest feasible wave speed over a 10m length of pipe that can give rise to the observed reflections.

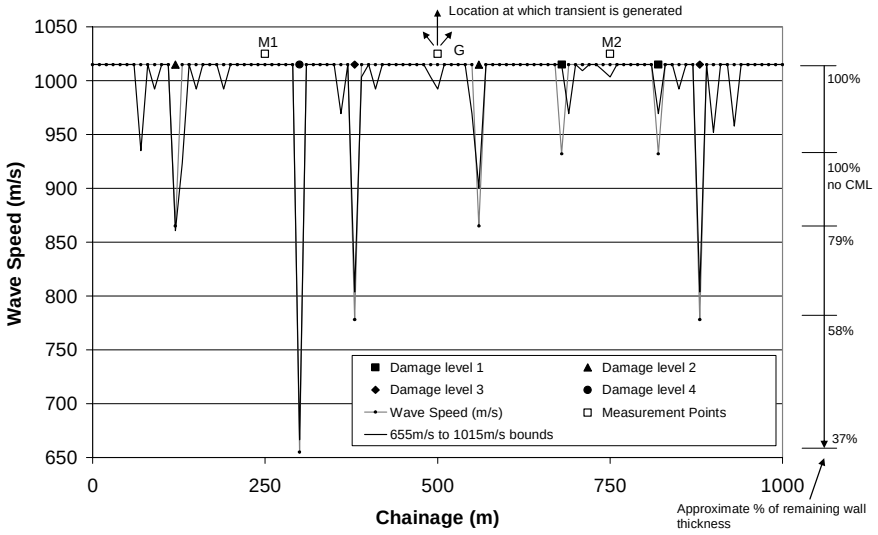

Figure 10-20 – Artificial pattern of damage versus fitted pattern of damage, in terms of wave speed and wall thickness reduction, for the numerical pipeline example

The artificial and fitted patterns of damage match closely after approximately 500000 evaluations using BSOLVER. Figure 10-21 shows the improvement in the objective function for the inverse fitting over the first 50000 evaluations. Most of the improvement in the fit occurs over the first 50000 of the 500000 evaluations. The discrepancies between the patterns of damage are problematic given the fitted damage was determined using the same forward transient response data in BSOLVER during the inverse analysis. Investigation into this discrepancy is continuing and it is

suspected to be partly related to the large number of parameters being fitted (i.e., 100 parameters).

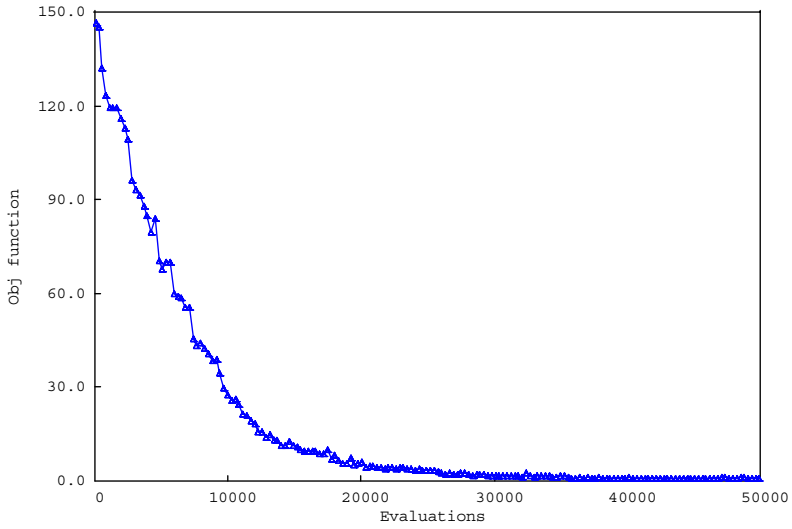

Figure 10-21 – Improvement in objective function over first 50000 evaluations using NLFIT, BSOLVER and a Genetic Algorithm

Figure 10-22 shows that the artificial numerical response and the response determined after fitting are similar at the location of the transient generator. This is despite the discrepancies between the artificial and fitted patterns of damage noted above. Figures 10-23 and 10-24 show that the artificial numerical responses and those determined after fitting are also similar at measurement locations 1 and 2. This indicates a loss of sensitivity in the inverse analysis as the weaker reflections are replicated and may help explain the residual discrepancies between the artificial and fitted patterns of damage. It is evident that approximately 0.45s passes before the wavefronts reach stations 1 and 2 and that there is less transient information available at these locations than at the transient generator. The inverse analysis is limited to 0.9s to avoid reflections from the artificial closed valve and reservoir boundary conditions influencing the results.

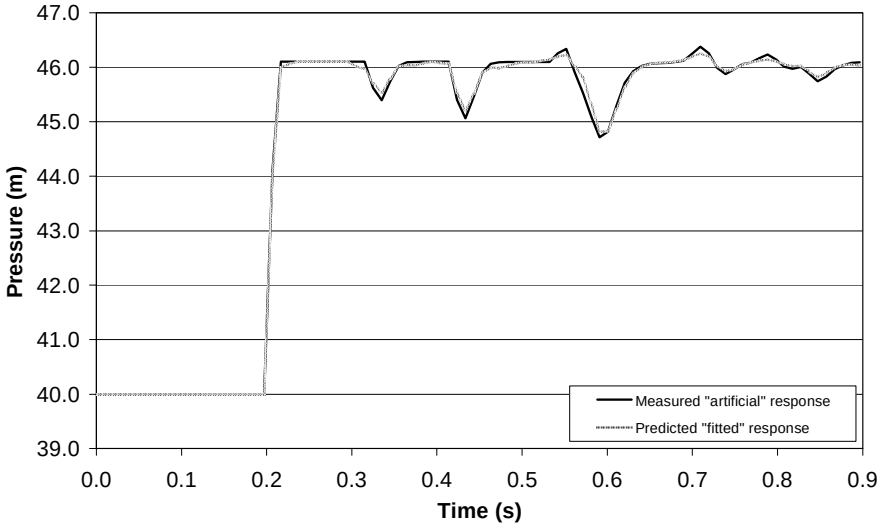

Figure 10-22 – Artificial and fitted transient responses at the transient generator

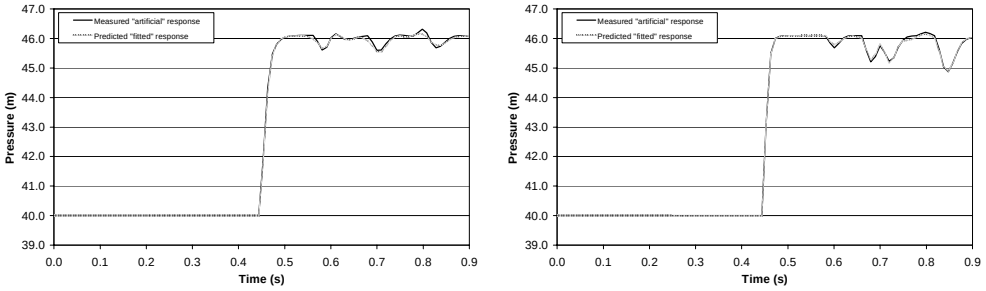

Figure 10-23 and 10-24 – Artificial and fitted transient responses at measurement locations 1 and 2, respectively

Search space issues

The larger the search space for the inverse problem the more difficult it is to identify parameters that give the best fit between measured and predicted responses. As mentioned above, increasing the number of divisions between the wave speed bounds increases the search space for the inverse problem. However, it also increases the accuracy with which a unique wave speed can be identified. The Genetic Algorithm in NLFIT is discrete (i.e., searches for discrete rather continuous parameter values). However, the search space between the wave speed bounds can be divided into binary

multiples of 2^2, 2^3, 2^4, 2^5, 2^6, 2^7, 2^8, 2^9 up to 2^{12}. That is, the search space can be divided into 4, 8, 16, 32, 64, 128, 256, 512 up to 4096 wave speeds such that the available values trend from 4 discrete values to 4096 finely spaced semi-continuous values, respectively. In the case of 4 divisions, the available wave speeds are 655, 775, 895 and 1015m/s. These values are reasonably close to the categories established earlier with wave speeds of 655, 778, 865, 932 and 1015m/s, respectively. Further division of the available values gives more flexibility to fit parameters closer to the arbitrary categories (i.e., for 4096 divisions the available wave speeds increase from 655m/s in 0.0879m/s increments such that 778, 865 and 932m/s are available). However, this additional division increases the size of the search space such that optimum solutions are not achieved. Sensitivity analysis has revealed that, for the numerical problem posed in this section, approximately 64 divisions gives the smallest relative objective function and this number of divisions will be used for the remainder of the analysis.

It was also mentioned above that the lower and upper bounds can be determined using the minimum and maximum wave speeds that feasibly give rise to the observed pattern of reflections. Figure 10-25 compares the results of the inverse analysis when lower bounds of 655m/s and 500m/s are used.

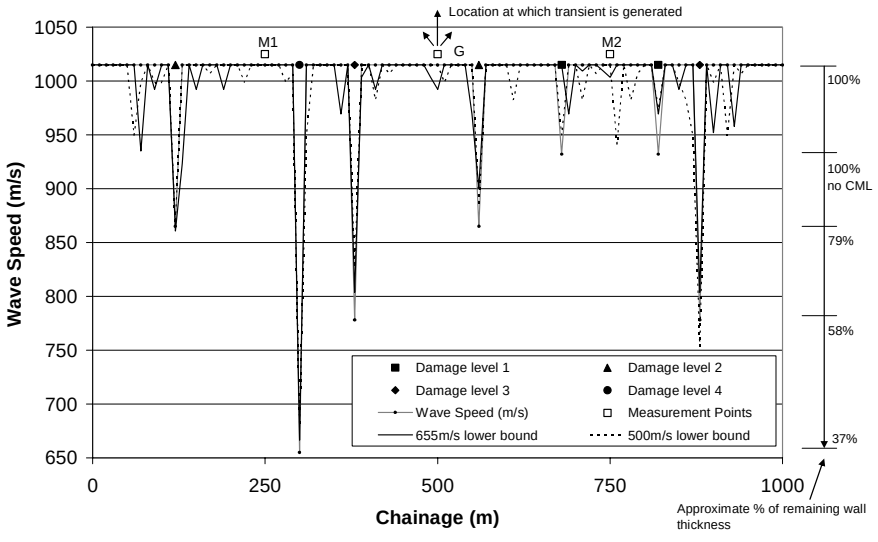

Figure 10-25 – Effect of reducing lower bound from 655m/s to 500m/s and increasing the inverse search space

The 655m/s bound covers the lowest feasible wave speed that can give rise to the observed reflections in the numerical example. By reducing the lower bound to 500m/s the search space is increased and less accurate results, in terms of the match between the artificial and fitted patterns of damage, are achieved after fitting. The loss in accuracy is most notable where less severe damage is fitted to the left and right of measurement stations 1 and 2, respectively.

Issues with positions and number of measurement stations

Reducing the size of the parameter search space is one strategy for improving the outcome of inverse analysis. Another strategy is to utilise more pressure response data. This gives the inverse model more information with which to correlate predicted reflection patterns and eliminate non-optimal parameter values. Typically, the pressure response of the Morgan Transmission Pipeline (MTP) has been measured at three locations throughout the field tests. This was a practical limitation driven by the range of the radios used for synchronising measurements. Global positioning system synchronisation has subsequently been implemented (outside of the scope of this research). As a result, four measurement stations up to 10kms apart can now be installed.

However, the usefulness of the transient measurements at such separations, and, in particular, distances from the transient generator, is reduced because of the effects of dispersion as documented in this research. In fact, the rate of observed dispersion for the Morgan Transmission Pipeline (MTP) is such that measurements more than 1km from the transient generator are less useful. Typically, only one or two air valve/fire plugs are available within 1km of the transient generator and so the use of three measurement stations (or occasionally four) is a practical limit. The use of three measurement stations over lengths of pipeline up to 2-3kms long, with one station upstream and another downstream of the location of the transient generator (at which the pressure response is also measured), provides for good coverage of the pipeline and measured data specific to each section along the pipeline. It also provides for the duplicate measurement of reflections from different positions and provides information with which correlations in the patterns of reflections can be confirmed. If

less than three measurements are taken, then the loss of information along the adjacent section of pipeline is significant. Figure 10-26 shows the effect of removing the measured response at the transient generator for the numerical pipeline example. Damage is erroneously predicted between measurement stations M1 and M2 (i.e., in the region where the transient generator measurement has been removed).

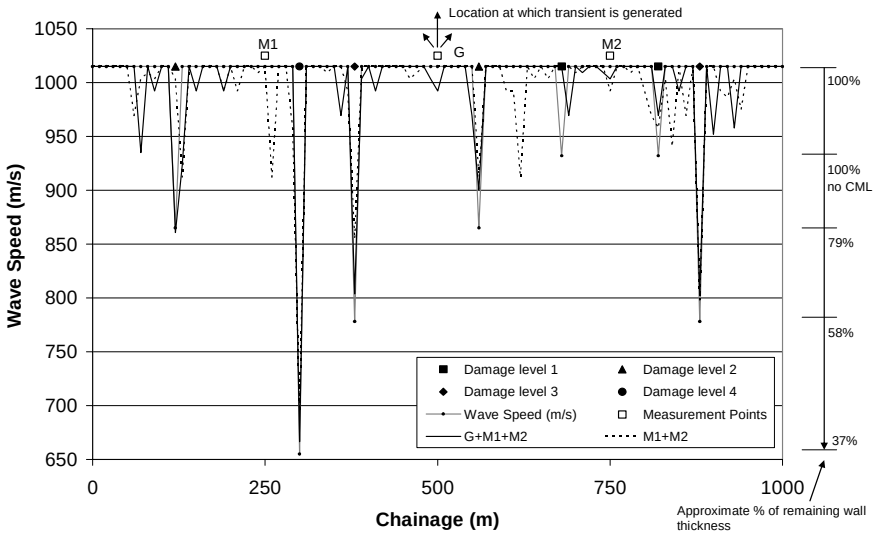

Figure 10-26 – Effect of removing measured response at the transient generator upon the results of the inverse analysis

Figures 10-27 and 10-28 show the effect of removing the measured response at stations M1 and M2, respectively. Erroneous damage is predicted in the region of the pipeline adjacent to measurement station M1 when it is removed from the inverse analysis. Similarly, erroneous damage is predicted in the region of the pipeline adjacent to measurement station M2 when it is removed. The extent of the erroneous damage is greater when M2 is removed. This is because the majority of the artificial damage is on the M1 side of the transient generator and the reflections that were recorded at M2 provided important information regarding this region of the pipeline. The results confirm that it is important to cover the length of pipeline under investigation with as many measurement locations as practical.

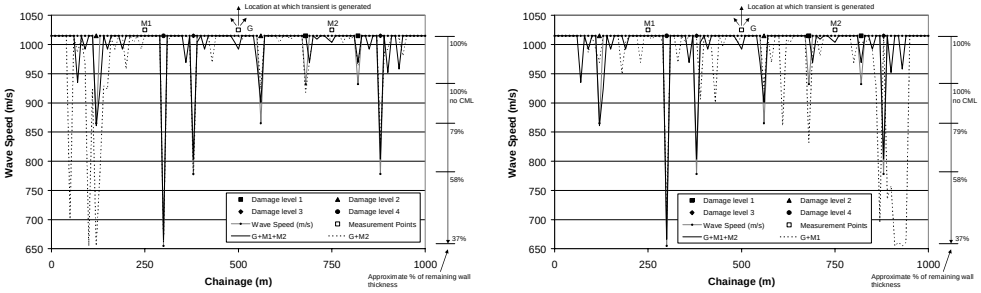

Figure 10-27 and 10-28 – Effect on the results of the inverse analysis of removing the measured responses at M1 and M2, respectively

Another issue is the location of the measurement stations relative to the source of the transient (i.e., the location of the transient generator). For the numerical example presented above M1, G and M2 are located at 250, 500 and 750m from the closed in-line valve boundary condition. Figure 10-29 shows the effect of moving M1 and M2 such that M1, G and M2 are located at 350, 500 and 650m from the closed in-line valve boundary condition. The comparison between the artificial and fitted damage patterns is improved between measurement stations M1 and M2, in the region of the transient generator, because more information is concentrated along this section of the pipeline.

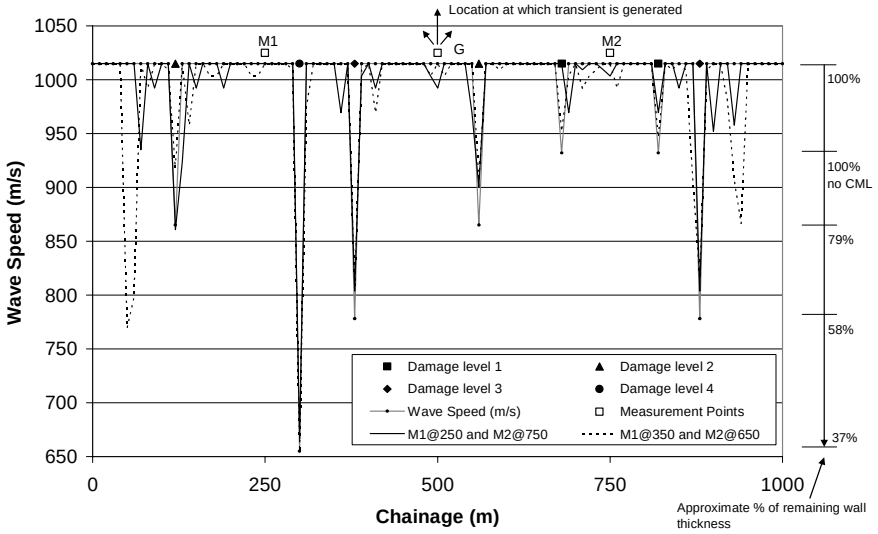

Figure 10-29 – Effect of moving measurement stations M1 and M2

Conversely, the comparison deteriorates upstream and downstream of stations M1 and M2, respectively. Erroneous damage is predicted near the closed in-line valve and reservoir boundary conditions where the inverse model has less reflection data to analyse. In this context, it is apparent that transient tests need to be conducted with at least three measurement stations within 500m to 1000m of the damaged section, and the transient generator and measurement stations.

Issues with the number of parameters

The number of parameters that need to be fitted has been identified as a major issue affecting the accuracy of the outcomes of the inverse fitting. The degree of damage (in terms of one undamaged and four damaged categories) along 100 by 10m long sub-pipe sections needs to be determined. This is a difficult inverse problem even when using artificial numerical data. The effect of the number of parameters that are fitted is investigated below by modifying the numerical example, as shown in Figure 10-30, such that the 7 by 10m long damaged sub-pipe segments are doubled to give 7 by 20m long sections of damaged pipeline. The same damage categories are applied as above and forward transient responses determined using BSOLVER.

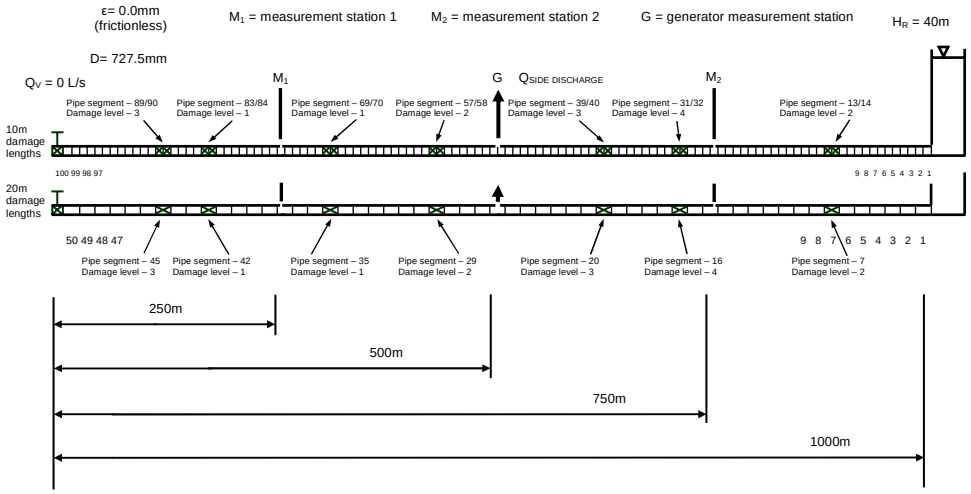

Figure 10-30 – Modified numerical pipelines with 7 by doubled 10m long and 7 by 20m long damaged sub-pipe sections with 100 and 50 parameters, respectively

In addition, a second model is established using a numerical pipeline with 50 by 20m long sub-pipe sections and damage along 7 by 20m long sub-pipe lengths that correspond with those defined by the doubled 10m long sub-pipe lengths (also as shown in Figure 10-30). The same damage categories are again applied and forward transient responses determined using BSOLVER. The same underlying model discretisation (10m) is used for both models such that similar predicted responses are obtained using both models.

Figure 10-31 shows the results of inverse analysis performed using the 100 and 50 parameter models, respectively. The comparison between the artificial and fitted damage patterns for the 100 parameter model (with 7 by doubled 10m long sub-pipe sections) is significantly less satisfactory than that obtained for the 50 parameter model (with 7 by 20m long sub-pipe sections). The fitted pattern of damage obtained using the 50 parameter model closely matches the artificial pattern. The fitted pattern of damage obtained using the 100 parameter model includes numerous erroneous predictions. The 50 parameter model is thought to be more accurate because fewer parameters are fitted.

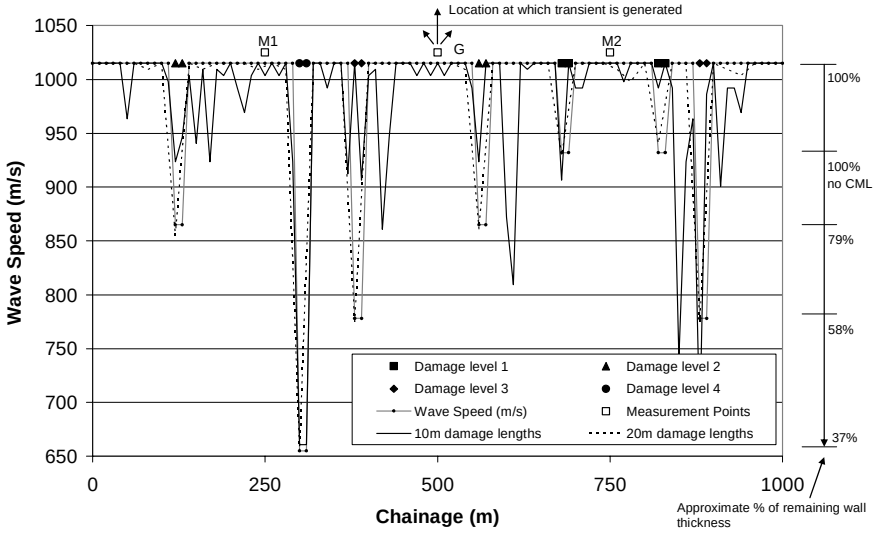

Figure 10-31 – Results of inverse analysis using 100 parameter and 50 parameter models with the same pattern of artificial damage in 20m long sub-pipe lengths

Figure 10-32 shows the measured artificial response and predicted fitted response at the transient generator when 10m long and 20m long sub-pipe sections are used to represent damage, respectively. The results obtained when the model with 50 parameters and 7 by 20m long damaged sub-pipe lengths is used match closely with the artificial damage pattern. The results obtained when the model with 100 parameters and 7 by doubled 10m long damaged sub-pipe lengths is used match relatively less closely. This discrepancy is consistent with the more and less accurate comparison between the artificial and fitted patterns of damage obtained using the 50 and 100 parameter models, respectively.

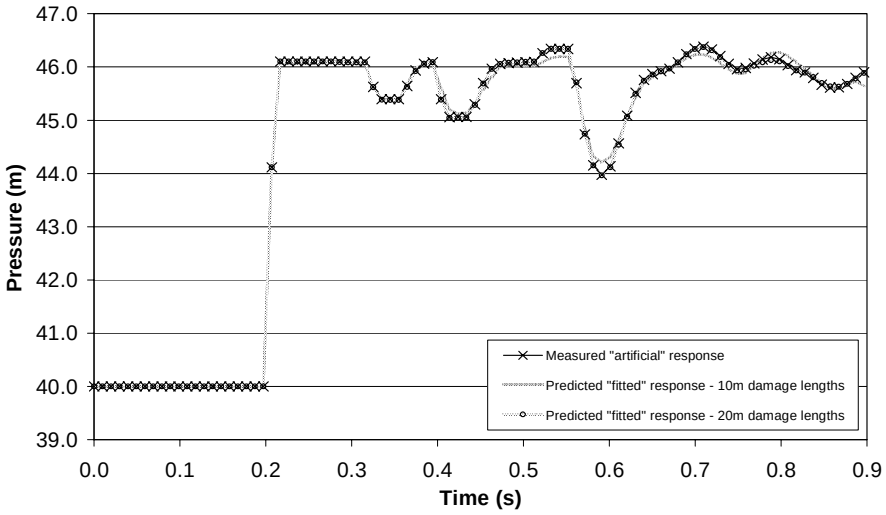

Figure 10-32 – Artificial and fitted transient responses at the transient generator obtained using 100 parameter and 50 parameter numerical models, respectively

Figures 10-33 and 10-34 show the measured artificial responses and predicted fitted responses at measurement stations M1 and M2, respectively. As at the transient generator, the results obtained using the 50 parameter model are more accurate than those obtained using the 100 parameter model. As mentioned above, the 50 parameter model is thought to be more accurate because fewer parameters are fitted. Further investigation, beyond the scope of this research is occurring into inverse methods and algorithms that can be used to fit large numbers of parameters with greater accuracy.

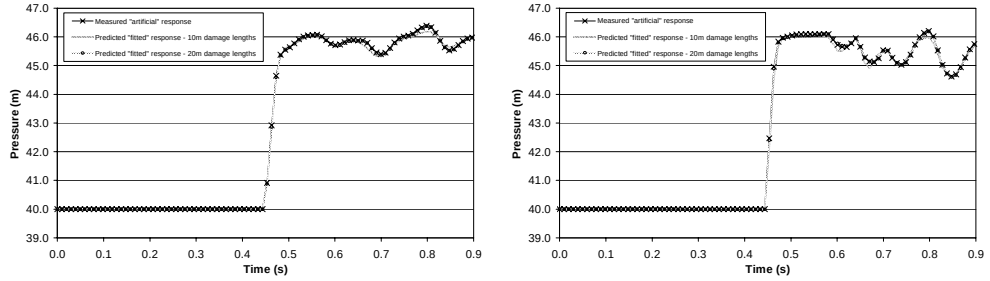

Figure 10-33 and 10-34 – Artificial and fitted transient responses, obtained using 100 and 50 parameter models, at measurement locations 1 and 2, respectively

10.4.7 Application of inverse transient software to pseudo-field pipe

Figure 10-35 shows a representation of the Morgan Transmission Pipeline (MTP) along the 1.5km section encompassing scour valve 22 and air valves 39 and 41. The pipeline is 1500m long and 727.5mm in diameter. The pipeline has an estimated roughness of 3mm and this is included in the transient modelling. Furthermore, the relative elevation of the pipeline is maintained along its entire length. An assumed reservoir depth of 32.6m is applied to give similar static pressures to those observed in the MTP at the locations of scour valve 22 and air valves 39 and 41. As for test 7, conducted on the MTP in August 2004, the pressure response is determined at three locations (namely measurement stations 1 and 2 and at the transient generator). These locations correspond with air valves 39 and 41 and scour valve 22, respectively.

As for the numerical example, and the trial and error fitting described above, four categories of damage are used to simulate the deterioration of the wall of the MTP over 10m lengths. The loss of cement mortar lining (CML) without corrosion of the steel pipeline wall is category 1, and categories 2, 3 and 4 have lost CML and 1mm, 2mm and 3mm of corroded wall thickness, respectively. The different categories of damage are shown in Figure 10-35 at 45 locations. The first 16 damaged sections from the closed in-line valve boundary condition are located on the basis of CCTV camera footage available along this section of the MTP. The next 10 damaged sections are located on the basis on the results of the trial and error fitting, for test 7 conducted on the MTP, as described above. The last 19 damaged sections up to the reservoir boundary are located on an arbitrary basis. The category of damage is based

on the results of the CCTV camera inspection or trial and error fitting over the relevant sections of the MTP.

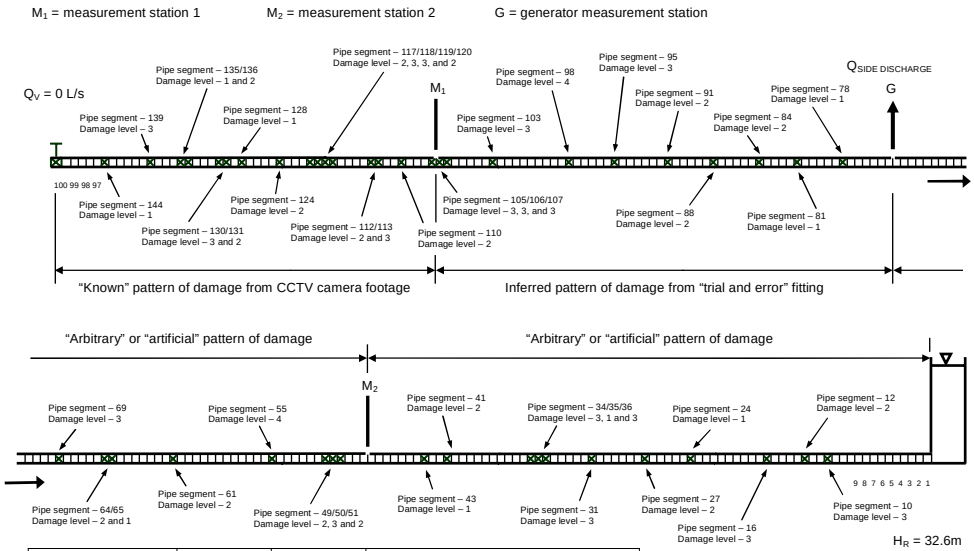

Label	Chainage	Elevation	Comment
M1	15290m	112.0m	Measurement station 1 at air valve 39
G	15710m	114.0m	Transient Generator at scour valve 22
M2	15990m	115.5m	Measurement station 2 at air valve 41
Closed end valve	14960m	110.0m	Artificial closed valve boundary condition
Reservoir	16460m	117.5m	Artificial reservoir/tank boundary condition

Figure 10-35 – Psuedo-field pipeline used to test the inverse transient model for wall condition assessment along a representative length of the MTP

Figure 10-36 shows the estimated pattern of damage along the pseudo-field pipeline, represented in terms of reduction in wave speed and loss of CML and/or corrosion of wall thickness, and the pattern of damage predicted after performing inverse analysis. In this problem, 150 sub-pipe segments are used to represent damage along 1500m of the MTP in 10m lengths. This means that 150 parameters need to be fitted during the inverse analysis. This is a more difficult inverse problem than tackled numerically above with an even larger search space. Furthermore, the measurement station locations are fixed, at the locations of scour valve 22 and air valves 39 and 41, and cannot be moved to positions that maximise the reflection information used during the inverse analysis.

The comparison between the estimated and fitted patterns of damage is not as good as for the numerical example. Nevertheless, the results are reasonable and the pattern of damage based on CCTV camera footage, trial and error fitting and a partial arbitrary distribution is fitted with relative accuracy. Even at this stage, the results provide a qualified basis upon which to infer the locations at which damage occurs along the section of the MTP subject to CCTV camera survey (which can be used to check the pattern of damage derived from the inverse analysis). Errors in the position of predicted damage along this section are in the order of ±30m while the errors in magnitude are up to, but generally less than, 50%. As mentioned previously, work is continuing outside the scope of this research to find methods for improving the inverse analysis including the identification of better search algorithms.

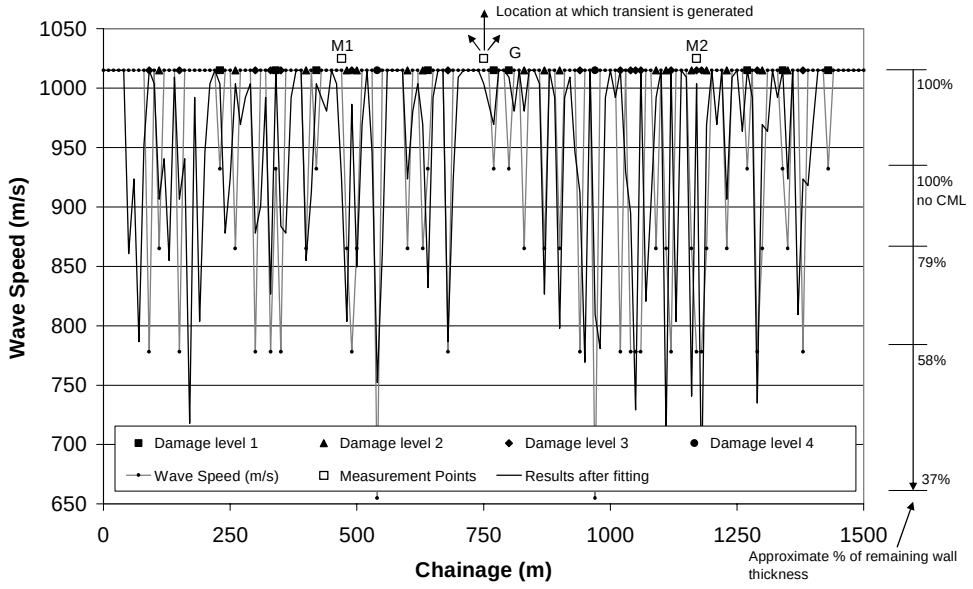

Figure 10-36 – Estimated and predicted patterns of damage along the 1500m long section of the MTP encompassing scour valve 22 and air valves 39 and 41

Figure 10-37 shows that the measured artificial and predicted fitted responses determined after the inverse analysis are similar at the location of the transient generator (i.e., scour valve 22). This is despite the discrepancies between the estimated and fitted patterns of damage noted above and indicates that the inverse algorithm is operating on relatively small differences in pressure once the match

between the measured and predicted responses becomes close. This means that the information contained in small trends and reflections in the measured responses are important if accuracy is to be maximised. Figures 10-38 and 10-39 show that the measured and predicted responses determined after fitting are also similar at measurement locations 1 (air valve 39) and 2 (air valve 41).

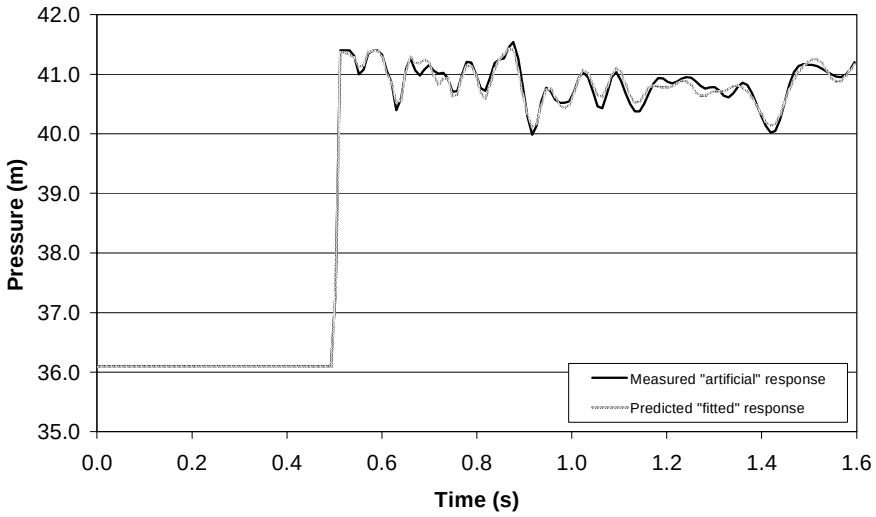

Figure 10-37 – Estimated and fitted transient responses at the transient generator (scour valve 22) after inverse analysis of the pseudo-field pipeline

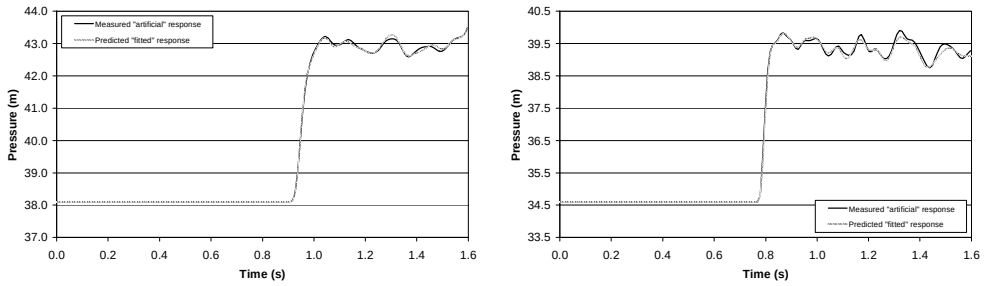

Figure 10-38 and 10-39 – Estimated and fitted transient responses at measurement locations 1 (air valve 39) and 2 (air valve 41), respectively

10.5 Summary

The hydraulic noise identified in Chapter 7, and found to be problematic in the context of Inverse Transient Analysis (ITA) for leak detection in Chapter 9, is examined in more detail in this chapter. The field tests conducted on the Morgan Transmission Pipeline (MTP) in August 2004, with a modified nozzle, to reduce the effects of flow turbulence or "flutter", exhibited relatively insignificant hydraulic noise prior to the induction of each controlled transient. However, significant hydraulic noise was observed following the induction of each transient. This hydraulic noise was structured and a consistent pattern of reflections was observed for repeated tests (even with different pipeline boundary conditions). Eventually, the pattern of reflections was dispersed and damped by a combination of the effects of fluid friction, entrained air and mechanical motion and vibration (and possibly the formation of flexural and shear waves).

The condition of the MTP between chainage 15000m and 15400m, 17200m and 17700m and, finally, 16000m and 16400m is described in this chapter based on CCTV camera investigation and information provided by the South Australian Water Corporation. This information is used to categorise 10m lengths of the MTP between the abovementioned chainages in terms of cement mortar lining delamination, wall corrosion and accumulations of pieces of lining. Physical explanations for the pattern of structured reflections observed in the measured responses, which may be related to the condition of the lining and pipe wall, are explored including reflections from trapped air pockets and discrete protrusions (formed by accumulations of delaminated lining). These physical mechanisms do not explain the observed reflections. Fluid Structure Interaction (FSI) has previously been considered in Chapter 7 and does not account for the observed reflections.

The hypothesis that the structured reflections are related to variations in wave speed (and pipeline impedance), where lining has delaminated and/or wall corrosion has occurred, is presented in this chapter. Four different categories of damage to the lining and wall condition of the MTP, together with the undamaged condition, are described in terms of wave speed over 10m (and also 5m) lengths of pipeline. Different distributions of these categories are then applied on a trial and error basis to infer the

condition of the MTP either side of the section between chainage 15000m and 15400m (for which the condition of the pipeline is known). The objective of the trial and error process was to match the predicted response, obtained using a forward transient model, with the measured response using a known or inferred pattern of damage.

The result has been a reasonable match between the predicted and measured transient responses using a combination of the known and inferred pipeline condition. This suggests that the inferred pipeline condition may be representative of the physical condition of the relevant lengths of pipeline. Significantly, the ability to interpret the structured reflections using forward transient models, and global optimisation algorithms (to replace trial and error inference of pipeline condition), may allow variations in the condition of pipeline linings and walls to be determined using measured transient responses.

Chapter 11

Distribution Pipeline Tests and Transient Modelling

No reported transient tests or analysis could be identified in the literature for individual pipelines within water distribution systems. This may be because of the physical complexity of such pipelines and the difficulties in inducing sufficiently sharp transients to acquire interpretable reflection information. Details of three pipelines within water distribution systems, at the scale of individual residential streets, are introduced in this chapter. The first two pipelines, called the Saint Johns Terrace Pipeline (SJTP) and Kookaburra Court Pipeline (KCP), are in close geographical proximity to each other (both being located within a small gravity distribution system called the Willunga Network). The third pipeline, called the Foster Street Pipeline (FSP), is geographically remote from the other two and located close to the City of Adelaide, South Australia. Figure 11-1 shows the location of SJTP and KCP within the Willunga Network.

The method for generating the transients involved the rapid closure of a side discharge valve transient generator as described in Chapter 6. Druck PDCR-810 pressure transducers, mounted inside “dummy” fire plug caps, were typically installed within existing fire plug chambers. The pressure measurement stations recorded the transient response of the distribution pipelines at either 500Hz or 2000Hz and were synchronised, as described in Chapter 6, using voltage pulses transmitted between stations along cables.

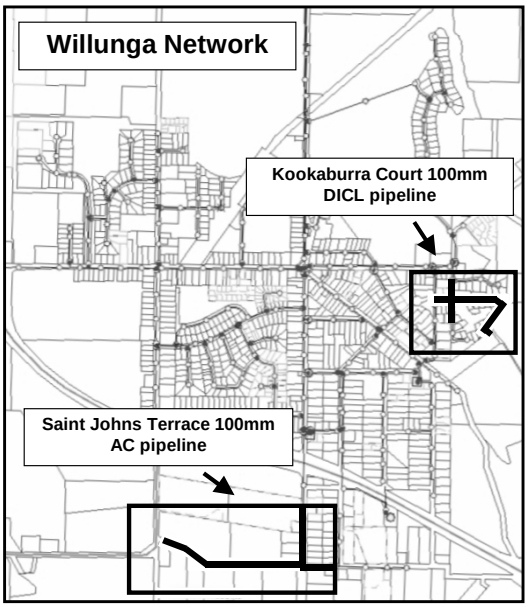

Figure 11-1 – Locality of Saint Johns Terrace Pipeline (SJTP) and Kookaburra Court Pipeline (KCP) within the Willunga Network, South Australia

As mentioned in Chapter 5, water distribution pipelines are subject to physical uncertainties including topological complexity, soil/pipe interaction and the effects of flexible pipe joints. Nevertheless, their small size means that reflections from faults, such as blockages, air pockets and leaks, are discernable. However, it is difficult to isolate the information from these faults amongst reflections from other sources. Existing algorithms for field complexities are applied to interpret the results of the field tests conducted on the distribution pipelines. It is anticipated that the application of existing algorithms will not be able to describe the measured transient responses. Rather, conceptual calibration models, based on the algorithms described in Chapter 5, will need to be developed.

11.1 Physical descriptions and test details

An assessment of conventional complexities such as demands, quantity of entrained air, wave speed and pipe wall condition, roughness and minor losses for the Saint Johns Terrace Pipeline (SJTP), Kookaburra Court Pipeline (KCP) and Foster Street Pipeline (FSP) is presented in Appendix W. This assessment confirms that the effects

of demands and entrained air are not significant during the transient tests (because of precautionary measures taken before the tests). Wave speeds for the three distribution pipelines are determined on the basis of the timed arrival of wave fronts at different measurement stations. Pipe roughness is determined using steady state pressure measurements and significant minor losses are identified.

In the context of below ground (i.e., buried) distribution system pipelines, physical complexities, in addition to the conventional complexities mentioned above, include the potential for mechanical motion and vibration as well as effects from complex water service connection topology, the behaviour of numerous individual flexible joints and soil/pipe interaction. The response of each of these physical complexities contributes to dispersion and damping of the measured transient responses of distribution pipelines. Apart from the theoretical complexities of the response of flexible joints and soil/pipe interaction, as discussed in Chapter 5, the sheer scope for physical variation, in terms of the numbers and condition of individual elements, suggests that the measured transient responses from such pipelines will be highly complex.

11.1.1 Physical description and test details for the SJTP

Physical description of the Saint Johns Terrace Pipeline (SJTP)

The general details and configuration of the pipeline during testing are shown in Figure 11-2. The SJTP is 575m long, comprises 100mm nominal diameter “Class D” Asbestos Cement (AC) pipe (manufactured in accordance with obsolete Australian Standard AS 1711 – 1975). The SJTP exists as a natural branch on the perimeter of the Willunga Network and the boundary conditions comprise a “T” intersection with the main network and a naturally occurring dead end. An existing in-line gate valve was used to simulate different extents of discrete blockage (as described in Chapter 6). The presence of the in-line gate valve partly along the length of the pipeline was the main motivation for conducting tests on the SJTP.

The in-line gate valve is located approximately 382.4m along the pipeline from the "T" intersection with the main network. An equivalent gate valve, removed from the Willunga Network, has been calibrated in the laboratories of the University of Adelaide, at different percentage openings, as described in Appendix I. The transient generator was installed on a fire plug located 273.5m from the "T" intersection. For a percentage of the transient tests, a baseflow was established along the SJTP and through an additional standpipe located at the end of the pipeline. A 25mm diameter orifice was installed to restrict the magnitude of this baseflow.

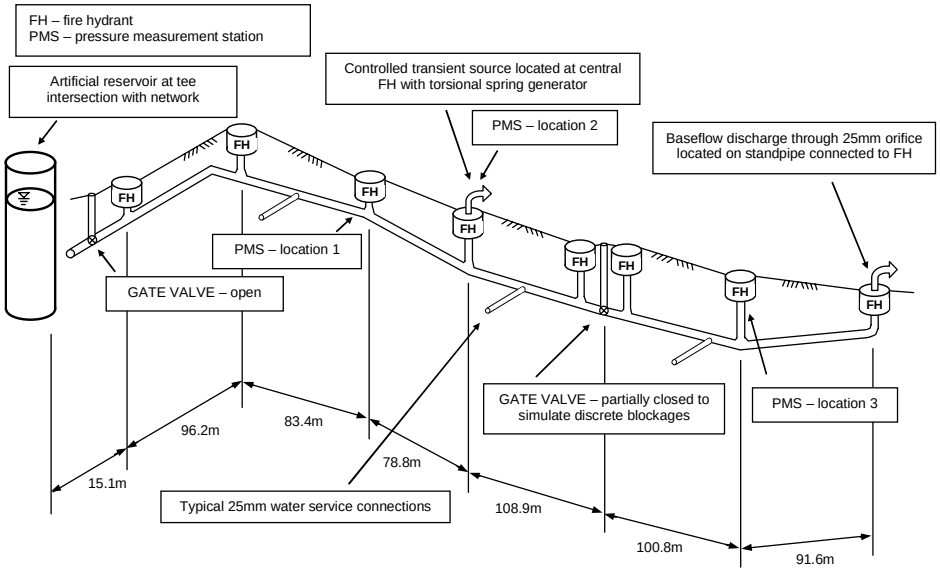

Figure 11-2 – Basic layout and details of the Saint Johns Terrace Pipeline (SJTP)

The SJTP was manually surveyed, as part of a larger survey of the Willunga Network, using a "Total Station" electronic level and position survey instrument and this information was verified using "as constructed" plans as described in Appendix K. There are 8 fire plugs located at road level along the length of the SJTP. Risers of various lengths are used to connect these fire plugs to the pipeline. There are 6 by 25mm water service connections.

Each in-line gate valve and fire plug is installed using flexible rubber ring collar joints as described in Chapter 5. Additional flexible joints are provided at a 3m to 6m spacing to join the sections of Asbestos Cement (AC) pipe comprising the SJTP. Each

joint reduces the level of restraint and increases the potential for mechanical losses (particularly at changes in direction or at dead ends). Soil/pipe interaction is anticipated because the ratio of the modulus of the backfill in the pipe trenches, as consolidated by road traffic, to the elastic modulus of the AC pipe (as determined in the laboratory and specified in Appendix D), is less than 500. Finally, water service connections are directly connected to the SJTP and water meters are installed on each water service connection.

Test details for the Saint Johns Terrace Pipeline (SJTP)

On the 23rd July 2003, five controlled transient tests were performed as listed in Table 11-1 which also specifies the configuration of the Saint Johns Terrace Pipeline (SJTP), including initial flow conditions, whether a side discharge valve closure or opening was used to induce controlled transients, the size of the nozzle mounted in the transient generator, recording rate and purpose of each test. The SJTP was in its "in-situ" condition without baseflow for all five tests.

Table 11-1 – Summary of controlled transient tests for the SJTP on 23rd July 2003

Test	Valve Configuration	Flow Condition	Type of Motion	Discharge Nozzle	Recording Stations	Rate	Purpose
1	Fully open	No baseflow	Closure	6mm	1, 2 and 3	500Hz	"In-situ" condition
2	Fully open	No baseflow	Closure	8mm	1, 2 and 3	500Hz	"In-situ" condition
3	Fully open	No baseflow	Closure	10mm	1, 2 and 3	500Hz	"In-situ" condition
4	Closed	No baseflow	Closure	6mm	1, 2 and 3	500Hz	Closed valve
5	Closed	No baseflow	Closure	10mm	1, 2 and 3	500Hz	Closed valve

On the 15th August 2003, a mix of fourteen controlled transient tests were performed as listed in Table 11-2, without and with baseflow along the pipeline, and with the in-line gate valve either open or only partially open. The baseflow was created by opening a 25mm diameter orifice, mounted on a standpipe, located at the dead end of the SJTP. Pressure transducers were located at measurement stations 2 and 3 (i.e., upstream and downstream of the gate valve) and an 8mm nozzle was installed in the transient generator.

Table 11-2 – Summary of controlled transient tests for the SJTP on 15th August 2003

Test	Valve Configuration	Flow Condition	Type of Motion	Discharge Nozzle	Stations	Rate	Purpose
1	Fully open	No baseflow	Closure	8mm	2 and 3	500Hz	"In-situ" condition
2	Fully open	No baseflow	Closure	8mm	2 and 3	500Hz	"In-situ" condition
3	Fully open	Baseflow	Closure	8mm	2 and 3	500Hz	"In-situ" condition
4	Fully open	Baseflow	Closure	8mm	2 and 3	500Hz	"In-situ" condition
5	"1/2" turn open	Baseflow	Closure	8mm	2 and 3	500Hz	Discrete blockage
6	"1/2" turn open	Baseflow	Closure	8mm	2 and 3	500Hz	Discrete blockage
7	"1/2" turn open	Baseflow	Closure	8mm	2 and 3	500Hz	Discrete blockage
8	"1/2" turn open	Baseflow	Closure	8mm	2 and 3	500Hz	Discrete blockage
9	"5/8" turn open	Baseflow	Closure	8mm	2 and 3	500Hz	Discrete blockage
10	"5/8" turn open	Baseflow	Closure	8mm	2 and 3	500Hz	Discrete blockage
11	"5/8" turn open	Baseflow	Closure	8mm	2 and 3	500Hz	Discrete blockage
12	"5/8" turn open	Baseflow	Closure	8mm	2 and 3	500Hz	Discrete blockage
13	"1" turn open	Baseflow	Closure	8mm	2 and 3	500Hz	Discrete blockage
14	"1" turn open	Baseflow	Closure	8mm	2 and 3	500Hz	Discrete blockage

On the 26th August 2003, a mix of ten controlled transient tests were performed as listed in Table 11-3, with baseflow along the pipeline, and with the in-line gate valve either open or only partially open. Pressure transducers were located at measurement stations 1 and 2 (i.e., both upstream of the gate valve) and an 8mm nozzle was installed in the transient generator.

Table 11-3 – Summary of controlled transient tests for the SJTP on 26th August 2003

Test	Valve Configuration	Flow Condition	Type of Motion	Discharge Nozzle	Stations	Rate	Purpose
1	Fully open	Baseflow	Closure	8mm	1 and 2	500Hz	In-situ condition
2	Fully open	Baseflow	Closure	8mm	1 and 2	500Hz	In-situ condition
3	"1/2" turn open	Baseflow	Closure	8mm	1 and 2	500Hz	Discrete blockage
4	"1/2" turn open	Baseflow	Closure	8mm	1 and 2	500Hz	Discrete blockage
5	"1/2" turn open	Baseflow	Closure	8mm	1 and 2	500Hz	Discrete blockage
6	"1/2" turn open	Baseflow	Closure	8mm	1 and 2	500Hz	Discrete blockage
7	"1/2" turn open	Baseflow	Closure	8mm	1 and 2	2000Hz	Discrete blockage
8	"1/2" turn open	Baseflow	Closure	8mm	1 and 2	2000Hz	Discrete blockage
9	"1/2" turn open	Baseflow	Closure	8mm	1 and 2	2000Hz	Discrete blockage
10	"1/2" turn open	Baseflow	Closure	8mm	1 and 2	2000Hz	Discrete blockage

The transients induced in the SJTP on the 23rd July 2003 gave maximum pressure rises of approximately 90kPa and 130kPa for the 8mm and 10 mm discharge nozzles, respectively. Similar transient pressure rises were induced during the tests conducted on the 15th and 26th August 2003. These pressure rises did not concern operators from United Water. Data was recorded over a limited period of 0.8s. This time marginally exceeded that required for the transient wavefront to travel to the open "T" intersection and return to the nearest measurement station location.

11.1.2 Physical description and test details for the KCP

Physical description of the Kookaburra Court Pipeline (KCP)

The general details and configuration of the pipeline during testing are shown in Figure 11-3 together with the locations at which an artificial air pocket and leak were introduced along the KCP. The details of the artificial air pocket and leak were described in Chapter 6. The transient generator was installed on a fire plug located 318.1m from the "T" intersection. The method for generating the transients involved both the rapid closure and opening of a side discharge valve.

The KCP is 379.2m long, comprises 100mm nominal diameter "Class K9" Ductile Iron Cement Mortar Line (DICL) pipe (manufactured in accordance with Australian Standard AS 2280 – 1999) and forms part of the Willunga Network. The KCP exists as a natural branch on the perimeter of the Willunga Network and the boundary conditions comprise a "T" intersection with the main network and a naturally occurring dead end. An artificial air pocket and leak were introduced as known faults. The location of the KCP at the extremity of the Willunga Network, and the fact that it was DICL, were the main motivations for conducting tests on the KCP.

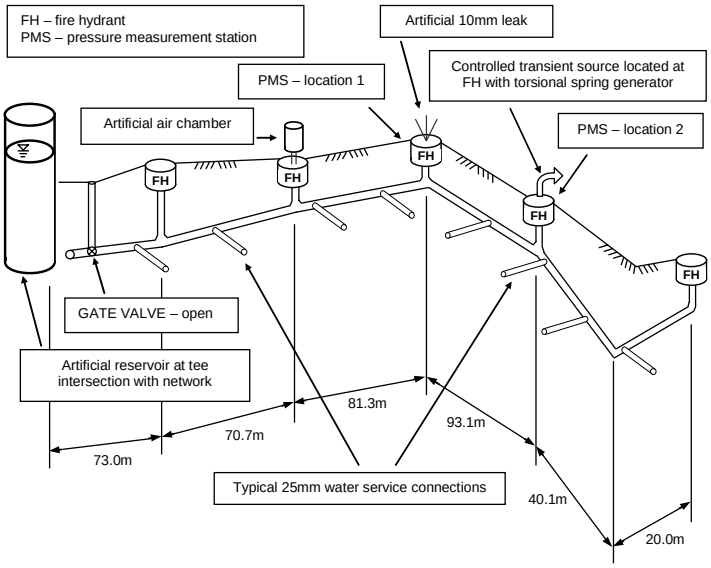

Figure 11-3 – Basic layout and details of the Kookaburra Court Pipeline (KCP)

The KCP was manually surveyed, as part of a larger survey of the Willunga Network, using a "Total Station" electronic level and position survey instrument and this information was verified using "as constructed" plans as described in Appendix K. There are 5 fire plugs located at road level along the length of the KCP. Risers of various lengths are used to connect these fire plugs to the pipeline. A 90 degree bend is located approximately 20m from the dead end of the KCP. There are 15 by 25mm water service connections.

Each in-line gate valve and fire plug is installed using flexible spigot and socket joints as described in Chapter 5. Additional flexible joints are provided at a 3m to 6m spacing to join the sections of Ductile Iron Cement Lined (DICL) pipe comprising the KCP. The effect of soil/pipe interaction is expected to be less significant for the KCP because the ratio of the modulus of the backfill in the pipe trenches, as consolidated by road traffic, to the elastic modulus of the DICL pipe is greater than 500. That said, the larger number of water service connections add significantly to the physical complexity of the pipeline.

Test details for the Kookaburra Court Pipeline (KCP)

On the 28th August 2003, twelve controlled transient tests were performed as listed in Table 11-4 which also specifies the configuration of the Kookaburra Court Pipeline (KCP), including initial flow conditions, whether a side discharge valve closure or opening was used to induce controlled transients, the size of the nozzle mounted in the transient generator, recording rate and purpose of each test. The KCP was either in its "in-situ" condition or had an artificial air pocket or leak installed at the locations shown above, and using the fittings, described in Chapter 6.

Table 11-4 – Summary of controlled transient tests for the KCP on 28th August 2003

Test	Configuration	Type of Motion	Discharge Nozzle	Recording Stations	Rate	Purpose
1	No air pocket or leak	Closure	6mm	1 and 2	500Hz	"In-situ" condition
2	No air pocket or leak	Closure	6mm	1 and 2	500Hz	"In-situ" condition
3	No air pocket or leak	Opening	6mm	1 and 2	500Hz	"In-situ" condition
4	No air pocket or leak	Opening	6mm	1 and 2	500Hz	"In-situ" condition
5	No air pocket or leak	Opening	6mm	2	2000Hz	"In-situ" condition
6	No air pocket or leak	Opening	6mm	2	2000Hz	"In-situ" condition
7	No air pocket or leak	Closure	6mm	2	2000Hz	"In-situ" condition
8	1.635L air pocket	Opening	6mm	1 and 2	500Hz	Air pocket response
9	1.635L air pocket	Opening	6mm	1 and 2	500Hz	Air pocket response
10	10 mm leak	Opening	6mm	2	500Hz	Leak response
11	10 mm leak	Opening	6mm	2	500Hz	Leak response
12	10 mm leak	Opening	6mm	2	2000Hz	Leak response

As reported in Table 11-4, side discharge valve closures and openings were used to generate controlled transients in the KCP on the 28th August 2003. Positive transients (i.e., transients associated with an increase in pressure in the pipeline) were induced in the KCP by closing the side discharge valve giving an initial maximum pressure rise of approximately 65kPa at station 2. A maximum pressure rise of 105kPa was recorded after wavefront reflection from the dead end of the KCP.

Negative transients (i.e., transients associated with a decrease in pressure in the pipeline) were induced in the KCP by opening the side discharge valve giving an

initial minimum pressure drop of approximately 55kPa at station 2. A minimum pressure drop of 105kPa was recorded after wavefront reflection from the dead end of the KCP. Data was recorded over a limited period of 0.7s. This time marginally exceeded that required for the transient wavefront to travel to the open "T" intersection and return to the nearest measurement station.

11.1.3 Physical description and test details for the FSP

Physical description of the Foster Street Pipeline (FSP)

The general details and configuration of the pipeline during testing are shown in Figure 11-4. The FSP is approximately 358.2m long by 80mm nominal diameter Cast Iron Cement Mortar Line (CICL) pipe. The pipeline was not manufactured in accordance with any known standard and was laid in 1932. The FSP exists as a connecting pipeline within a grid-like larger network and the boundary conditions comprise "T" intersections at either end. The main motivation for conducting tests on the FSP was a record of low pressure and water quality complaints from two residents near the middle of the street. It was thought that these complaints indicated the presence of tuberculation along the parts of the pipeline.

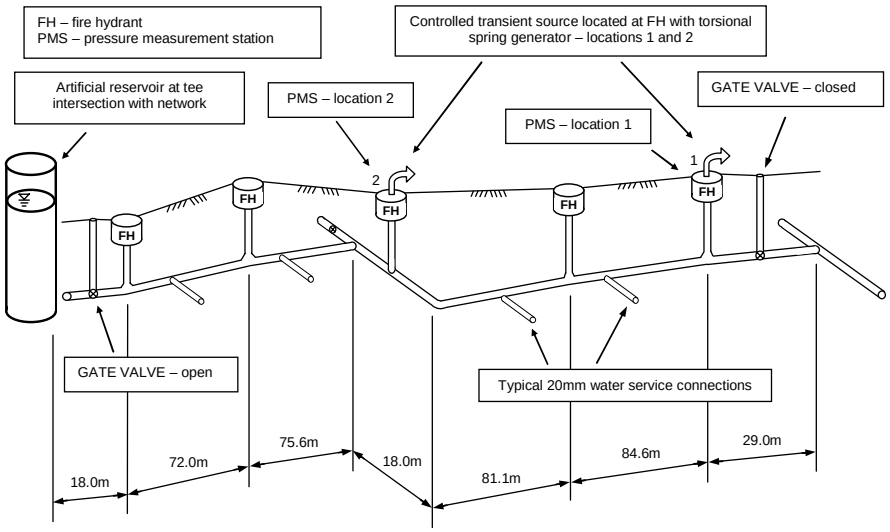

Figure 11-4 – Basic layout and details of the Foster Street Pipeline (FSP)

"Total Station" survey was not undertaken for the FSP because United Water operators had obtained manual survey information in order to develop a contract for the replacement of the pipeline in April 2005. This survey information was compared to existing "as constructed" records and the plan and elevation information describing the FSP was found to be consistent. There are 5 fire plugs located at road level along the length of the FSP. Risers of various lengths are used to connect these fire plugs to the pipeline. There are 22 by 20mm water service connections.

Each in-line gate valve and fire plug is installed using flexible spigot and socket joints as described in Chapter 5. Additional flexible joints are provided at a 3m to 6m spacing to join the sections of Cast Iron Cement Lined (CICL) pipe comprising the FSP. As for the Kookaburra Court Pipeline (KCP), the effect of soil/pipe interaction is expected to be less significant than for the Saint Johns Terrace Pipeline (SJTP). However, there is a greater number of water service connections for the FSP than KCP as well as existing sections of pipeline with significant tuberculation.

Given that the FSP was not a natural branch, it was necessary to close the in-line gate valve at the western end of the pipeline to isolate it from the influence of the existing network beyond this location. At the same time, the in-line gate valve at the eastern end of the pipeline needed to remain open to maintain continuity of supply to the residents and transient generator. In effect, the local network was decomposed to favourably configure the FSP for the transient tests without interrupting supply. The formation of an artificial branch pipeline allowed the FSP to be individually assessed. The concept of network decomposition is further explained in Appendix W. Transient inputs were generated at two locations to increase the likelihood of identifying reflections from either end of any tuberculated sections.

Test details for the Foster Street Pipeline (FSP)

On the 16th July and 7th August 2003, four controlled transient tests were performed as listed in Table 11-5 which also specifies whether a side discharge valve closure or opening was used, the size of the nozzle mounted in the transient generator and

recording rate. The purpose of the tests was to obtain measured transient responses from a pipeline with in-situ extended blockage (i.e., tuberculation).

Table 11-5 – Summary of controlled transient tests for the FSP on the 16th July and 7th August 2003

Test	Date	Transient Generator Location	Type of Motion	Discharge Nozzle	Recording Stations	Rate
1	16/07/2003	Station 1	Closure	6mm	1 and 2	500Hz
2	16/07/2003	Station 1	Closure	6mm	1 and 2	500Hz
3	7/08/2003	Station 2	Closure	6mm	1 and 2	500Hz
4	7/08/2003	Station 2	Closure	6mm	1 and 2	500Hz

11.2 Positive and negative transients for the KCP

Figure 11-5 shows the response of the Kookaburra Court Pipeline (KCP), measured at station 2, to controlled positive transients. Various features are apparent in the measured response including reflections from the dead end of the KCP and the "T" intersection with the Willunga Network at approximately 0.21s and 0.55s, respectively. A collapse and then partial recovery in the pressure plateau following the reflection from the dead end is apparent. Distinct reflections in the response of the KCP, which cannot be attributed to any known element, are apparent. These reflections represent the cumulative response of the combined physical complexities of the KCP. The oscillation following the induction of the transient is due to "ringing" in the transient generator and will be discussed later in this chapter.

Figure 11-6 shows the response of the KCP, measured at station 2, to controlled negative transients. Various features are again apparent in the measured response including reflections from the dead end of the KCP and the "T" intersection with the Willunga Network at approximately 0.21s and 0.55s, respectively. Notably, there is no collapse in the magnitude of the negative pressure plateau after the reflection from the dead end of the KCP. As for positive transient test, distinct reflections in the response of the KCP, which cannot be attributed to any known element, are apparent. However, there appears to be significantly less damping.

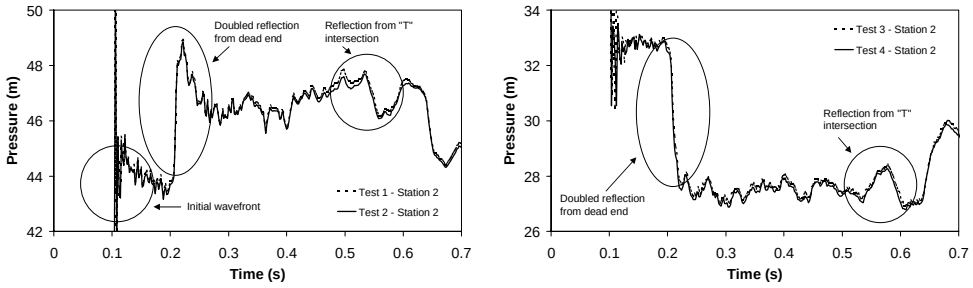

Figures 11-5 and 11-6 – Measured responses for tests 1 and 2 and tests 3 and 4, conducted on 28th August 2003, over 0.7 seconds at station 2

The induction of positive and negative transients in the KCP, and the responses to each, provides an important insight into the effect of the physical complexities, including mechanical motion and vibration, flexible joints and soil/pipe interaction, and how they might be acting to disperse and damp the observed transients. Figure 11-7 shows the dimensionless comparison of measured responses for test 1, a positive transient, and test 3, a negative transient (inverted), at station 2. The initial dimensionless pressure rise for both tests is approximately 1.

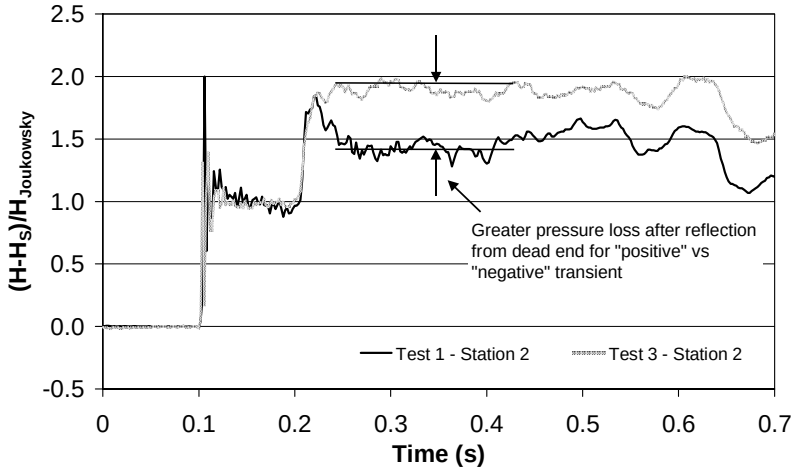

Figure 11-7 – Measured positive response for test 1 versus inverted negative response for test 3 over 0.7 seconds at station 2

A significant discrepancy emerges between the responses to the positive and negative transients after the reflection from the dead end of the KCP. A collapse in the pressure plateau is evident for test 1. In contrast, the pressure plateau is relatively constant for the negative transient induced during test 3 (as inverted). The fact that no positive thrust is exerted at the dead end of the KCP may partly explain these observations. Instead of a volume of water being forced into and along the KCP towards the dead end, following the induction of a positive transient, a volume of water is abstracted from the KCP, including the section up to the dead end, and this creates a negative thrust or pulls on the dead end. Furthermore, physical complexities such as water service connections, fire plugs and risers, existing roughness and flexible joints may dissipate more energy following a rapid increase in pressure (i.e., for a positive transient) as axial and outward circumferential thrust is transferred, via mechanical vibration and/or movement, to surrounding soils.

The proposed hypothesis is therefore that there is considerable mechanical motion and vibration at flexible joints (sliding friction) due to variable restraint from soil/pipe (joint) interaction and that this is responsible for a significant proportion of the observed dispersion and damping of the measured responses of the KCP (and also other distribution pipelines with similar physical complexity). The observation that more damping occurs when the pressure is increased, as opposed to when it is decreased, supports the hypothesis. There are numerous precedents in other fields of engineering where mechanical friction and damping (directly proportional to a pressure increase or internal dynamic load in the case of a positive transient) is replicated using equivalent “viscous” dispersion and damping. This hypothesis forms part of the justification for the development of the conceptual transient model proposed in Chapter 5.

11.3 Development of traditional transient models

As mentioned in Chapter 7, an explicit Method of Characteristics (MOC) scheme has been implemented in a transient model (called BSOLVER) to determine the response of single and branched pipe systems. The model includes algorithms for the calculation of the effect of unsteady friction and discrete air pockets and/or entrained

air, as elaborated in Appendices E and O, and a listing of the Fortran source code developed by the author is included in Appendix M.

The program is applied to conduct the forward transient modelling of the Saint Johns Terrace Pipeline (SJTP) and the Kookaburra Court Pipeline (KCP) reported below. The forward transient modelling of the Foster Street Pipeline (FSP) is conducted using the same program in Chapter 13 after the detailed condition of the pipeline, including the extent of tuberculation, is described. The forward transient program is modified and linked to the NLFIT suite of Bayesian non-linear regression programs, developed by Kuczera (1994), in order to perform the inverse analysis described in Chapters 12, 13 and 14. The modified subroutines developed by the author for this analysis are presented in Appendix M.

The results of the forward transient modelling will be compared to the measured responses from the SJTP and KCP without any artificially introduced faults in this chapter. Complex calibrated conceptual models will be investigated in Chapter 12. Comparisons between measured and predicted transient responses obtained using traditional and more complex calibrated conceptual models, with artificial faults, are presented in Chapters 13 and 14.

11.3.1 Traditional model for the Saint Johns Terrace Pipeline

The Saint Johns Terrace Pipeline (SJTP) has a total length of 574.8m and is discretised into 496 sub-pipe segments (each 1.16m long). A wave speed varying between 1061m/s and 1159m/s is applied giving a time step in the calculations of 1ms and a minimum Courant number of 0.915. A linear timeline interpolation scheme is implemented in the model and a pipe roughness of 1mm is used. The wave speeds and pipe roughness are taken from the assessment presented in Appendix W. The transient generator is located approximately 273.5m along the pipeline measured from the open “T” intersection end. Boundary conditions are formed by the natural dead end of the SJTP and the open “T” intersection with the network. The pressure at the “T” intersection is varied to match the measured pressure at the start of each transient test

but is not thereafter adjusted (i.e., the pressure at the "T" intersection is not a variable boundary condition).

It was not possible to accurately survey the 6 private water service connections along the SJTP. Even if the original details of the pipe work had been able to be ascertained, the physical condition of the plumbing, at the time of the tests, was unknown. As a consequence, the 6 water service connections have been approximated by including 10m long branches of 25mm diameter pipe at each offtake. Individual water meters are represented using 20mm orifices located approximately 3.5m along each offtake (measured from the SJTP). The transient generator, and other vertical risers beneath the fire plugs along the SJTP, have been included in the forward transient model as vertical branches using the nearest multiple of the sub-pipe segment length.

Results of traditional transient modelling without baseflow

Figures 11-8 and 11-9 show the comparison between the measured and predicted responses, obtained using a traditional forward transient model with unsteady friction over a time scale of 0.8s, at station 1, for tests 2 and 3 from the 23rd July 2003, respectively. Discrepancies, comprising a loss and then recovery of pressure along the measured transient plateau, relative to the predicted response, are apparent following the arrival of the incident wavefront. Further discrepancies, following the arrival of the reflection from the "T" intersection are not relevant to the analysis because an artificial boundary condition is assumed at the "T" intersection.

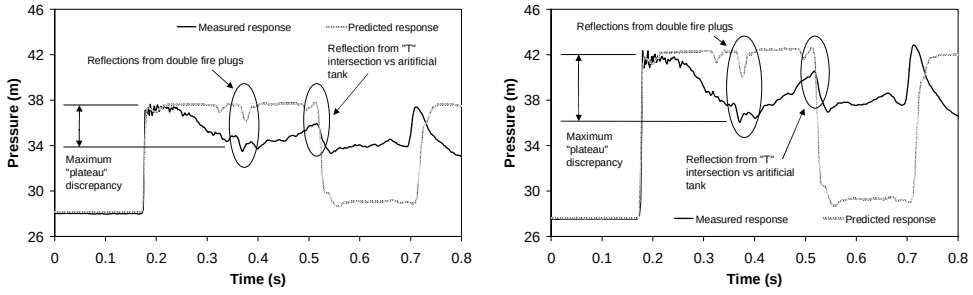

Figures 11-8 and 11-9 – Measured and predicted responses for tests 2 and 3, with 8mm and 10mm nozzles and without baseflow, at station 1

Figures 11-10 and 11-11 show the comparison between the measured and predicted responses, obtained using a traditional forward transient model with unsteady friction over a time scale of 0.8s, at station 2, for tests 2 and 3 from the 23rd July 2003, respectively. Discrepancies, comprising a loss and then recovery of pressure along the measured transient plateau, relative to the predicted response, are again apparent. The forward transient model approximately reproduces a "ringing" effect at the transient generator, associated with the standpipe between the nozzle and the SJTP below, and the reflections from known point features including the fire plug risers either side of the in-line gate valve.

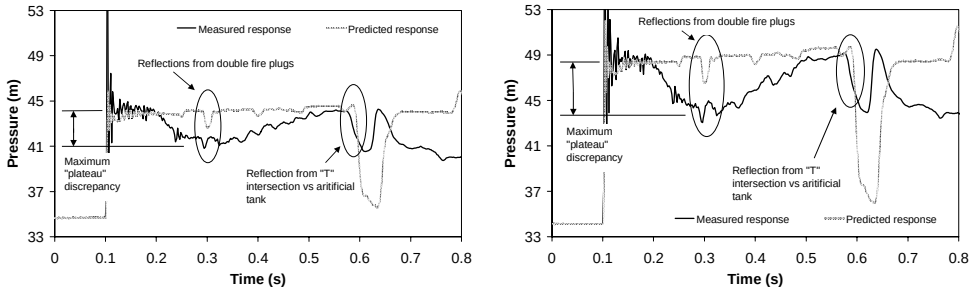

Figures 11-10 and 11-11 – Measured and predicted responses for tests 2 and 3, with 8mm and 10mm nozzles and without baseflow, at station 2

Results of traditional transient modelling with baseflow

Figures 11-12 and 11-13 show the comparison between the measured and predicted responses, obtained using a traditional forward transient model with unsteady friction over a time scale of 0.8s, for test 3 from the 15th August 2003, conducted with baseflow, at stations 2 and 3, respectively. The comparison at station 2 shows that there is a discrepancy along the transient plateau that is similar to that observed without baseflow. The comparison at station 3 shows a discrepancy along the transient plateau and between the measured and predicted reflection from the discharging orifice used to establish the baseflow at the dead end of the Saint Johns Terrace Pipeline (SJTP).

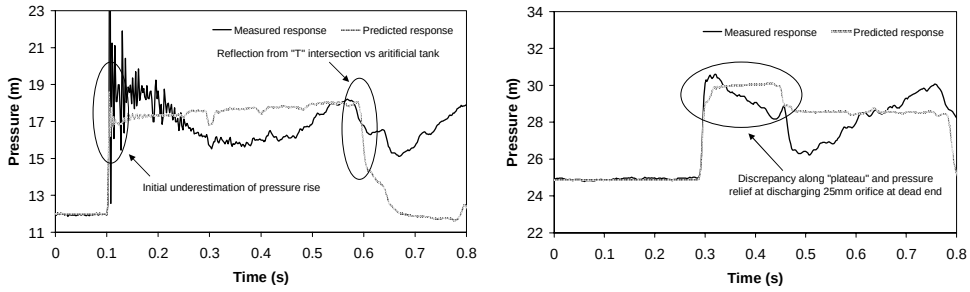

Figures 11-12 and 11-13 – Measured and predicted responses for test 3, with an 8mm nozzle and with baseflow, at stations 2 and 3

Figures 11-14 and 11-15 show the comparison between the measured and predicted responses, obtained using a traditional forward transient model with unsteady friction over a time scale of 0.8s, for test 1 from the 26th August 2003, conducted with baseflow, at stations 1 and 2, respectively. The comparison at both stations again reveals a discrepancy between the measured and predicted responses along the transient plateaus.

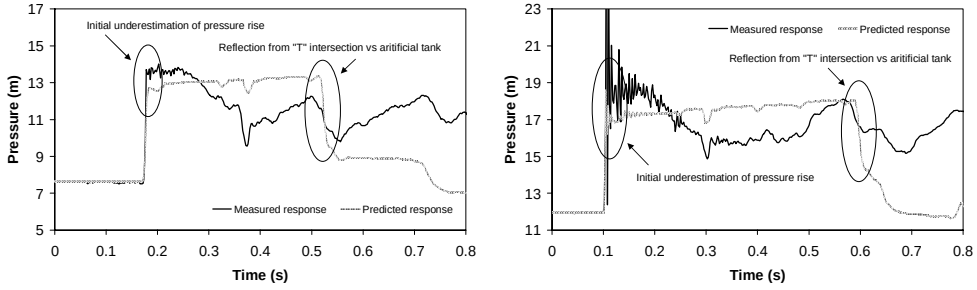

Figures 11-14 and 11-15 – Measured and predicted responses for test 1, with an 8mm nozzle and with baseflow, at stations 1 and 2

Transient generator effect for the Saint Johns Terrace Pipeline

The 1.25m high transient generator standpipe, in combination with the rapid closure of the 15mm diameter ball valve regulating discharge through the nozzles, over approximately 4ms, produces a short lived and localised oscillating pressure response within the standpipe described above and hereafter as “ringing” (a more stable rise or

fall in pressure is established in the main pipeline). Figure 11-16 shows the measured transient responses at station 2, recorded at rates of 500Hz and 2000 Hz, for tests 5 and 7, conducted on the 15th and 26th August 2003, respectively. Discrepancies are apparent between the responses measured at 500Hz and 2000Hz with the form of the "ringing" better captured at the higher frequency. The higher frequency oscillations damp out within approximately 0.05s following the induction of the transient.

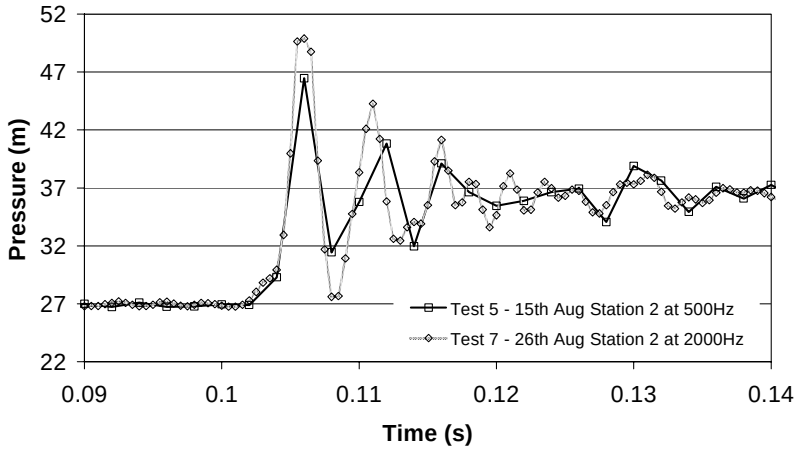

Figure 11-16 – Measured responses for tests 5 and 7, at station 2, over 0.05 seconds, recorded at 500Hz and 2000Hz, respectively

At the time the tests were conducted, no other practical way of mounting a side discharge standpipe, with a rapid operation valve mechanism, on fire plug valves located in underground access chambers had been developed. Furthermore, access to the main pipe can generally only be achieved through existing fire plugs. Significantly, these fire plugs are mounted on 0.5m to 1.5m long vertical risers, as the embedment depth of the main varies, so that a standard access chamber depth of 0.9m can be maintained. As a consequence, transients induced through existing fire plugs will exhibit some form of oscillatory response, regardless of whether a transient generator standpipe or some other device is used. That said, the magnitude of the oscillatory effect can be reduced if the combined length of standpipe and riser is minimised.

The speed of operation of the valve mechanism also contributes to the "ringing" effect. Using a slower closure or opening will reduce the effect of the "ringing". However, the sharpness of the incident transient wavefront is critical if structure, including faults such as discrete blockages, air pockets and leaks, are to be clearly identified. It was considered more important to generate a sharp input, and include the "ringing" effect in any subsequent analysis, than to use a slower input and compromise the information content of the measured transient responses.

11.3.2 Traditional model of the Kookaburra Court Pipeline

The Kookaburra Court Pipeline (KCP) has a total length 378.1m and is discretised into 321 sub-pipe segments (each 1.18m long). A wave speed varying between 1087m/s and 1178m/s is applied giving a time step in the calculations of 1ms and a minimum Courant number of 0.930. A linear timeline interpolation scheme is implemented in the model and a pipe roughness of between 1mm and 4mm is used. The wave speeds and pipe roughness are taken from the assessment presented in Appendix W. The transient generator is located approximately 318.1m along the pipeline measured from the open "T" intersection end. Boundary conditions are formed by the natural dead end of the KCP and the open "T" intersection with the network. The pressure at the "T" intersection is varied to match the measured pressure at the start of each transient test but is not thereafter adjusted (i.e., the pressure at the "T" intersection is not a variable boundary condition).

As for the Saint Johns Terrace Pipeline (SJTP), it was not possible to accurately survey the 15 private water service connections along the KCP. As a consequence, the 15 water service connections have been approximated by including 10m long branches of 25mm diameter pipe at each offtake. Individual water meters are represented using 20mm orifices located approximately 3.5m along each offtake (measured from the KCP). The transient generator, and other vertical risers beneath the fire plugs along the KCP, have been included in the forward transient model as vertical branches using the nearest multiple of the sub-pipe segment length.

Results of traditional transient modeling for a negative transient

Figure 11-17 shows the comparison between the measured and predicted responses, obtained using a traditional forward transient model with unsteady friction over a time scale of 0.7s, at station 2, for test 3, conducted during August 2003. Discrepancies, including overestimation of the predicted pressure, relative to the measured transient plateau, following the arrival of the reflected wavefront from the dead end of the Kookaburra Court Pipeline (KCP), together with reflections from unknown features along the KCP, are apparent. This is despite the inclusion of the best available physical information regarding pipe diameter, class, water service locations (and sizes) and fire plug risers. Further discrepancies, following the arrival of the reflection from the "T" intersection are not relevant to the analysis because an artificial boundary condition is assumed at the "T" intersection

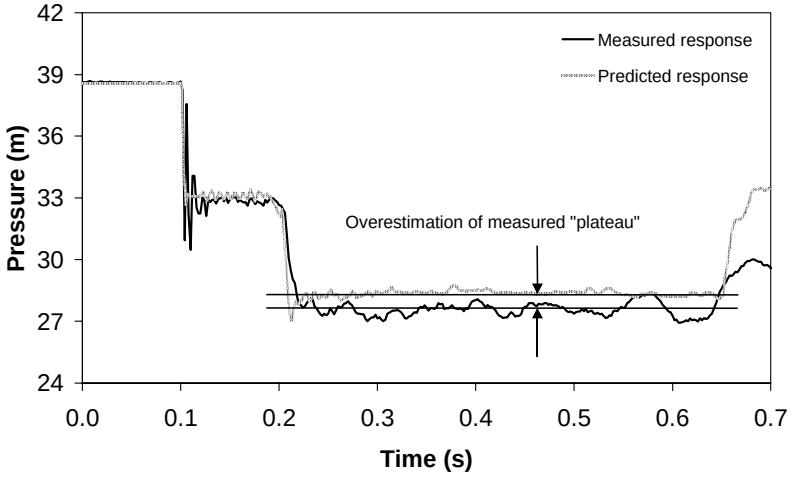

Figure 11-17 – Measured and predicted responses for test 3 (negative transient), with a 6mm nozzle, at station 2

There is circumstantial evidence, comprising anecdotal operator experience specific to the KCP, steady state roughness analysis and a 16.7% reduction in apparent wave speed, relative to the estimated theoretical wave speed, that suggests that there are physical complexities associated with the KCP which are neither known nor included in the forward transient model. It is possible that the effect of these complexities, when subject to a negative transient wavefront, is to magnify the negative reflection

from the dead end of the KCP. In this context, the behaviour of the dead end of the KCP, when subject to suction or pulling thrust during a negative transient, is a major uncertainty. The results from the negative transient tests (e.g., test 3) are used to develop a conceptual calibration model in Chapter 12 because the measured responses appear less affected by mechanical friction and damping (relative to the measured responses for the positive transients).

Transient generator effect for the Kookaburra Court Pipeline

As for the results from the tests on the Saint Johns Terrace Pipeline (SJTP), the 1.25m high transient generator standpipe, in combination with the rapid closure or opening of the 15mm diameter ball valve regulating discharge through the nozzles, over approximately 4ms, produces a short lived and localised oscillating pressure response within the standpipe ("ringing"). Figure 11-18 shows the measured transient responses at station 2, recorded at rates of 500Hz and 2000 Hz, for tests 1 and 7, conducted on the 28th August 2003, respectively. Discrepancies are apparent between the responses measured at 500Hz and 2000Hz with the form of the "ringing" effect for these positive transient tests better captured at the higher frequency. The high frequency oscillations damp out within approximately 0.03s following the induction of the positive transients.

Figure 11-19 shows the measured transient responses at station 2, recorded at rates of 500Hz and 2000Hz, for tests 3 and 5, conducted on the 28th August 2003, respectively. The "ringing" effect for these negative transient tests is better captured at a recording rate of 2000Hz over the first 0.05s of the responses. The high frequency oscillations damp out within approximately 0.02s. The magnitude of oscillation induced following the negative transients is significantly reduced relative to that following the positive transients. It is likely that sustained discharge through the 6mm nozzle is responsible for the extra damping.

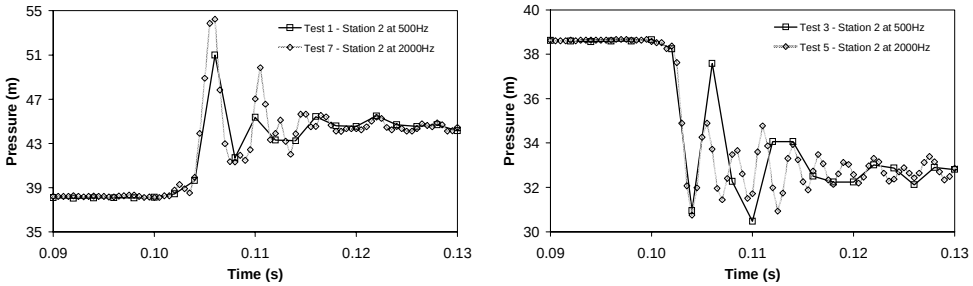

Figures 11-18 and 11-19 – Measured responses for tests 1 and 7, and tests 3 and 5, at station 2, over 0.04 seconds, recorded at 500 and 2000Hz, respectively

11.4 Summary

Physical complexities relevant to distribution pipelines have been summarised in this chapter and include pipe, valve, flexible joint and water service connection elements. When subject to a transient event, these physical components can provide conditions suitable for, or contribute to, effects from mechanical motion and vibration (particularly at flexible joints) and soil/pipe interaction. Controlled transient tests performed on three distribution pipelines, the Saint Johns Terrace Pipeline (SJTP), the Kookaburra Court Pipeline (KCP) and the Foster Street Pipeline (FSP), are listed in this chapter. Results are presented for the SJTP and the KCP. The results of the tests on the FSP are presented in Chapter 13.

Traditional transient models have been developed in this chapter to obtain predicted transient responses for comparison with the measured responses. Comparisons between the measured and predicted response of the SJTP have been presented for the tests conducted with the pipeline in its in-situ condition. Some tests were conducted with a baseflow to determine the in-situ response of the SJTP, without discrete blockage, under these conditions. The significance of conducting tests with a baseflow is explained, in the context of blockage detection, in Chapter 13. Significant discrepancies between the measured and predicted responses have been identified in this chapter (for tests without and with baseflow). Explanations for these discrepancies, and the development of a conceptual calibration model for the SJTP to account for them, are investigated in Chapter 12.

A comparison between the measured and predicted response of the KCP, for a test conducted by opening the side discharge valve in the transient generator, and inducing a negative transient, has been presented for the pipeline in its in-situ condition. As for the SJTP, discrepancies between the measured and predicted responses have been identified. The development of a conceptual calibration model for the KCP is presented in Chapter 12.

The effect of the standpipe, as part of the transient generator, has been presented in this chapter. A significant oscillation is introduced to the measured responses obtained at the location of the transient generator regardless of whether a side discharge closure or opening is performed. This oscillation has been labelled “ringing” and reduces the interpretable reflection information near the location of the transient generator. Modifications to the transient generator are currently being performed, outside of the scope of this research, to reduce the “ringing” effect.

Chapter 12

Development of Transient Models for Distribution Pipelines

Based on the calibration model presented in Chapter 5, and the development and calibration of such a model for the Hanson Transmission Pipeline (HTP), as presented in Chapter 8, conceptual calibration models are developed and calibrated, for both the SJTP and KCP, in this chapter. As for the model developed in Chapter 8, Kelvin-Voigt mechanical elements are used to introduce a "viscous" mechanism to approximate equivalent mechanical dispersion and damping. However, the models developed in this chapter utilise multiple Kelvin-Voigt mechanical elements, with different creep deformation spring and retardation time dashpot parameters, distributed spatially in distinct zones along each pipeline to replicate increased physical variability. This significantly increases the number of parameters used to calibrate the proposed models and regression diagnostics are examined to identify signs of redundancy in model structure or parameter correlations indicative of an over-parameterised model. The sensitivity of the calibration to the number of spatial zones for each pipeline, and hence also the number of Kelvin-Voigt mechanical elements, is assessed. Furthermore, the sensitivity of the models, developed for the KCP, to the inclusion or omission of the physically approximated water service connections is tested. Finally, limitations to the physical interpretation of the calibrated "viscous" dispersion and damping parameters are discussed in this chapter.

12.1 Non-conventional physical complexities

As for transmission pipelines, the degree of restraint along a distribution pipeline is likely to govern potential mechanical motion and vibration. The effects of this motion and vibration may be replicated using a "viscous" mechanism to approximate

equivalent dispersion and damping. However, significant additional complexity is introduced, in the case of distribution pipelines, via uncertainties in the topology and condition of water service connections. Each connection to a distribution pipeline can potentially abstract transient energy. Furthermore, the type and nature of the energy abstraction will vary with the multitude of different restraints and materials, their physical condition and the number of energy absorbing fixtures. Even if a practical inventory of the physical details and condition of each connection could be collated, theoretical deficits in the understanding of the response of individual elements is likely to continue to compromise the accuracy of the forward transient model.

As mentioned in Chapter 5, the degree of restraint is coupled with the type and number of flexible joints and the support from surrounding soils at each joint. Previous research has confirmed that mechanical movement and rotation at flexible joints can lead to significant energy losses under dynamic loads. Furthermore, although Coulomb sliding friction typically best describes the physical mechanisms at a flexible joint, equivalent "viscous" damping is used to replicate the overall energy loss. With regard to soil/pipe interaction, some work has been conducted to assess the reduction in pipe wall stress and strain that occurs during a transient event due to support from surrounding soils and viscoelastic models have been developed by, amongst others, Rajani et al. (1996) to account for the interaction of buried pipelines with externally applied dynamic loads.

Significant discrepancies between measured and predicted transient responses for the Saint Johns Terrace Pipeline (SJTP), presented in Chapter 11, were apparent when the pipeline was subject to rapid increases in pressure (i.e., positive transients). Significant discrepancies between the measured and predicted transient responses for the Kookaburra Court Pipeline (KCP) were also apparent when the pipeline was subject to rapid decreases in pressure (i.e., negative transients). The predicted responses were obtained using a traditional forward transient model including available information relating to conventional physical complexities. The remainder of this chapter presents the development and calibration of conceptual transient models utilising multiple Kelvin-Voigt mechanical elements, distributed spatially along the SJTP and KCP in distinct zones, to introduce "viscous" dispersion and

damping and approximately replicate physically variable non-conventional complexities.

12.2 Extension of models to include spatial variability

12.2.1 Using "viscous" mechanisms to model dispersion and damping

The physical uncertainties affecting the transient response of a distribution pipeline, which cannot be directly accounted for using a traditional forward transient model, include the restraint of the main pipe, the restraint and condition of water service connections, the behaviour and condition of flexible joints and the interaction of the pipeline with surrounding soils. For buried pipelines, there is likely to be some interaction between these general categories of uncertainty. In particular, the soils surrounding the pipeline are likely to influence the degree of restraint along the main pipe (and at water service connections) and the degree of support at flexible joints. Importantly, all of these uncertainties have been, in analogous research contexts, modelled using "viscous" or viscoelastic mechanisms (refer to Ferri (1988) for viscous replication of restraint and joint effects and Rajani and Tesfamarian (2004) for viscoelastic replication of soil/pipe interaction). This approach has been relied upon when developing the conceptual forward transient models presented below.

12.2.2 Development of a spatially zoned Kelvin-Voigt model

It is unrealistic to expect to calibrate a conceptual calibration model with only one Kelvin-Voigt element (two parameters) to the complex responses observed at the scale of individual distribution pipelines. Given the spatial (and physical) variability of water service connections, flexible joints and soil/pipe interaction along the main pipe, a conceptual forward transient model has been developed which includes numerous spatial zones and Kelvin-Voigt elements. This model allows for the calibration of independent Kelvin-Voigt elements, distributed along the length of the main pipe, and is called the spatially zoned "viscous" calibration model (SZVCM). The number of spatial zones, and corresponding Kelvin-Voigt elements, required to adequately replicate the measured responses varies and is confirmed by examining the

predicted responses, regression diagnostics and parameter correlations obtained after inverse calibration.

In this regard, the problem of over-parameterisation must be considered. This problem is often encountered in other fields of inverse engineering (e.g., groundwater hydrology) where high levels of spatial variability often tempt modellers to increase numbers of spatial zones until good fits are achieved. There is a balance between increasing the structural complexity of a conceptual model, and consequently increasing its ability to replicate a measured response, and over-parameterising it (and thereby creating redundant parameters that are not independently fitted during inverse calibration). A number of regression diagnostics are available to assess the parsimony of a parameterised model including the posterior parameter correlations (Carrera and Neuman (1986a)).

12.3 Calibration of spatially zoned model of the SJTP

12.3.1 Description of the spatially zoned "viscous" model

The number of spatial zones, and hence Kelvin-Voigt elements, along the Saint Johns Terrace Pipeline (SJTP) is initially set to 16. This gives 32 Kevin-Voigt parameters (i.e., 16 creep deformation spring (J) and 16 dashpot retardation time (τ) parameters). Figure 12-1 (below) shows a schematic of the SJTP with 16 spatial zones each 35.9m long (i.e., approximately 31 by 1.16m sub-pipe segments long). Pairs of creep deformation spring and dashpot retardation time parameters are separately calibrated to replicate the dispersive and damping effect of mechanical motion and vibration, flexible joints and soil/pipe interaction within each zone. Figure 12-2 (below) shows a schematic of the 16 element (32 parameter) Kelvin-Voigt model.

Calibrations are performed using measured responses from tests 1, 2 and 3, conducted on the 23rd July 2003, without baseflow, test 3, conducted on the 15th August 2003, with baseflow, and test 1, conducted on the 26th August 2003, with baseflow. In each case, the measured responses from each recording station (three for the tests conducted on the 23rd July 2003 and two for the other tests) are used to perform the

inverse calibration. The results for test 2 (at stations 1 and 2), conducted on the 23rd July 2003, and test 3 (at stations 2 and 3), conducted on the 15th August 2003, are presented below. Calibration using fixed τ parameters is performed to assess the sensitivity of the calibration to these parameters. The results are presented in tabular form, with those obtained when simultaneously calibrating the τ parameters, below.

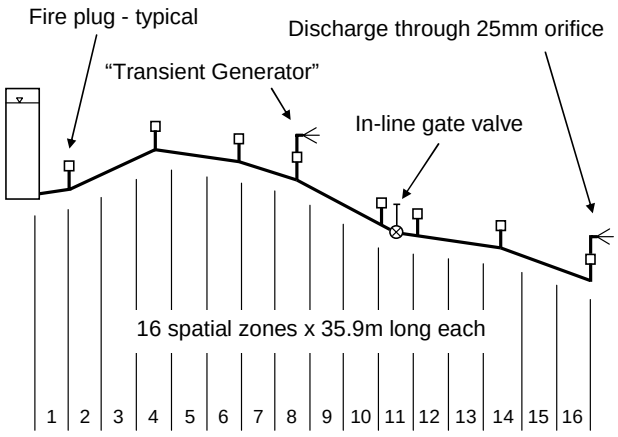

Figure 12-1 – Saint Johns Terrace Pipeline divided into spatial zones for calibration using 16 pairs of Kelvin-Voigt spring and dashpot parameters

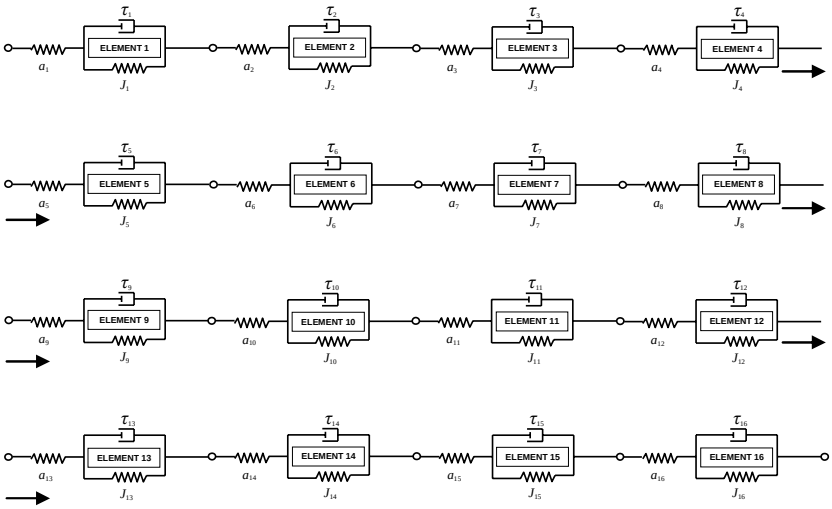

Figure 12-2 – Spatially zoned "viscous" calibration model (SZVCM) with 16 zones

12.3.2 Calibration for test 2 conducted on 23rd July 2003

Figures 12-3 and 12-4 show the measured versus predicted responses for test 2, conducted on the 23rd July 2003, following calibration using the spatially zoned "viscous" calibration model (SZVCM) with 16 zones, at stations 1 and 2, respectively. The predicted responses obtained using the traditional forward transient model, developed in Chapter 11, are plotted for comparison. There is a marked improvement in the predicted responses obtained using the 16 zone SZVCM relative to those obtained using the traditional forward transient model.

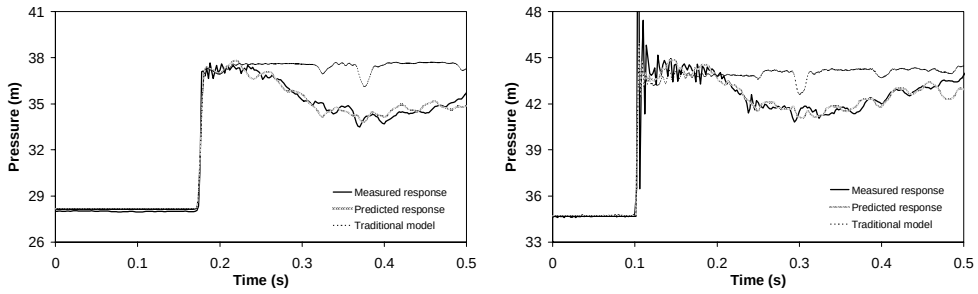

Figures 12-3 and 12-4 – Measured and predicted responses for test 2, conducted on the 23rd July 2003, at stations 1 and 2, respectively

The coefficients of determination for the measured and predicted responses are 99.1% and 88.9% at stations 1 and 2, respectively. These coefficients of determination indicate that the predicted responses approximately replicate the measured responses. The coefficient of determination is lower for station 2 because of inaccuracies in the replication of the "ringing" effect of the transient generator.

Figures 12-5 and 12-6 show the standardised residual plotted against time for test 2, at stations 1 and 2, respectively. The discrepancies between the measured and predicted responses along the transient plateaus manifest as relatively random "runs" of positive and negative residuals. Variations in the standardised residual, associated with inadequacies in the replication of the "ringing" effect from the transient generator, are apparent for a short time following the induction of the transient at station 2.

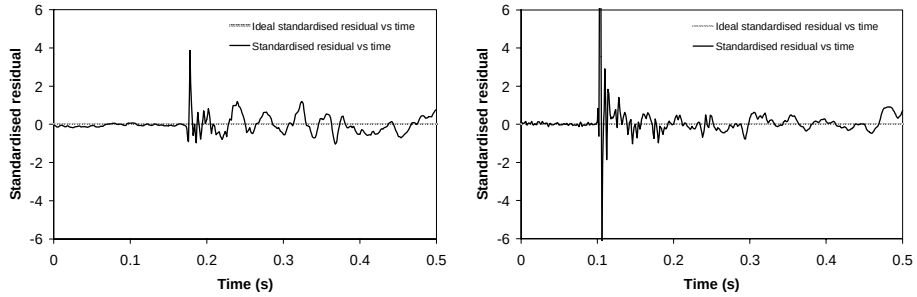

Figures 12-5 and 12-6 – Standardised residual versus time plots for test 2, conducted on the 23rd July 2003, at stations 1 and 2, respectively

12.3.3 Calibration for test 3 conducted on the 15th August 2003

Figures 12-7 and 12-8 show the measured versus predicted responses for test 3, conducted on the 15th August 2003, following calibration using the spatially zoned "viscous" calibration model (SZVCM) with 16 zones, at stations 2 and 3, respectively. The predicted responses obtained using the traditional forward transient model are plotted for comparison. There is a marked improvement in the predicted responses obtained using the SZVCM relative to those obtained using the traditional forward transient model. The reflection from the standpipe discharging at the end of the Saint Johns Terrace Pipeline (SJTP) is not replicated accurately (as shown in Figure 12-8).

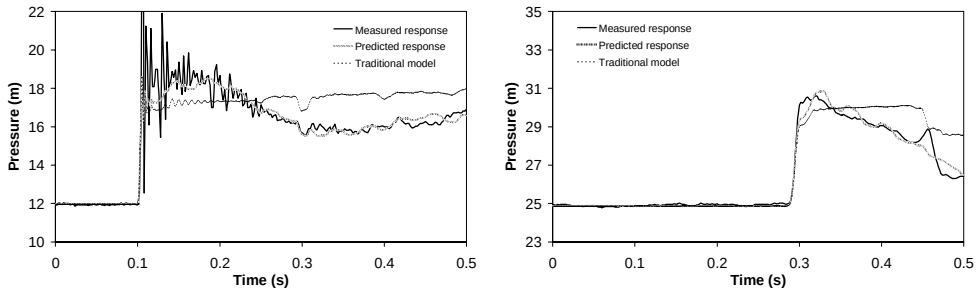

Figures 12-7 and 12-8 – Measured and predicted responses for test 3, conducted on the 15th August 2003, at stations 2 and 3, respectively

The coefficients of determination for the measured and predicted responses are 80.1% and 98.0% at stations 2 and 3, respectively. These coefficients of determination

indicate that the predicted responses approximately replicate the measured responses. The coefficient of determination is again lower for station 2 because of inaccuracies in the replication of the "ringing" effect of the transient generator.

Figures 12-9 and 12-10 show the standardised residual plotted against time for test 3, at stations 2 and 3, respectively. The discrepancies between the measured and predicted responses along the transient plateaus manifest as relatively random "runs" of positive and negative residuals. Variations in the standardised residual, associated with inadequacies in the replication of the "ringing" effect from the transient generator, are apparent for a short time following the induction of the transient at station 2.

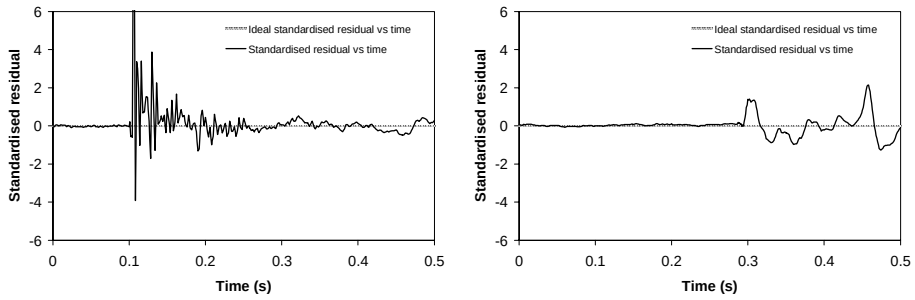

Figures 12-9 and 12-10 – Standardised residual versus time plots for test 3, conducted on the 15th August 2003, at stations 2 and 3, respectively

12.3.4 Assessment of 16 zone SZVCM and parameterisation

SZVCM performance and parameters for test 2 on 23rd July 2003

Table 12-1 shows the results of the calibration for creep deformation spring (J) parameters, with fixed 0.1, 0.2, 0.3, 0.4, 0.5 and 0.6s dashpot retardation time (τ) parameters, and then for simultaneous calibration of both J and τ parameters, for test 2 conducted on 23rd July 2003. There is considerable variation in the fitted J parameters for each zone as the value of the fixed τ parameter is increased. Nevertheless, there are consistent trends in the fitted J parameters for each of the calibrations. The lowest objective function is obtained for the calibration with fitted J and τ parameters. The

next lowest objective function is obtained for the calibration with a fixed τ parameter of 0.3s.

Table 12-1 – Calibrated creep deformation spring (J) parameters, using fixed and fitted dashpot retardation time (τ) parameters, for test 2, on the 23rd July 2003

Zone	Fixed τ Parameter						Average (x e-10)	Fitted J and τ	
	0.1	0.2	0.3	0.4	0.5	0.6		J (x e-10)	τ
1	1.68	-0.44	1.96	-0.61	-0.88	1.45	**0.53**	**3.94**	0.37
2	0.96	1.40	0.82	1.32	1.83	1.49	**1.30**	**1.14**	0.40
3	0.48	0.49	1.06	1.23	1.00	1.15	**0.90**	**1.27**	0.56
4	0.22	0.21	-0.38	-0.75	-0.65	-0.65	**-0.33**	**0.31**	0.46
5	0.53	0.74	1.36	1.84	1.99	2.00	**1.41**	**0.95**	0.35
6	-0.10	0.02	-0.02	-0.15	0.22	0.74	**0.12**	**0.46**	0.39
7	0.19	0.13	0.23	0.30	0.18	-0.08	**0.16**	**0.14**	0.39
8	-0.13	-0.19	-0.32	-0.45	-0.71	-0.99	**-0.47**	**-0.69**	0.37
9	-0.15	-0.11	-0.24	-0.40	-0.16	0.39	**-0.11**	**0.14**	0.39
10	0.84	1.71	2.60	3.89	4.47	4.59	**3.02**	**2.35**	0.29
11	0.73	0.49	0.16	-0.58	-0.96	-0.94	**-0.18**	**-0.24**	0.54
12	-0.47	-0.78	-0.91	-0.99	-0.99	-1.00	**-0.86**	**-0.98**	0.40
13	-0.46	-0.75	-0.99	-0.99	-0.99	-0.99	**-0.86**	**-1.00**	0.41
14	0.35	0.84	1.09	1.35	1.45	1.11	**1.03**	**1.55**	0.40
15	0.97	1.59	2.36	2.95	3.77	5.08	**2.79**	**3.21**	0.41
16	0.18	-0.03	-0.02	-0.02	-0.24	-0.56	**-0.12**	**-0.36**	0.48
Obj. Func.	1.893	1.835	1.831	1.839	1.862	1.901	1.860	1.826	Avg. 0.41

Figure 12-11 shows the variation of the fitted J parameters with spatial zone along the Saint Johns Terrace Pipeline (SJTP). The magnitude of the calibrated J parameters, and consequently the magnitude of "viscous" damping, varies with position along the SJTP. It is difficult to identify any consistent trend for zones 1 to 4. However, consistent trends are evident, despite variations in magnitude, for zones 5 to 16. These variations in magnitude are correlated with changes in the fixed τ parameter. Interestingly, the average magnitudes of the fitted J parameters, determined for each zone using fixed τ parameters, are similar to those of the fitted J parameters, determined for each zone, while simultaneously fitting for the τ parameters.

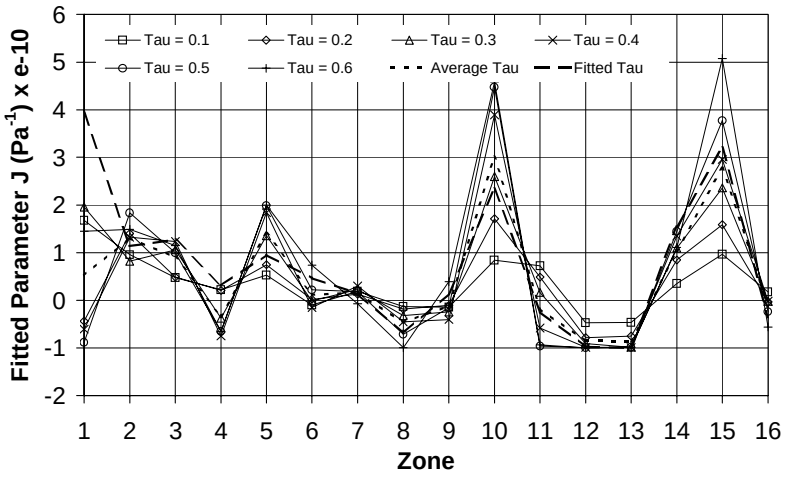

Figure 12-11 – Fitted *J* parameters for test 2, conducted on the 23rd July 2003, without baseflow, for fixed and fitted τ parameter calibrations

Table 12-2 shows the correlation of calibrated *J* parameters for the different zones along the SJTP, when the τ parameters have been simultaneously fitted. Generally, the fitted *J* parameters for each of the 16 zones are not highly correlated. The general lack of correlation between the fitted *J* parameters suggests that the 16 zone SZVCM, while having 32 parameters, is not over-parameterised. The fitted τ parameters are neither highly correlated between zones nor with the fitted *J* parameters.

Table 12-2 – *J* parameter correlations for different zones for test 2

	J1	***J2***	***J3***	***J4***	***J5***	***J6***	***J7***	***J8***	***J9***	***J10***	***J11***	***J12***	***J13***	***J14***	***J15***	***J16***
J1	**1.00**	0.37	0.43	0.06	0.33	0.44	0.44	0.16	0.24	0.11	0.21	0.21	0.22	0.21	0.04	0.29
J2	0.37	**1.00**	0.20	0.13	0.08	0.19	0.33	0.41	0.09	0.26	0.68	0.61	0.04	0.04	0.24	0.14
J3	0.43	0.20	**1.00**	0.69	0.68	0.62	0.52	0.20	0.73	0.71	0.57	0.53	0.47	0.47	0.48	0.50
J4	0.06	0.13	0.69	**1.00**	0.70	0.59	0.59	0.17	**0.84**	**0.82**	0.59	0.58	0.49	0.49	0.58	0.61
J5	0.33	0.08	0.68	0.70	**1.00**	**0.84**	0.61	0.36	**0.83**	0.58	0.46	0.44	0.32	0.26	0.51	0.73
J6	0.44	0.19	0.62	0.59	**0.84**	**1.00**	**0.89**	0.01	0.75	0.46	0.17	0.12	0.23	0.27	0.50	**0.84**
J7	0.44	0.33	0.52	0.59	0.61	**0.89**	**1.00**	0.35	0.66	0.47	0.04	0.01	0.21	0.36	0.51	**0.82**
J8	0.16	0.41	0.20	0.17	0.36	0.01	0.35	**1.00**	0.37	0.07	0.38	0.44	0.13	0.05	0.12	0.03
J9	0.24	0.09	0.73	**0.84**	**0.83**	0.75	0.66	0.37	**1.00**	0.77	0.49	0.46	0.40	0.52	0.68	0.73
J10	0.11	0.26	0.71	**0.82**	0.58	0.46	0.47	0.07	0.77	**1.00**	0.66	0.54	0.44	0.54	0.54	0.41
J11	0.21	0.68	0.57	0.59	0.46	0.17	0.04	0.38	0.49	0.66	**1.00**	0.92	0.09	0.10	0.56	0.29
J12	0.21	0.61	0.53	0.58	0.44	0.12	0.01	0.44	0.46	0.54	0.92	**1.00**	0.30	0.11	0.48	0.30
J13	0.22	0.04	0.47	0.49	0.32	0.23	0.21	0.13	0.40	0.44	0.09	0.30	**1.00**	0.58	0.12	0.03
J14	0.21	0.04	0.47	0.49	0.26	0.27	0.36	0.05	0.52	0.54	0.10	0.11	0.58	**1.00**	0.43	0.15
J15	0.04	0.24	0.48	0.58	0.51	0.50	0.51	0.12	0.68	0.54	0.56	0.48	0.12	0.43	**1.00**	0.73
J16	0.29	0.14	0.50	0.61	0.73	**0.84**	**0.82**	0.03	0.73	0.41	0.29	0.30	0.03	0.15	0.73	**1.00**

SZVCM performance and parameters for test 3 on 15th August 2003

Table 12-3 shows the results of the calibration for creep deformation spring (J) parameters, with fixed 0.1, 0.2, 0.3, 0.4, 0.5 and 0.6s dashpot retardation time (τ) parameters, and then for simultaneous calibration of both J and τ parameters, for test 3 conducted on the 15th August 2003. There is considerable variation in the fitted J parameters for each zone as the value of the fixed τ parameter is increased. Nevertheless, there are consistent trends in the fitted J parameters for each of the calibrations. The lowest objective function is obtained for the calibration with fitted J and τ parameters. The next lowest objective function is obtained for the calibration with a fixed τ parameter of 0.3s. This outcome is the same as that for the no baseflow tests.

Table 12-3 – Calibrated creep deformation spring (J) parameters, using fixed and fitted dashpot retardation time (τ) parameters, for test 3, on the 15th August 2003

Zone	Fixed τ Parameter						Average (x e-10)	Fitted J and τ	
	0.1	0.2	0.3	0.4	0.5	0.6		J (x e-10)	τ
1	4.44	4.56	3.68	4.19	5.38	6.95	**4.86**	**4.10**	0.36
2	5.10	4.37	2.91	5.40	0.49	4.57	**3.81**	**3.23**	0.30
3	3.02	3.17	1.26	-0.34	1.89	1.85	**1.81**	**2.41**	0.36
4	2.14	3.16	2.88	3.24	2.76	1.52	**2.61**	**1.66**	0.40
5	0.93	1.32	2.01	3.03	3.44	3.47	**2.37**	**2.69**	0.37
6	0.16	0.55	1.70	1.44	2.65	3.58	**1.68**	**1.85**	0.46
7	-0.22	-0.29	-0.33	0.09	-0.75	-0.71	**-0.37**	**-0.30**	0.44
8	-0.74	-0.98	-0.99	-1.00	-0.97	-0.99	**-0.95**	**-0.96**	0.23
9	0.08	0.10	-0.35	-0.98	-0.94	-0.97	**-0.51**	**-0.35**	0.40
10	0.75	1.28	1.35	2.19	2.81	2.60	**1.83**	**2.01**	0.43
11	-0.46	-0.29	-0.23	-0.42	-0.80	-0.45	**-0.44**	**-0.54**	0.45
12	-0.15	-0.86	-0.70	-0.78	-0.88	-0.36	**-0.62**	**-0.85**	0.44
13	-0.29	-0.34	-0.40	-0.77	-0.69	-0.95	**-0.57**	**-0.83**	0.46
14	0.36	0.31	0.21	0.66	0.02	-0.87	**0.11**	**0.53**	0.42
15	1.60	3.22	4.30	3.96	6.62	7.10	**4.47**	**4.31**	0.33
16	3.36	1.73	1.01	4.16	1.28	1.41	**2.16**	**0.20**	0.41
Obj. Func.	1.355	1.352	1.381	1.401	1.411	1.430	1.388	1.347	Avg. 0.39

Figure 12-12 shows the variation of the fitted J parameters with spatial zone along the Saint Johns Terrace Pipeline (SJTP). The magnitude of the calibrated J parameters, and consequently the magnitude of "viscous" damping, varies with position along the SJTP. It is difficult to identify any consistent trend for zones 1 to 4. However,

consistent trends are evident, despite variations in magnitude, for zones 7 to 16. The trends for zones 5 to 6 are less consistent than for the tests without baseflow.

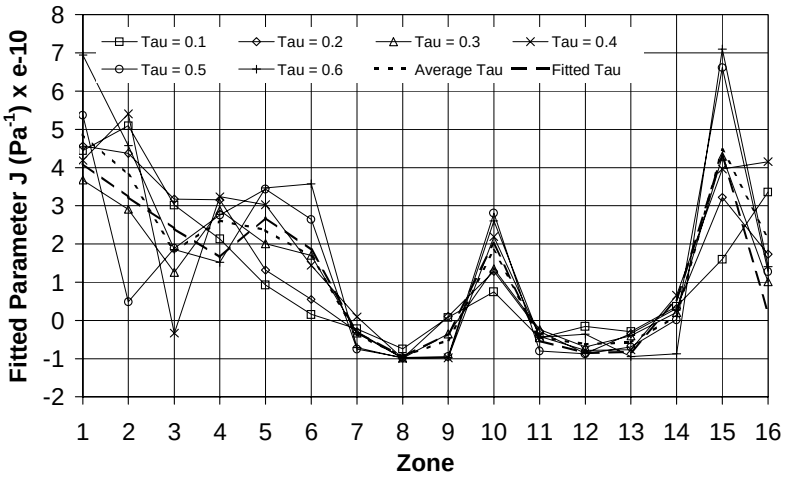

Figure 12-12 – Fitted *J* parameters for test 3, conducted on the 15th August 2003, with baseflow, for fixed and fitted τ parameter calibrations

Table 12-4 – *J* parameter correlations for different zones for test 3

	J1	J2	J3	J4	J5	J6	J7	J8	J9	J10	J11	J12	J13	J14	J15	J16
J1	**1.00**	0.21	0.03	0.01	0.28	0.01	0.19	0.01	0.20	0.06	0.26	0.02	0.13	0.10	0.17	0.04
J2	0.21	**1.00**	0.04	0.39	0.45	0.14	0.00	0.28	0.01	0.06	0.42	0.39	0.06	0.72	0.04	0.39
J3	0.03	0.04	**1.00**	**0.80**	0.01	0.02	0.48	0.02	0.36	0.39	0.37	0.79	**0.98**	0.05	0.50	0.34
J4	0.01	0.39	**0.80**	**1.00**	0.42	0.03	0.19	0.21	0.09	0.29	0.63	**0.99**	**0.83**	0.48	0.15	0.13
J5	0.28	0.45	0.01	0.42	**1.00**	0.12	0.01	0.33	0.03	0.13	**0.86**	0.48	0.01	0.57	0.06	0.43
J6	0.01	0.14	0.02	0.03	0.12	**1.00**	0.41	0.06	0.41	0.79	0.09	0.06	0.03	0.17	0.28	0.53
J7	0.19	0.00	0.48	0.19	0.01	0.41	**1.00**	0.04	**0.94**	0.08	0.36	0.27	0.42	0.12	**0.84**	0.74
J8	0.01	0.28	0.02	0.21	0.33	0.06	0.04	**1.00**	0.20	0.06	0.22	0.21	0.02	0.39	0.08	0.35
J9	0.20	0.01	0.36	0.09	0.03	0.41	**0.94**	0.20	**1.00**	0.21	0.35	0.19	0.30	0.10	**0.88**	0.76
J10	0.06	0.06	0.39	0.29	0.13	0.79	0.08	0.06	0.21	**1.00**	0.12	0.20	0.30	0.00	0.16	0.30
J11	0.26	0.42	0.37	0.63	**0.86**	0.09	0.36	0.22	0.35	0.12	**1.00**	0.70	0.33	0.49	0.22	0.17
J12	0.02	0.39	0.79	**0.99**	0.48	0.06	0.27	0.21	0.19	0.20	0.70	1.00	**0.83**	0.49	0.22	0.08
J13	0.13	0.06	**0.98**	**0.83**	0.01	0.03	0.42	0.02	0.30	0.30	0.33	**0.83**	1.00	0.01	0.47	0.31
J14	0.10	0.72	0.05	0.48	0.57	0.17	0.12	0.39	0.10	0.00	0.49	0.49	0.01	1.00	0.19	0.60
J15	0.17	0.04	0.50	0.15	0.06	0.28	**0.84**	0.08	**0.88**	0.16	0.22	0.22	0.47	0.19	1.00	0.76
J16	0.04	0.39	0.34	0.13	0.43	0.53	0.74	0.35	0.76	0.30	0.17	0.08	0.31	0.60	0.76	1.00

Table 12-4 (above) shows the correlation of calibrated *J* parameters for the different zones along the SJTP, when the τ parameters have been simultaneously fitted, for test 3, conducted on the 15th August 2003. Generally, the fitted *J* parameters for each of the 16 zones are not highly correlated. As for the case without baseflow, the fitted τ

parameters are neither highly correlated between zones nor with the fitted *J* parameters.

Comparison of results from tests without and with baseflow

Figure 12-13 compares the calibrated *J* parameters, determined as an average of the results for each fixed τ parameter, with the *J* parameters, calibrated while simultaneously fitting for τ parameters, for test 2, conducted without baseflow on the 23rd July 2003, and test 3, conducted with baseflow on the 15th August 2003, respectively. There is a marked divergence between the calibrated *J* parameters for zones 1 to 6 for the tests conducted without and with baseflow. That said, the calibrated *J* parameters are relatively similar for zones 7 to 16.

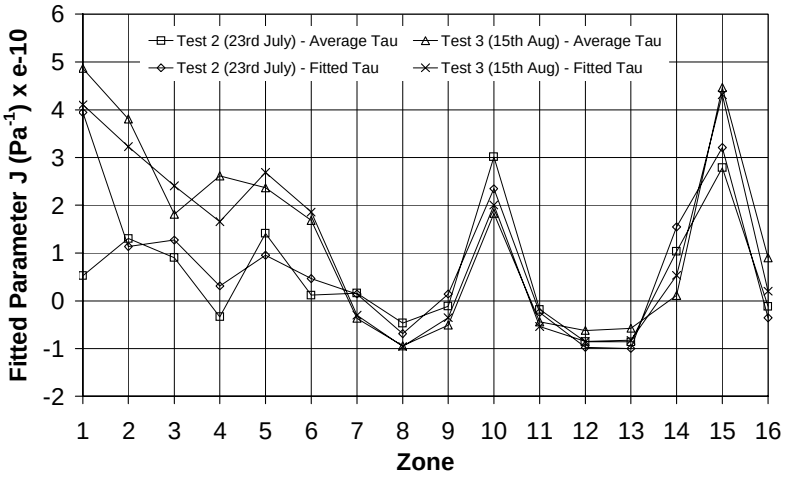

Figure 12-13 – Comparison of fitted *J* parameters for test 2, conducted on the 23rd July 2003, and for test 3, conducted on the 15th August 2003

It is possible that the difference for zones 1 to 6 is related to the reduction of pressure along the Saint Johns Terrace Pipeline (SJTP) for test 3, with baseflow, and, in particular, the reduction of pressure along the sections with higher elevations and less static pressure. The "viscous" damping associated with mechanical motion and vibration, flexible joints and soil/pipe interaction may, depending on the physical processes involved, be greater if the SJTP is subject to less static pressure.

Nevertheless, the consistency in the calibrated *J* parameters for zones 7 to 16 supports the hypothesis that "viscous" damping can be used to replicate the effects of physical complexity along at least part of the SJTP.

12.3.5 Assessment of lower number of spatial zones for SZVCM

While a spatially zoned "viscous" calibration model (SZVCM) with 16 zones has been adopted for the calibration described above, a smaller number of spatial zones may facilitate adequate replication of the effects of the physical variability, and changes in the magnitude of "viscous" damping, along the Saint Johns Terrace Pipeline (SJTP). In order to assess the sensitivity of the results to the number of spatial zones, SZVCMs with 8 and 4 zones have been calibrated below.

The calibrations are performed using the measured response from test 2, conducted on the 23rd July 2003, without baseflow. Given the general consistency of the calibrated *J* and τ parameters obtained for this test with those obtained for the other tests, test 2 was considered sufficient to gauge the performance of the 8 and 4 zone SZVCMs. Furthermore, it was considered sufficient to perform the calibration using only fitted, and not fixed, τ parameters.

Assessment of 8 zone SZVCM

Figures 12-14 and 12-15 show the measured versus predicted responses for test 2 following calibration using a spatially zoned "viscous" calibration model (SZVCM) with 8 zones, and fitted τ parameters, at stations 1 and 2, respectively. The predicted responses obtained using the 16 zone SZVCM and traditional forward transient model are plotted for comparison. There is a marked improvement relative to the predicted results obtained when using a traditional forward transient model. Figures 12-16 and 12-17 show that the calibrated response obtained using the 8 zone SZVCM is marginally less accurate than that obtained using the 16 zone SZVCM.

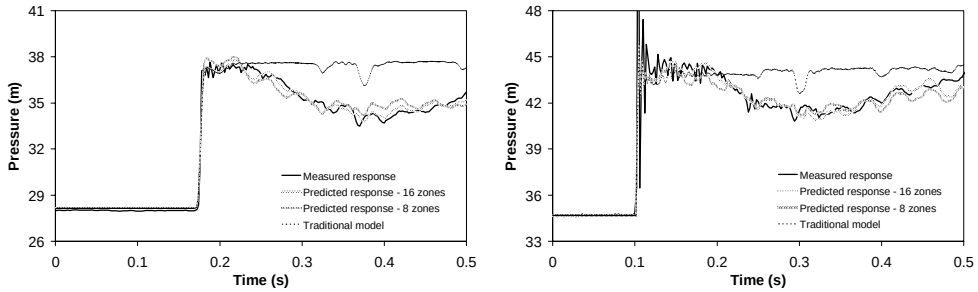

Figures 12-14 and 12-15 – Measured and predicted responses, obtained using 16 and 8 zone SZVCMs, for test 2, at stations 1 and 2, respectively

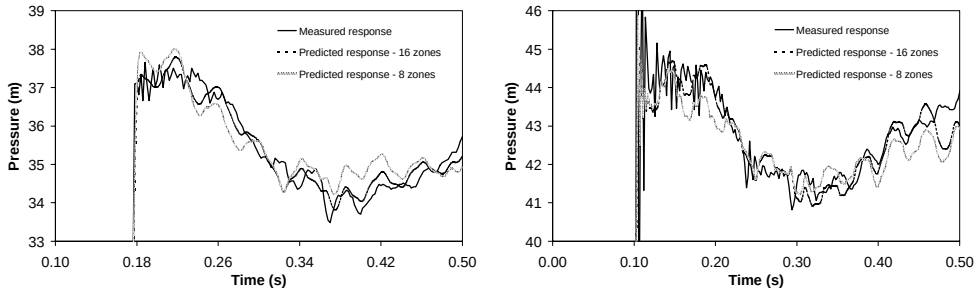

Figures 12-16 and 12-17 – Measured and predicted responses, obtained using 16 and 8 zone SZVCMs, over a pressure range of 6m, at stations 1 and 2, respectively

The coefficients of determination for the measured and predicted responses are 98.4% and 88.6%, for the calibrations performed using the 8 zone SZVCM, at stations 1 and 2, respectively (compared to 99.1% and 88.9% when calibrating using the 16 zone SZVCM). These coefficients of determination indicate that the predicted responses approximately replicate the measured responses. The coefficient of determination is lower for station 2 because of the inaccuracies in the replication of the "ringing" effect of the transient generator.

Figures 12-18 and 12-19 show the standardised residual plotted against time for test 2, for the calibrations performed using the 16 and 8 zone SZVCMs, at stations 1 and 2, respectively. Relative to the results obtained using the 16 zone SZVCM, marginally longer "runs" of positive and negative residuals are obtained using the 8 zone SZVCM. Variations in the standardised residual, associated with inadequacies in the

replication of the "ringing" effect from the transient generator, are particularly apparent for a short time following the induction of the transient at station 2.

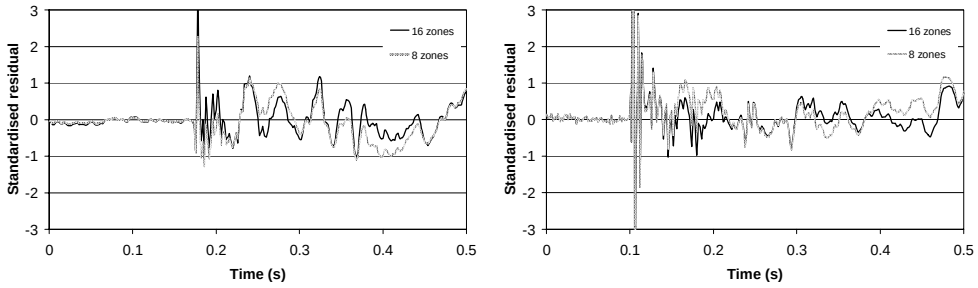

Figures 12-18 and 12-19 – Standardised residual versus time plots, obtained using 16 and 8 zone SZVCMs, for test 2, at stations 1 and 2, respectively

Assessment of 4 zone SZVCM

Figures 12-20 and 12-21 show the measured versus predicted responses for test 2 following calibration using a spatially zoned "viscous" calibration model (SZVCM) with 4 zones, and fitted τ parameters, at stations 1 and 2, respectively. There is a marked improvement, relative to the predicted results obtained when using a traditional forward transient model, when using the 4 zone SZVCM. However, Figures 12-22 and 12-23 show that the calibrated response obtained using the 4 zone SZVCM is significantly less accurate than that obtained using the 16 zone SZVCM (and 8 zone SZVCM).

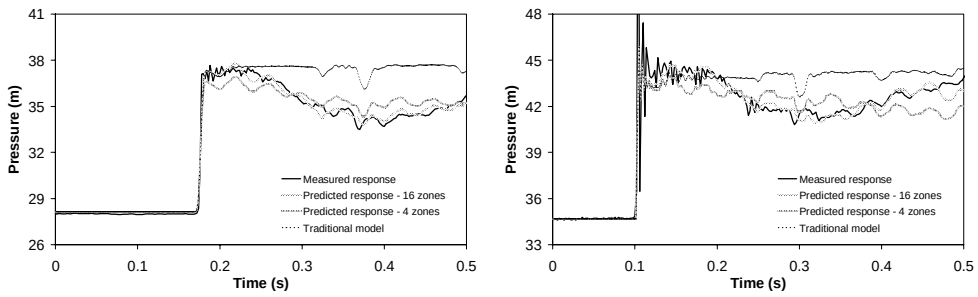

Figures 12-20 and 12-21 – Measured and predicted responses, obtained using 16 and 4 zone SZVCMs, for test 2, at stations 1 and 2, respectively

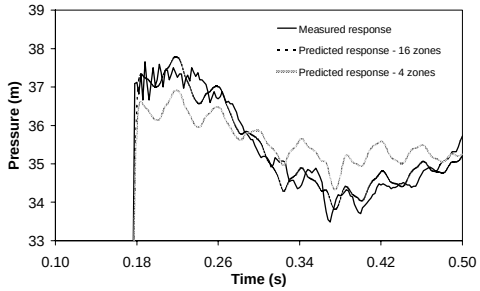

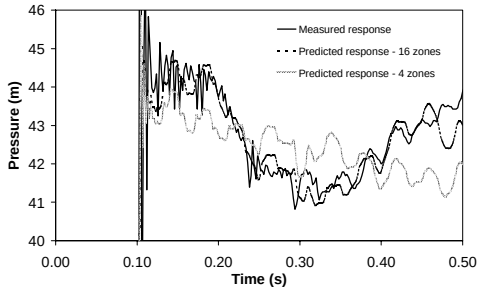

Figures 12-22 and 12-23 – Measured and predicted responses, obtained using 16 and 4 zone SZVCMs, over a pressure range of 6m, at stations 1 and 2, respectively

The coefficients of determination for the measured and predicted responses are 97.1% and 84.1%, for the calibrations performed using the 4 zone SZVCM, at stations 1 and 2, respectively (compared to 99.1% and 88.9% when calibrating using the 16 zone SZVCM). The loss of accuracy relative to the results obtained using the 16 and 8 zone SZVCMs is significant.

Figures 12-24 and 12-25 show the standardised residual plotted against time for test 2, for the calibrations performed using the 8 and 4 zone SZVCMs, at stations 1 and 2, respectively. Relative to the results obtained using the 8 zone SZVCM, significantly longer "runs" of positive and negative residuals are obtained using the 4 zone SZVCM. This confirms that the error for the 4 zone SZVCM is less random than for the 8 and 16 zone SZVCMs.

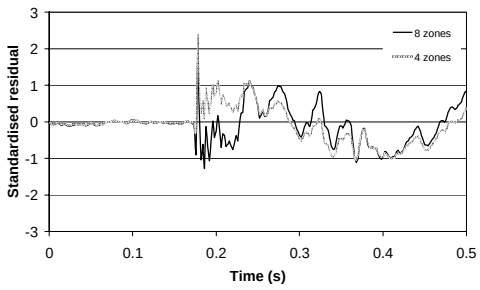

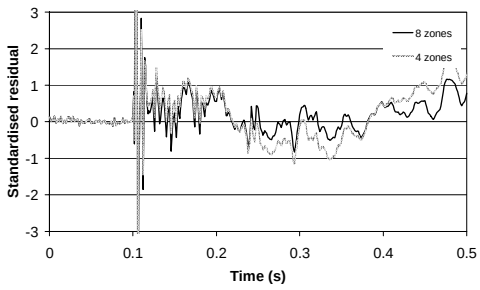

Figures 12-24 and 12-25 – Standardised residual versus time plots, obtained using 8 and 4 zone SZVCMs, for test 2, at stations 1 and 2, respectively

Parameter correlations for the 8 and 4 zone SZVCMs

Table 12-5 shows the correlation of calibrated J and τ parameters, for the different zones along the Saint Johns Terrace Pipeline (SJTP), obtained using the spatially zoned "viscous" calibration model (SZVCM) with 8 zones, for test 2. Generally, the fitted J and τ parameters for each of the 8 zones are not highly correlated. The general lack of correlation between the fitted J parameters suggests that the 8 zone SZVCM is not over-parameterised. Table 12-6 shows the correlation of calibrated J and τ parameters, for the different zones along the SJTP, obtained using the 4 zone SZVCM, for test 2. The fitted J and τ parameters for each of the for zones are, again, not generally highly correlated.

Table 12-5 – J and τ parameter correlations for 8 zone SZVCM for test 2

	J1	τ1	J2	τ2	J3	τ3	J4	τ4	J5	τ5	J6	τ6	J7	τ7	J8	τ8
J1	**1.00**	**0.98**	0.01	0.09	0.18	0.24	0.21	0.21	0.21	0.20	0.09	0.04	0.15	0.21	0.07	0.06
τ1	**0.98**	**1.00**	0.19	0.12	0.08	0.13	0.19	0.19	0.18	0.16	0.07	0.03	0.13	0.20	0.07	0.06
J2	0.01	0.19	**1.00**	**0.97**	0.13	0.10	0.08	0.07	0.13	0.18	0.26	0.21	0.19	0.02	0.06	0.06
τ2	0.09	0.12	**0.97**	**1.00**	0.31	0.30	0.06	0.06	0.11	0.16	0.22	0.18	0.18	0.00	0.05	0.05
J3	0.18	0.08	0.13	0.31	**1.00**	**0.98**	0.51	0.52	0.48	0.46	0.01	0.12	0.03	0.01	0.19	0.18
τ3	0.24	0.13	0.10	0.30	**0.98**	**1.00**	**0.35**	0.37	0.37	0.37	0.06	0.03	0.00	0.00	0.11	0.11
J4	0.21	0.19	0.08	0.06	0.51	**0.35**	**1.00**	**1.00**	**0.86**	0.77	0.20	0.39	0.16	0.06	0.40	0.37
τ4	0.21	0.19	0.07	0.06	0.52	0.37	**1.00**	**1.00**	**0.87**	0.78	0.18	0.37	0.15	0.06	0.39	0.36
J5	0.21	0.18	0.13	0.11	0.48	0.37	**0.86**	**0.87**	**1.00**	**0.99**	0.27	0.06	0.17	0.23	0.30	0.28
τ5	0.20	0.16	0.18	0.16	0.46	0.37	0.77	0.78	**0.99**	**1.00**	0.42	0.21	0.28	0.29	0.25	0.23
J6	0.09	0.07	0.26	0.22	0.01	0.06	0.20	0.18	0.27	0.42	**1.00**	**0.97**	**0.80**	0.58	0.22	0.20
τ6	0.04	0.03	0.21	0.18	0.12	0.03	0.39	0.37	0.06	0.21	**0.97**	**1.00**	0.77	0.55	0.30	0.28
J7	0.15	0.13	0.19	0.18	0.03	0.00	0.16	0.15	0.17	0.28	**0.80**	0.77	**1.00**	**0.91**	0.14	0.15
τ7	0.21	0.20	0.02	0.00	0.01	0.00	0.06	0.06	0.23	0.29	0.58	0.55	**0.91**	**1.00**	0.02	0.04
J8	0.07	0.07	0.06	0.05	0.19	0.11	0.40	0.39	0.30	0.25	0.22	0.30	0.14	0.02	**1.00**	**1.00**
τ8	0.06	0.06	0.06	0.05	0.18	0.11	0.37	0.36	0.28	0.23	0.20	0.28	0.15	0.04	**1.00**	**1.00**

Table 12-6 – J and τ correlations for 4 zone SZVCM for test 2

	J1	τ1	J2	τ2	J3	τ3	J4	τ4
J1	**1.00**	0.58	**0.88**	**0.88**	0.41	0.38	0.04	0.03
τ1	0.58	**1.00**	0.38	0.39	0.17	0.14	0.01	0.00
J2	**0.88**	0.38	**1.00**	**1.00**	0.74	0.69	0.20	0.17
τ2	**0.88**	0.39	**1.00**	**1.00**	0.73	0.69	0.22	0.19
J3	0.41	0.17	0.74	0.73	**1.00**	**0.97**	0.38	0.34
τ3	0.38	0.14	0.69	0.69	**0.97**	**1.00**	0.49	0.46
J4	0.04	0.01	0.20	0.22	0.38	0.49	**1.00**	**1.00**
τ4	0.03	0.00	0.17	0.19	0.34	0.46	**1.00**	**1.00**

Performance of the 16, 8 and 4 zone SZVCMs

Table 12-7 shows the results of the calibration for creep deformation spring (J) and dashpot retardation time (τ) parameters for test 2, using spatially zoned "viscous" calibration models (SZVCMs) with 16, 8 and 4 zones. The objective functions obtained for the calibrations are 1.83, 2.22 and 3.07, respectively. On the basis of lowest objective function, and an assessment of the regression diagnostics, the 16 zone SZVCM is superior to the 8 and 4 zone SZVCMs. Furthermore, the parameter correlations for the 16 zone SZVCM indicate that it is not over-parameterised.

Table 12-7 – Calibrated creep deformation spring (J) and dashpot retardation time (τ) parameters for test 2 using 16, 8 and 4 zone SZVCMs

Zone	Number of spatial zones in model					
	16		8		4	
	Fitted J (x e-10) Pa^{-1}	Fitted τ (s)	Fitted J (x e-10) Pa^{-1}	Fitted τ (s)	Fitted J (x e-10) Pa^{-1}	Fitted τ (s)
1	3.94	0.37	1.29	0.43	0.20	0.05
2	1.14	0.40	0.21	0.31	0.60	0.65
3	1.27	0.56	0.65	0.36	0.30	0.26
4	0.31	0.46	-0.76	0.46	1.14	0.65
5	0.95	0.35	2.72	0.60	NA	NA
6	0.46	0.39	-0.41	0.43	NA	NA
7	0.14	0.39	-0.24	0.25	NA	NA
8	-0.69	0.37	2.31	0.54	NA	NA
9	0.14	0.39	NA	NA	NA	NA
10	2.35	0.29	NA	NA	NA	NA
11	-0.24	0.54	NA	NA	NA	NA
12	-0.98	0.40	NA	NA	NA	NA
13	-1.00	0.41	NA	NA	NA	NA
14	1.55	0.40	NA	NA	NA	NA
15	3.21	0.41	NA	NA	NA	NA
16	-0.36	0.48	NA	NA	NA	NA
	1.83 Obj Func	Avg. 0.42	2.22 Obj Func	Avg. 0.41	3.07 Obj Func	Avg. 0.40

Figure 12-26 shows the variation of the fitted J parameters with spatial zone along the Saint Johns Terrace Pipeline (SJTP), for calibrations obtained for test 2 using the 16 and 8 zone SZVCMs. Despite halving the number of zones, the magnitudes of the calibrated J parameters, and consequently the magnitude of "viscous" damping, are relatively consistent along the SJTP for both models. This suggests that the 8 zone SZVCM is sufficiently flexible, in terms of representing variations in the physical complexities that disperse and damp the response of the SJTP, to be relatively

accurately calibrated. Coincidentally, it confirms that the 16 zone SZVCM is also adequate and that additional zones are not likely to lead to a significant change in the distribution of "viscous" damping along the SJTP.

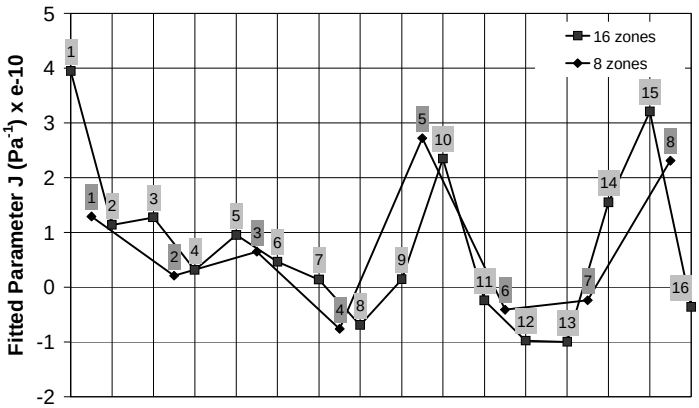

Figure 12-26 – Calibrated *J* parameters for test 2 using 16 and 8 zone SZVCMs

Figure 12-27 shows the variation of the fitted *J* parameters with spatial zone along the SJTP, for calibrations obtained for test 2 using the 16 and 4 zone SZVCMs. The magnitudes of the calibrated *J* parameters obtained using the 4 zone SZVCM are not consistent with those obtained using the 16 zone SZVCM. The 4 zone SZVCM lacks flexibility and is unable to represent variations in the physical complexities that disperse and damp the response of the SJTP.

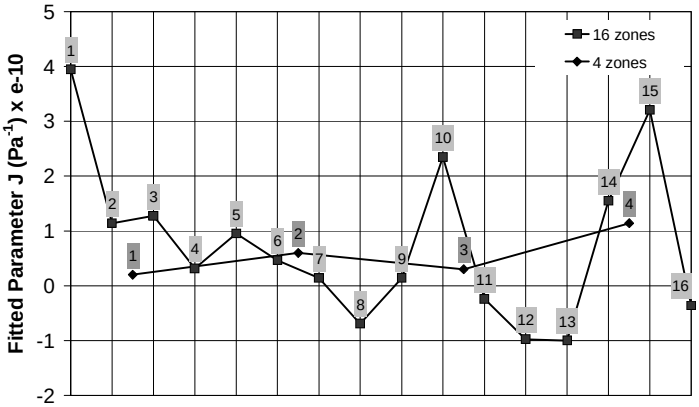

Figure 12-27 – Calibrated *J* parameters for test 2 using 16 and 4 zone SZVCMs

12.4 Calibration of spatially zoned model of the KCP

12.4.1 Description of the spatially zoned "viscous" model

The number of spatial zones, and hence Kelvin-Voigt elements, along the Kookaburra Court Pipeline (KCP) is initially set to 8 because the KCP is shorter than the Saint Johns Terrace Pipeline (SJTP). This gives 16 Kevin-Voigt parameters (i.e., 8 creep deformation spring (J) and 8 dashpot retardation time (τ) parameters). Figure 12-28 shows a schematic of the KCP with 8 spatial zones each 47.3m long (i.e., approximately 40 by 1.18m sub-pipe segments long).

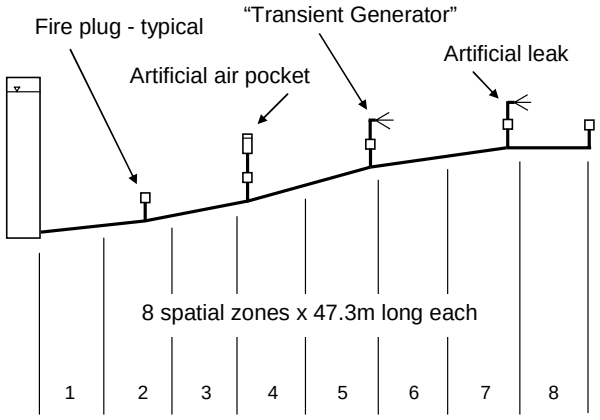

Figure 12-28 – Kookaburra Court Pipeline divided into spatial zones for calibration using 8 pairs of Kelvin-Voigt spring and dashpot parameters

Pairs of creep deformation spring and dashpot retardation time parameters are separately calibrated to replicate the dispersive and damping effect of mechanical motion and vibration, flexible joints and soil/pipe interaction within each zone. Calibration is performed using the measured responses for test 3, conducted on the 28th August 2003, from stations 1 and 2. Calibration using fixed τ parameters is performed to assess the sensitivity of the calibration to these parameters. The results are presented with those obtained when simultaneously calibrating the τ parameters.

It was not possible to accurately determine either the topology or physical condition of the 15 water service connections along the KCP (this scenario is likely to be typical of the general situation for other distribution pipelines). A complex forward transient model of the KCP, as described in Chapter 11, has been developed and includes 15 by 10m long branches of 25mm pipe, with 20mm orifices for individual water meters, located approximately 3.5m along each offtake (measured from the KCP), representing each water service connection.

While the size of the offtakes and location of the water meters are topologically correct, the approximation of each water service connection, using a 10m length of pipe, is likely to be deficient. Given this uncertainty, a topologically simplified forward transient model has been developed (excluding the 10m lengths of pipe used to approximate each water service connection). The results of the calibration of a spatially zoned "viscous" calibration model (SZVCM) with 8 zones, and simplified topology, will be compared with those obtained using a complex topology.

12.4.2 Calibration of complex spatially zoned "viscous" model

Figures 12-29 and 12-30 show the measured versus predicted responses for test 3, conducted on the 28th August 2003, following calibration using a topologically complex spatially zoned "viscous" calibration model (SZVCM) with 8 zones, at stations 1 and 2, respectively. Only a proportion of the measured and predicted reflections correlate with each other. Given the uncertainty in the topology, condition and anticipated response of the water service connections, this result is not unexpected. The coefficients of determination for the measured and predicted responses are 99.6% and 98.3% at stations 1 and 2, respectively. The coefficient of determination is lower for station 2 because of inaccuracies in the replication of the "ringing" effect of the transient generator.

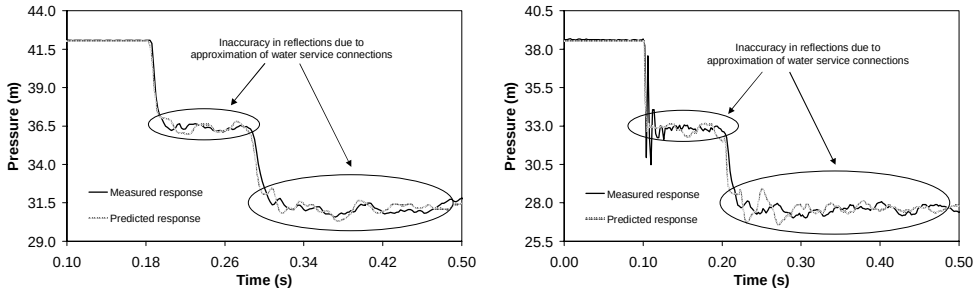

Figures 12-29 and 12-30 – Measured and predicted responses obtained using a complex SZVCM for test 3, at stations 1 and 2, respectively

Figures 12-31 and 12-32 show the standardised residual plotted against time for test 3, at stations 1 and 2, respectively. The discrepancies between the measured and predicted responses along the transient plateaus manifest as relatively random "runs" of positive and negative residuals. Variations in the standardised residual, associated with inadequacies in the replication of the "ringing" effect from the transient generator, are apparent for a short time following the induction of the transient at station 2.

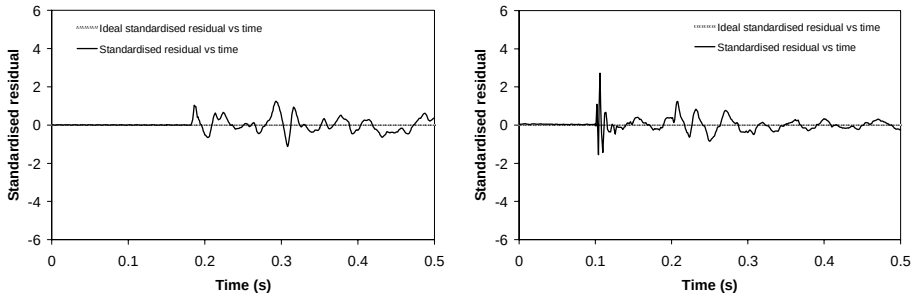

Figures 12-31 and 12-32 – Standardised residual versus time plots, obtained using a complex SZVCM, for test 3, at stations 1 and 2, respectively

12.4.3 Calibration of simplified spatially zoned "viscous" model

Figures 12-33 and 12-34 show the measured versus predicted responses for test 3 following calibration using a topologically simplified spatially zoned "viscous" calibration model (SZVCM) with 8 zones, at stations 1 and 2, respectively. The

calibrated responses obtained using the simplified SZVCM are devoid of reflections apart from those from the vertical fire plug risers (which are retained in the simplified model). This confirms that the water service connections (as approximated) affect the predicted responses of the KCP. The coefficients of determination for the measured and predicted responses are 99.1% and 98.0% at stations 1 and 2, respectively (compared to 99.6% and 98.3% when calibrating using the complex SZVCM).

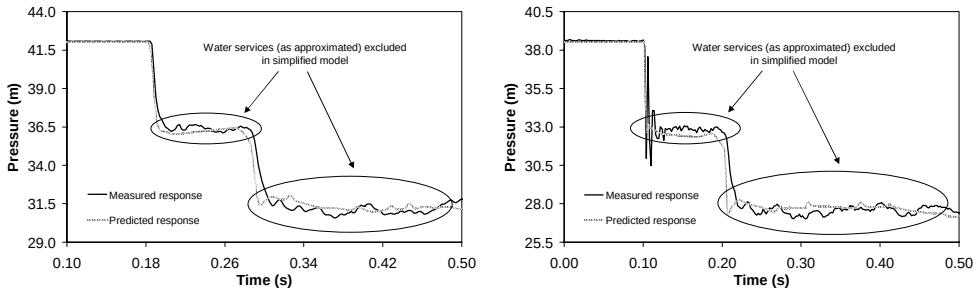

Figures 12-33 and 12-34 – Measured and predicted responses obtained using a simplified SZVCM for test 3, at stations 1 and 2, respectively

Figures 12-35 and 12-36 show the standardised residual plotted against time for test 3, at stations 1 and 2, respectively. The discrepancies between the measured and predicted responses along the transient plateaus manifest as "runs" of positive and negative residuals. These "runs" are significantly longer than for the results obtained using the complex SZVCM.

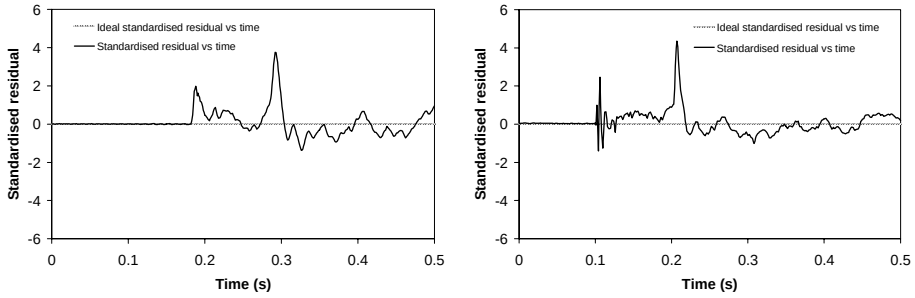

Figures 12-35 and 12-36 – Standardised residual versus time plots, obtained using a simplified SZVCM, for test 3, at stations 1 and 2, respectively

12.4.4 Assessment of SZVCM and parameterisation

Complex SZVCM performance and parameters

Table 12-8 shows the results of the calibration, using a topologically complex spatially zoned "viscous" calibration model (SZVCM) with 8 zones, of creep deformation spring (J) parameters, with fixed 0.1, 0.2, 0.3, 0.4, 0.5 and 0.6s dashpot retardation time (τ) parameters, and then simultaneous calibration of both J and τ parameters. There is considerable variation in the fitted J parameters for each zone as the value of the fixed τ parameter is increased. Nevertheless, there are consistent trends in the fitted J parameters. The lowest objective function is obtained for the calibration with fitted J and τ parameters. The next lowest objective function is obtained for the calibration with a fixed τ parameter of 0.3s.

Table 12-8 – Calibrated creep deformation spring (J) parameters, using fixed and fitted dashpot retardation time (τ) parameters, for test 3

Zone	Fixed Tau Parameter						Average (x e-10)	Fitted J and Tau	
	0.1	0.2	0.3	0.4	0.5	0.6		J (x e-10)	Tau
1	4.30	8.02	9.95	5.73	9.98	8.21	**7.70**	**3.99**	0.39
2	-0.05	0.09	0.30	0.47	0.80	1.08	**0.45**	**0.25**	0.39
3	-0.11	-0.20	-0.35	-0.34	-0.62	-0.80	**-0.40**	**-0.23**	0.43
4	-0.07	-0.03	-0.09	-0.05	0.11	0.15	**0.00**	**0.01**	0.37
5	-0.14	-0.25	-0.06	-0.32	-0.36	-0.37	**-0.25**	**-0.40**	0.43
6	0.11	0.24	-0.06	0.37	0.31	0.22	**0.20**	**0.44**	0.36
7	-0.35	-0.53	-0.72	-0.83	-1.00	-1.00	**-0.74**	**-0.99**	0.44
8	0.14	0.17	0.29	0.21	0.29	0.26	**0.23**	**0.17**	0.27
Obj. Func.	0.452	0.443	0.439	0.481	0.468	0.470	0.459	0.434	Avg. 0.39

Figure 12-37 shows the variation of the fitted J parameters with spatial zone along the Kookaburra Court Pipeline (KCP). The magnitude of the calibrated J parameters, and consequently the magnitude of "viscous" damping, varies with position along the KCP. These variations in magnitude appear to be correlated with changes in the fixed τ parameter. Figure 12-38 shows the variation of the J parameters over a scale of $\pm$1.0e-10Pa^{-1} for zones 2 to 8. The fitted J parameters for zones 3, 5 and 7, are negative. It is difficult to physically interpret this result. The SZVCM is designed to

incorporate "viscous" damping and not "viscous" excitation of the KCP. That said, the overall effect of the calibrated *J* parameters is to positively damp the KCP.

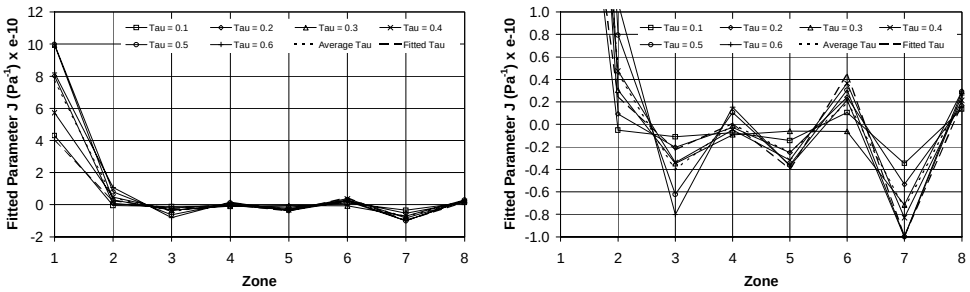

Figures 12-37 and 12-38 – Comparison of fitted *J* parameters for test 3, obtained using an 8 zone SZVCM, over different vertical scales

Table 12-9 shows the correlation of calibrated *J* and τ parameters for the different zones along the KCP. Generally, the fitted *J* and τ parameters for each of the 8 zones are not highly correlated.

Table 12-9 – *J* and τ parameter correlations for 8 zone SZVCM for test 3

	J1	*τ1*	*J2*	*τ2*	*J3*	*τ3*	*J4*	*τ4*	*J5*	*τ5*	*J6*	*τ6*	*J7*	*τ7*	*J8*	*τ8*
J1	**1.00**	**1.00**	0.47	0.47	0.61	0.61	0.43	0.48	0.16	0.19	0.13	0.12	0.20	0.20	0.56	0.54
τ1	**1.00**	**1.00**	0.47	0.47	0.61	0.61	0.43	0.48	0.16	0.19	0.13	0.12	0.20	0.20	0.56	0.54
J2	0.47	0.47	**1.00**	**0.99**	0.23	0.21	0.32	0.33	0.10	0.13	0.05	0.04	0.09	0.07	0.23	0.18
τ2	0.47	0.47	**0.99**	**1.00**	0.16	0.14	0.35	0.36	0.08	0.11	0.04	0.03	0.09	0.08	0.23	0.19
J3	0.61	0.61	0.23	0.16	**1.00**	**1.00**	0.37	0.42	0.17	0.23	0.19	0.16	0.09	0.08	0.49	0.45
τ3	0.61	0.61	0.21	0.14	**1.00**	**1.00**	0.34	0.39	0.14	0.20	0.22	0.19	0.06	0.05	0.49	0.45
J4	0.43	0.43	0.32	0.35	0.37	0.34	**1.00**	**0.99**	0.44	0.42	0.12	0.10	0.17	0.18	0.50	0.52
τ4	0.48	0.48	0.33	0.36	0.42	0.39	**0.99**	**1.00**	0.37	0.35	0.16	0.14	0.15	0.16	0.53	0.55
J5	0.16	0.16	0.10	0.08	0.17	0.14	0.44	0.37	**1.00**	**1.00**	0.58	0.59	0.50	0.49	0.03	0.06
T5	0.19	0.19	0.13	0.11	0.23	0.20	0.42	0.35	**1.00**	**1.00**	0.52	0.53	0.46	0.45	0.06	0.03
J6	0.13	0.13	0.05	0.04	0.19	0.22	0.12	0.16	0.58	0.52	**1.00**	**1.00**	**0.87**	**0.87**	0.01	0.06
T6	0.12	0.12	0.04	0.03	0.16	0.19	0.10	0.14	0.59	0.53	**1.00**	**1.00**	**0.87**	**0.88**	0.03	0.04
J7	0.20	0.20	0.09	0.09	0.09	0.06	0.17	0.15	0.50	0.46	**0.87**	**0.87**	**1.00**	**1.00**	0.49	0.43
T7	0.20	0.20	0.07	0.08	0.08	0.05	0.18	0.16	0.49	0.45	**0.87**	**0.88**	**1.00**	**1.00**	0.48	0.42
J8	0.56	0.56	0.23	0.23	0.49	0.49	0.50	0.53	0.03	0.06	0.01	0.03	0.49	0.48	**1.00**	**0.98**
T8	0.54	0.54	0.18	0.19	0.45	0.45	0.52	0.55	0.06	0.03	0.06	0.04	0.43	0.42	**0.98**	**1.00**

Comparison of results obtained for complex and simplified SZVCMs

Table 12-10 shows the results of the calibration for creep deformation spring (*J*) and dashpot retardation time (τ) parameters for test 3, conducted on the 28th August 2003,

using topologically complex and simplified spatially zoned "viscous" calibration models (SZVCMs) with 8 zones. The objective functions are 0.43 and 0.64 for the calibration of the complex and simplified SZVCMs, respectively. On the basis of lowest objective function, and an assessment of the regression diagnostics, the SZVCM with complex topology is marginally superior.

Table 12-10 – Calibrated creep deformation spring (J) and dashpot retardation time (τ) parameters using 8 zone SZVCMs with complex and simplified topologies

Zone	Fitted J and τ – complex topology		Fitted J and τ – simplified topology	
	J (x e-10)	τ	J (x e-10)	τ
1	3.99	0.39	-0.24	0.43
2	0.25	0.39	0.60	0.31
3	-0.23	0.43	-0.75	0.40
4	0.01	0.37	-0.06	0.53
5	-0.40	0.43	-0.25	0.47
6	0.44	0.36	0.46	0.35
7	-0.99	0.44	-0.95	0.25
8	0.17	0.27	0.42	0.22
Obj. Func.	0.434	Avg. 0.39	0.638	Avg. 0.37

Figure 12-39 shows the variation of the fitted J parameters with spatial zone along the Kookaburra Court Pipeline (KCP), when both J and τ parameters are simultaneously calibrated using the complex and simplified 8 zone SZVCMs. Relatively consistent J parameters are obtained for each of the zones, except for zone 1, regardless of whether the model with complex or simplified topology is used. Figure 12-40 shows the variation of the J parameters, over a scale of ±1.0e-10Pa^{-1}, for zones 1 to 8.

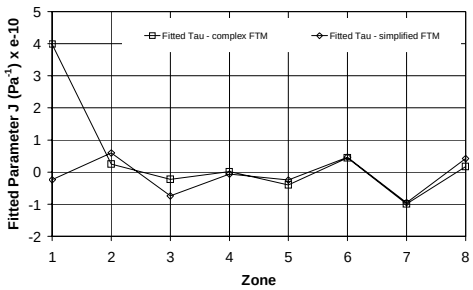

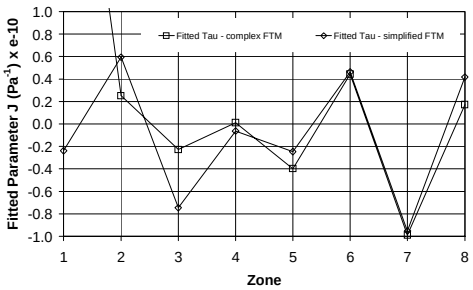

Figures 12-39 and 12-40 – Comparison of fitted J parameters obtained using 8 zone SZVCMs, with complex and simplified topologies, over different vertical scales

The consistency in the calibrated J parameters may be explained if the effects of mechanical motion or vibration, flexible joints and soil/pipe interaction, rather than the topology and physical condition of the water service connections, dominate the "viscous" damping. Alternatively, the damping effects of the water service connections may be being incorporated during the calibration. Both interpretations suggest that the inclusion of the precise physical details of the water service connections may not be significant for damping calibration.

That said, the use of the model with simplified topology leads to the omission of significant reflections. Figures 12-41 and 12-42 show the standardised residual plotted against time for test 3, for the calibrations performed using the complex and simplified 8 zone SZVCMs with fitted τ parameters, at stations 1 and 2, respectively. Relative to the results obtained using the complex model, marginally longer "runs" of positive and negative residuals are obtained.

The neglect of the water service connections leads to the predicted wavefront pre-empting the arrival of the measured reflected wavefront from the dead end of the KCP (this manifests as the distinctive spike at both stations 1 and 2). Each water service connection acts as a volumetric accumulator and their omission from a model will result in predicted wavefronts arriving earlier than measured wavefronts. This observation is important when the time of arrival of a wavefront at a station is used to determine wave speed and/or infer the condition of the wall of a distribution pipeline.

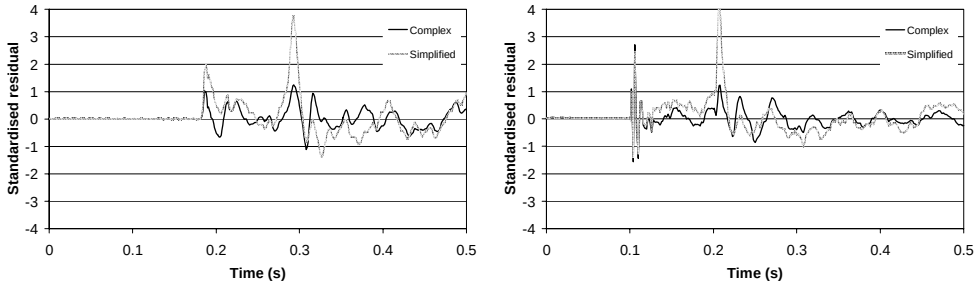

Figures 12-41 and 12-42 – Standardised residual versus time plots, obtained using SZVCMs with complex and simplified topologies, at stations 1 and 2, respectively

That said, it has been presumed that the inclusion of more information regarding the topology and condition of the water service connections will result in reflections being accurately predicted. This is only true if the information is accurate. The amount of physical information that can be gathered for any particular distribution pipeline will vary significantly and, in some cases, no information regarding the position, size, extent or condition of water service connections will be available. In these situations, the use of a model with simplified topology may be necessary.

12.5 Summary

Physical complexities, including effects from mechanical motion and vibration, flexible joints and soil/pipe interaction, are more likely to be significant for distribution pipelines and require the development of conceptual transient models with parameters that can be calibrated using measured transient responses. Furthermore, the presence of water service connections, with ill-defined or unknown topology and/or physical condition, represents a significant additional complexity. The conceptual approach described in Chapter 5, and applied to reproduce the measured responses of the Hanson Transmission Pipeline (HTP) in Chapter 8, has been further developed in this chapter by introducing spatial zones and increasing the number of Kelvin-Voigt mechanical elements to replicate variable dispersion and damping observed in the measured responses from the Saint Johns Terrace Pipeline (SJTP) and Kookaburra Court Pipeline (KCP).

A spatially zoned “viscous” calibration model (SZVCM) has been developed and calibrated to the measured responses of the SJTP. Selected positive transient tests were used to perform the calibration without any artificial fault. Regression diagnostics have been examined and the SZVCM with 16 distinct spatial zones, and 32 creep deformation spring (J) and dashpot retardation time (τ) parameters, was not over-parameterised. The number of spatial zones, and hence parameters, was reduced from 16 to 8 to 4 to assess the adequacy of these models. The 8 zone SZVCM could be calibrated with marginally less accuracy than the 16 zone SZVCM. However, the 4 zone SZVCM could not be satisfactorily calibrated.

A SZVCM has also been developed and calibrated to the measured response of the KCP. A selected negative transient test was used to perform the calibration without any artificial fault. Models with complex, but approximated, water service connection topology and condition, as well as models with simplified topology, have been calibrated. The water service connections were omitted for the simplified SZVCM. The results of the calibrations confirm that the topology and condition of the water service connections is important, but that using approximate representations gave results only marginally better than those obtained when omitting the water service connections.

Given the physical complexity of the Saint Johns Terrace Pipeline (SJTP) and Kookaburra Court Pipeline (KCP), the calibrated values of the creep deformation spring (J) parameters cannot be ascribed any specific physical meaning. This is partly due to uncertainty regarding whether mechanical motion or vibration, flexible joints and/or soil/pipe interaction, are responsible for the damping in the main pipe. Furthermore, the contribution of uncertainty in the topology and condition of water service connections to the observed damping is unknown. That said, the spatially zoned “viscous” calibration models (SZVCMs) presented in this chapter do facilitate calibration to the no-fault measured responses of the SJTP and the KCP. The significance of these calibrations is demonstrated in the context of detecting artificially introduced blockages, air pockets and leaks, using Inverse Transient Analysis (ITA), in Chapters 13 and 14.